NASA TECHNICAL NOTE

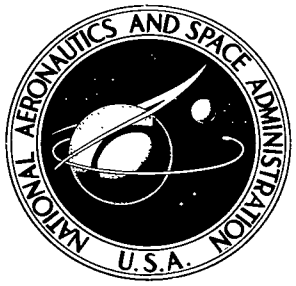

NASA TN D-6788

NASA TN D-6788

ANALYSIS OF A TURBULENT BOUNDARY LAYER OVER A MOVING GROUND PLANE

by Alan T. Roper and Garl L. Gentry, Jr.

Langley Research Center
Hampton, Va. 23365

NATIONAL AERONAUTICS AND SPACE ADMINISTRATION • WASHINGTON, D. C. • JULY 1972

1. Report No.	2. Government Accession No.	3. Recipi
NASA TN D-6788		

4. Title and Subtitle	5. Report Date
ANALYSIS OF A TURBULENT BOUNDARY LAYER OVER A MOVING GROUND PLANE	July 1972
	6. Performing Organization Code

7. Author(s)	8. Performing Organization Report No.
Alan T. Roper, Rose-Hulman Institute of Technology; and Garl L. Gentry, Jr.	L-7872
	10. Work Unit No.
9. Performing Organization Name and Address	136-63-02-07
NASA Langley Research Center Hampton, Va. 23365	11. Contract or Grant No.
	13. Type of Report and Period Covered
12. Sponsoring Agency Name and Address	Technical Note
National Aeronautics and Space Administration Washington, D.C. 20546	14. Sponsoring Agency Code

15. Supplementary Notes

16. Abstract

Four methods of predicting the integral and friction parameters for a turbulent boundary layer over a moving ground plane are evaluated by using test information obtained in the 76.2- by 50.8-centimeter tunnel at the Langley Research Center. The tunnel was operated in the open-sidewall configuration. These methods are

(1) Relative integral parameter method

(2) Modified power law method

(3) Relative power law method

(4) Modified law of the wall method

Methods (1) and (3) can be used to predict moving-ground-plane parameters with reasonable accuracy provided the corresponding stationary-ground-plane parameters are known. The general usefulness of these methods is dependent upon the universality of basic approximations upon which they are based. Method (2) is shown to be an invalid formulation. Investigation of method (4) is inconclusive. No attempt is made to establish the accuracy of the local skin-friction coefficients predicted by the various methods. Comparatively, however, the modified law of the wall method predicts a more rapid decrease in skin friction with an increase in the ratio of belt velocity to free-stream velocity than do methods (1) and (3).

17. Key Words (Suggested by Author(s))	18. Distribution Statement
Boundary-layer parameters Moving-belt ground plane	Unclassified – Unlimited

19. Security Classif. (of this report)	20. Security Classif. (of this page)	21. No. of Pages	22. Price*
Unclassified	Unclassified	72	$3.00

*For sale by the National Technical Information Service, Springfield, Virginia 22151

ANALYSIS OF A TURBULENT BOUNDARY LAYER OVER A MOVING GROUND PLANE

By Alan T. Roper* and Garl L. Gentry, Jr.
Langley Research Center

SUMMARY

Four methods of predicting the integral and friction parameters for a turbulent boundary layer over a moving ground plane are evaluated by using test information obtained in the 76.2- by 50.8-centimeter tunnel at the Langley Research Center. The tunnel was operated in the open-sidewall configuration. These methods are

(1) Relative integral parameter method

(2) Modified power law method

(3) Relative power law method

(4) Modified law of the wall method

Methods (1) and (3) can be used to predict moving-ground-plane parameters with reasonable accuracy provided the corresponding stationary-ground-plane parameters are known. The general usefulness of these methods is dependent upon the universality of basic approximations upon which they are based. Method (2) is shown to be an invalid formulation. Investigation of method (4) is inconclusive.

No attempt is made to establish the accuracy of the local skin-friction coefficients predicted by the various methods. Comparatively, however, the modified law of the wall method predicts a more rapid decrease in skin friction with an increase in the ratio of belt velocity to free-stream velocity than do methods (1) and (3).

INTRODUCTION

One system being considered in high-speed ground transportation studies is that of a vehicle traveling in a tube. At high speeds, the aerodynamic forces are important in determining the stability and performance of this system. It is, therefore, necessary that the flow phenomena producing these forces be understood.

*Professor, Department of Mechanical and Aerospace Engineering, Rose-Hulman Institute of Technology, Terre Haute, Indiana.

When viewed from the vehicle frame of reference, the tube wall has a velocity equal in magnitude and opposite in sign to that of the vehicle. The vehicle is stationary in this frame of reference and, therefore, the relative velocity between the fluid and the tube wall and that between the fluid and vehicle are different. Since the fluid velocity is higher than the vehicle velocity due to blockage effects, the tube-wall boundary layer is analogous to a boundary layer developing over a moving ground plane. This nonzero wall velocity has a profound effect upon the boundary layer.

An understanding of the turbulent-boundary-layer development on both the vehicle and the tube wall is the key to successful near-field drag prediction. The vehicle boundary layer is commonplace and can be handled by existing techniques. The tube-wall boundary layer, however, has some unusual characteristics which are similar to those encountered in the growth of boundary layers behind moving shock waves and in the development of boundary layers in a Ludwieg tube.

A boundary layer, whether laminar or turbulent, is characterized by vorticity in what may be an otherwise irrotational field. The edge of the boundary layer marks the limit of the outward extent of the vorticity generated at the solid boundary. Consider two boundary layers under the same conditions except that one develops over a moving ground plane and the other develops over a stationary ground plane (fig. 1). If vorticity travels outward at an average velocity V, then the time $t = \delta/V$ is required for the vorticity to reach the vertical distance δ. Since vorticity is convected downstream at the local velocity, the layer above the stationary ground plane, having the lower average velocity, attains a thickness δ in a shorter distance x than the layer above the moving ground plane. Thus, one effect of the moving ground plane is to reduce the boundary-layer thickness.

In order to promote the understanding of the nonstationary wall boundary layer, velocity measurements were taken over a smooth-texture moving ground belt (representing a moving ground plane) installed in the 76.2- by 50.8-centimeter tunnel at the Langley Research Center. The tunnel was operated in the open-sidewall configuration. These data are used to evaluate two methods of predicting integral and friction parameter behavior which currently appear in the literature and two methods generated during the present study.

SYMBOLS

The units used for the physical quantities in this report are given in both the International System of Units (SI) and the U.S. Customary Units. Measurements and calculations were made in the U.S. Customary Units.

A, A'
B, B' } empirically determined constants

$a(x)$	vertical displacement of ground plane, meters (feet)
C_f	total skin-friction coefficient, $\frac{2}{x}\int_0^x \frac{c_f}{2}\,dx'$
$C_f(0)$	stationary-ground-plane total skin-friction coefficient
C_p	pressure coefficient, $\frac{p - p_i}{\frac{1}{2}\rho U^2}$
c	chord of fairing plate, meters (feet)
c_f	local skin-friction coefficient
$c_f(0)$	stationary-ground-plane local skin-friction coefficient
$g(R)$	empirically determined polynomial
H	shape factor, δ^*/θ
$H(0)$	stationary-ground-plane shape factor
N	reciprocal of power in relative power law formulation, $n(R = 0)$
n	reciprocal of power in power law formulation
p	static pressure, newtons/meter^2 (pounds/foot^2)
p_i	static pressure at fairing plate tip, newtons/meter^2 (pounds/foot^2)
R	velocity ratio (nominal value), V_B/U
R_c	critical Reynolds number
R_x	Reynolds number based on x
R_y	Reynolds number based on y and U
t	time

U	x-component of mean velocity at edge of boundary layer, meters/second (feet/second)
u	local x-component of mean velocity, meters/second (feet/second)
u_τ	friction velocity, $\sqrt{\tau_0/\rho}$, meters/second (feet/second)
V	vorticity diffusion velocity in boundary layer
V_B	velocity of ground belt, meters/second (feet/second)
v	local y-component of mean velocity, meters/second (feet/second)
x	longitudinal distance from leading edge of ground belt, meters (feet)
x', θ'	dummy variables
y	vertical distance from ground belt, centimeters (inches)
δ	boundary-layer thickness, centimeters (inches)
$\delta(0)$	stationary-ground-plane boundary-layer thickness
δ^*	displacement thickness, $\int_0^\delta \left(1 - \frac{u}{U}\right) dy$, centimeters (inches)
$\delta^*(0)$	displacement thickness for stationary ground plane, centimeters (inches)
η	reciprocal of the exponent in the modified Blasius shear-stress formulation
θ	momentum thickness, $\int_0^\delta \frac{u}{U}\left(1 - \frac{u}{U}\right) dy$, meters (feet)
$\theta(0)$	momentum thickness for stationary ground plane, meters (feet)
μ	dynamic viscosity, newton-seconds/meter^2 (pound-seconds/foot^2)
ν	kinematic viscosity, μ/ρ, meters^2/second (feet^2/second)
ρ	mass density, kilograms/meter^3 (slugs/foot^3)
τ	shearing stress, newtons/meter^2 (pounds force/foot^2)

Subscript:

o measured at $y = 0$

A tilde (~) over a symbol indicates a relative velocity or a quantity based upon velocity relative to the ground plane; for example,

$$\tilde{\delta}^* = \int_0^{\tilde{\delta}} \left(1 - \frac{\tilde{u}}{\tilde{U}}\right) dy$$

ANALYSIS

Experimental Data

Data analyzed in this study were obtained in the 76.2- by 50.8-centimeter tunnel at the Langley Research Center. The tunnel was fitted with a moving smooth ground belt (representing a moving ground plane) and operated in the open-sidewall configuration (ref. 1). Velocity profiles were measured by means of total-pressure probe traverses. Probe position was controlled by a lead screw with vertical position indicated by a potentiometer readout. The general test arrangement is shown in figure 2. Lateral and longitudinal pressure distributions were measured on the fairing plate (fig. 2(a)) prior to testing to ensure that positioning of the fairing had not produced any large or adverse pressure gradients. A representative set of such readings are presented in figure 3 in terms of pressure coefficient based on static pressure at the first fairing plate tap and on free-stream dynamic pressure. All pressure data were recorded on a slant-tube alcohol manometer.

In all tests, the tunnel boundary layer was bled off through a porous suction plate located immediately ahead of the belt leading edge. The boundary layer is, therefore, assumed to originate at the leading edge of the belt. In practice, it was not possible to remove the entire tunnel boundary layer. The effects of this incomplete boundary-layer removal are shown for the $R = 1.0$ (nominal) profiles in figure 4. Additional disturbances were caused at the leading edge by a small slot (between the suction plate and the belt) and the natural entrainment of air from this slot by the belt motion. Further inaccuracies were encountered for readings taken nearest the belt because of the tendency of the belt to lift slightly when in motion. The data are uncorrected for these disturbances.

The vertical positions of measured total-pressure values were corrected for the displacement effect of the probe disturbance upon the flow. The method used for correction is outlined in reference 2.

Total-pressure probe traverses were made at a nominal dynamic pressure of 526.68 N/m^2 (11 lbf/ft^2), velocity of 29.26 m/sec (96.00 ft/sec), and Reynolds number per

unit length of 1.87×10^6 per meter (5.70×10^5 per foot) at stations 0.347 m (1.14 ft), 0.506 m (1.66 ft), 0.713 m (2.34 ft), 0.860 m (2.82 ft), and 1.079 m (3.54 ft) aft of the belt leading edge. Tunnel static pressure during testing was nominally atmospheric. For these conditions the range of test Reynolds numbers was $0.65 \times 10^6 < R_x < 2.0 \times 10^6$. Data were recorded at values of V_B/U of approximately 0, 0.19, 0.39, 0.58, 0.77, and 1.00.

Boundary-layer transition from laminar to turbulent flow occurred on the belt forward of the station at $x = 0.347$ m (1.14 ft). (See fig. 5(a).) Due to the shortness of the belt and the relatively low Reynolds numbers which could be achieved, none of the stations are spatially far removed from the transition region. Local skin-friction coefficients presented in figure 5(a) were determined by the approach suggested by Clauser (ref. 3) which is illustrated in figure 5(b). These low Reynolds number effects, as well as those effects associated with leading-edge disturbances mentioned previously, are present in all data but are particularly serious at the station at $x = 0.347$ m (1.14 ft) and for $V_B/U = 1.0$ (all stations). For this reason, the data at $x = 0.347$ m and $V_B/U = 1.0$ are not included in the analysis of this study, although the raw data for all conditions are presented in tabular form.

Velocity profiles measured during this study are presented in figures 6(a) to 6(e) in ln-ln form; the velocity data are also given in table I. Summary charts of the x-variation of boundary-layer thickness δ, and the integral parameters δ^*, θ, and H are presented in figures 7(a) to 7(d); these data are also given in table II. Cross-plotting the data of figure 7(a) and including the rough-belt data of reference 4 yields figure 8, which shows that the experimental boundary-layer thickness decreases with belt speed ratio. This result tends to support the simplified argument presented in the Introduction.

Theoretical Methods

Brief descriptions are presented of four methods which have been suggested for predicting the development of the turbulent boundary layer over a moving ground plane. Evaluation of each method is accomplished by comparison with data measured during this investigation.

Relative integral parameter method.- The boundary-layer equations for two-dimensional incompressible flow over a flat plate

$$u \frac{\partial u}{\partial x} + v \frac{\partial u}{\partial y} = \frac{1}{\rho} \frac{\partial \tau}{\partial y} \tag{1a}$$

$$\frac{\partial u}{\partial x} + \frac{\partial v}{\partial y} = 0 \tag{1b}$$

together with the boundary conditions

$$u(x,0) = V_B \qquad u(x,\delta) = U \qquad v(x,0) = 0$$

define the moving-ground-plane problem.

The integral form of the momentum equation is obtained from equations (1) as

$$\frac{d\theta}{dx} = \frac{\tau_o}{\rho U^2} = \frac{c_f}{2} \tag{2}$$

This equation remains unchanged from the stationary-ground-plane expression which implies that the form of the dependence of local skin-friction coefficient upon θ remains unchanged when the ground belt is set in motion.

The relative integral parameters $\tilde{\delta}^*$, $\tilde{\theta}$, and $\tilde{H}$ can be generated by replacing the absolute velocity ratio u/U in the usual integral definitions by the relative velocity ratio

$$\frac{\tilde{u}}{\tilde{U}} = \frac{u - V_B}{U - V_B} = \frac{(u/U) - R}{1 - R} \tag{3}$$

The equations relating $\tilde{\delta}^*$, $\tilde{\theta}$, and $\tilde{H}$ to the integral parameters δ^*, θ, and H are easily generated by using equation (3) and the integral quantity definitions. These equations are

$$\delta^* = (1 - R)\tilde{\delta}^* \tag{4a}$$

$$\theta = (1 - R)^2\tilde{\theta} + R(1 - R)\tilde{\delta}^* \tag{4b}$$

$$H = \frac{\tilde{H}}{1 + R(\tilde{H} - 1)} \tag{4c}$$

Test data available at the time this method was developed (ref. 5) indicated that $\tilde{H}$ is nearly independent of R and $\theta/\theta(0)$ is approximately independent of x. Thus,

$$\tilde{H} \approx \tilde{H}(0) = H(0) \tag{5a}$$

$$\frac{\theta}{\theta(0)} = \frac{C_f}{C_f(0)} = g(R) \tag{5b}$$

where $g(R)$ is a polynomial in R obtained by fitting measured data. The general form of this function is taken to be

$$g(R) = (1 - R)\left[1 + AR + BR(1 + R)\right] \tag{6}$$

where A and B are empirically determined constants.

On the basis of these assumptions, the following equations can be generated for the integral parameters by using equations (4) and (5):

$$\theta = g(R)\theta(0) \tag{7}$$

$$\delta^* = \frac{H(0)}{1 + R\left[H(0) - 1\right]} g(R)\theta(0) \tag{8}$$

$$H = \frac{H(0)}{1 + R\left[H(0) - 1\right]} \tag{9}$$

The coefficients A and B in equation (6) were found to be -0.411 and 0.013, respectively, in reference 5; whereas to fit the data of the present study, values of -1.1756 and 0.7863 were necessary. These changes are not unexpected since the data used to determine A and B in reference 5 were measured in a fully developed turbulent boundary layer over a rough belt, whereas data for the present study were obtained over a smooth belt for a layer not far removed from transition. The possibility exists, however, that A and B may not be truly universal constants even for smooth belts. If this proves to be true, the usefulness of this method would be greatly reduced.

A comparison of g(R) with measured values of $\theta/\theta(0)$ is presented in figure 9. With the exception of the station at x = 0.506 m (1.66 ft), the x-dependence of $\theta/\theta(0)$ is small. Since data for this station are most susceptible to errors generated by the leading-edge flow disturbances peculiar to the test arrangement (see "Experimental Data" section), the relative x-independence of g(R) seems a justifiable assumption.

Even a cursory inspection of figure 10 is sufficient to show that the assumption $\tilde{H} = H(0)$ is rather seriously violated, the variation of $\tilde{H}$ being approximately of the same order as the variation in H itself. However, rather large incremental changes in both $\tilde{H}$ and H represent relatively small percentage variations (of the order of 25 percent) compared with those of other integral parameters. Further, the assumption of R-independence of H is a less critical assumption than the x-independence of g(R).

Measured values of θ, δ^*, and H are compared with those predicted from equations (7) to (9) in figures 11(a) to 11(d). Correlation between measured and predicted values of θ is generally good, as indeed it must be, since the equation was obtained through an empirical fit of the data. Correlations of δ^* and H are also reasonably good; this further underscores the secondary importance of the assumption $\tilde{H} = H(0)$.

With one additional assumption it is possible to extend this method to include the prediction of local skin-friction coefficients. Multiplying and dividing equation (2) by the stationary-ground-plane local skin-friction coefficient $c_f(0)$ yields

$$\frac{d\theta}{dx} = \frac{1}{2}\frac{c_f}{c_f(0)}\,c_f(0)$$

Assuming $c_f/c_f(0)$ $\left(\text{like } C_f/C_f(0)\right)$ is a function of R alone and integrating results in

$$\int_0^{\theta} d\theta' = \frac{1}{2}\frac{c_f}{c_f(0)}\int_0^{x} c_f(0)\,dx'$$

or

$$\theta = \frac{1}{2}\frac{c_f}{c_f(0)}\,C_f(0)x$$

Dividing by $\theta(0)$ gives

$$\frac{\theta}{\theta(0)} = \frac{1}{2}\frac{c_f}{c_f(0)}\frac{C_f(0)}{\theta(0)}\,x$$

Rearranging and using equation (5b) yields

$$\frac{1}{2}\frac{C_f(0)}{\theta(0)}\,x = \frac{g(R)}{c_f/c_f(0)}$$

Since the left-hand side of this equation is a function of x and the right-hand side (within the validity of the original assumption) varies with R only, it follows that

$$\frac{c_f}{c_f(0)} = g(R) = \frac{\theta}{\theta(0)} \tag{10}$$

Thus, $c_f/c_f(0)$ should be equal to θ/θ_o provided $\dfrac{c_f}{c_f(0)} \neq f(x)$.

Modified power law method.- Reference 6 has suggested representation of the moving-ground-plane velocity variation as a power law profile. The usual formulation is modified so that the wall is displaced to a position $y = a(x)$ at which the local velocity u equals the ground-plane velocity V_B (fig. 12). Mathematically,

$$\frac{u}{U} = \left[\frac{y + a(x)}{\delta + a(x)}\right]^{1/n} \tag{11}$$

where n is an appropriate number which the authors of reference 6 took to be 7. Application of the boundary condition $u(x,0) = V_B$ produces the following definition:

$$a(x) = \frac{\delta R^n}{1 - R^n} \tag{12}$$

Implicit in this approach is the assumption that $n \neq n(R)$; thus, all velocity profiles from equation (11) should collapse to a single line of slope $1/n$ when presented in logarithmic form. Values of n were determined by a least-squares fit of the $R = 0$ profiles measured in this study. By using these values, the measured data are presented in the form suggested by equation (11) in figures 13(a) to 13(d). It can be seen that the results do not collapse as predicted by this method.

Relative power law method.- Existing data, from both the rough belt (ref. 4) and the smooth belt tests, indicate that the relative velocity ratio (eq. (3)) does admit to the power law formulation

$$\frac{\tilde{u}}{\tilde{U}} = \left(\frac{y}{\tilde{\delta}}\right)^{1/N} \tag{13}$$

where $\tilde{\delta}$ is the boundary-layer thickness based upon the relative velocity distribution $\left(\frac{\tilde{u}}{\tilde{U}} = 0.99\right)$ and N is essentially independent of R.

For the formulation suggested by equation (13), the measured relative velocity profiles collapse to a single line of relatively constant slope (figs. 14(a) to 14(d)). The data from reference 4 are presented in the same form in figures 14(e) and 14(f) and display the same behavior. A summary of the variation of the slopes of the absolute velocity profiles in ln-ln form denoted by $n(R)$ and those of the relative velocity profiles N are presented in figure 15. These values were obtained by a least-squares (straight line) fit of the data points in the form ($-\ln y/\delta$, $-\ln u/U$) and ($-\ln \tilde{y}/\tilde{\delta}$, $-\ln \tilde{u}/\tilde{U}$). Although a slight degradation of N from the $R = 0$ value is apparent with increasing R, the $N(0)$ value was used for all calculations.

From equation (13) and the definition of relative integral parameters, it follows that

$$\frac{\tilde{\delta}^*}{\tilde{\delta}} = \frac{1}{N+1} \tag{14a}$$

$$\frac{\tilde{\theta}}{\tilde{\delta}} = \frac{N}{(N+1)(N+2)} \tag{14b}$$

$$\tilde{H} = \frac{N+2}{N} \tag{14c}$$

Substituting equations (4) into equations (14) yields

$$\frac{\delta^*}{\delta} = \frac{1-R}{N+1}\frac{\tilde{\delta}}{\delta} \tag{15a}$$

$$\frac{\theta}{\delta} = (1-R)\frac{N+2R}{(N+1)(N+2)}\frac{\tilde{\delta}}{\delta} \tag{15b}$$

$$H = \frac{N+2}{N+2R} \tag{15c}$$

It should be noted that the quantity $\tilde{\delta}/\delta$ in equations (15a) and 15(b) is 1 only when $R = 0$; that is, the y value at which $\frac{u}{U} = 0.99$ is not generally the same as that at which $\frac{\tilde{u}}{\tilde{U}} = 0.99$. The variation of $\tilde{\delta}/\delta$ with R, as determined from experimental data, is presented in figure 16.

Although the parameter ratios given by equations (15) are of interest, it is perhaps of greater interest to be able to predict the quantities δ^*, θ, and H from known values of these parameters for the stationary ground plane. Dividing each of equations (15) with its form for $R = 0$ produces the desired ratios:

$$\frac{\delta^*}{\delta^*(0)} = (1-R)\frac{\tilde{\delta}}{\delta(0)} \tag{16}$$

$$\frac{\theta}{\theta(0)} = (1-R)\frac{N+2R}{N}\frac{\tilde{\delta}}{\delta(0)} = \frac{C_f}{C_f(0)} \tag{17}$$

$$\frac{H}{H(0)} = \frac{N}{N + 2R} \tag{18}$$

Values of $\tilde{\delta}/\delta(0)$ were determined from experimental data and are presented in figure 16. With the exception of the station at $x = 0.506$ m (1.66 ft), the results show only a small scatter. The values of $\tilde{\delta}/\delta(0)$ obtained from the fairing in figure 16 and the values of N obtained from the least-squares fit of the stationary-ground-plane logarithmic profiles were used with equations (16), (17), and (18) to obtain values of $\delta^*/\delta^*(0)$ and $H/H(0)$. These predicted values are compared with the experimentally determined ratios in figures 17(a) to 17(d). Correlations appear to be satisfactory for most purposes except at the station at $x = 0.506$ m (1.66 ft).

The empirical determination of $\tilde{\delta}/\delta(0)$ appears to be the weakest link in this particular approach. The possibility exists that the variation obtained is peculiar only to the experimental setup used in this study.

For incompressible turbulent flow past a semi-infinite flat plate, Blasius gives the variation of τ_o with δ to be (ref. 7)

$$\frac{\tau_o}{\rho U^2} = 0.0225\left(\frac{\nu}{U\delta}\right)^{1/4} \tag{19}$$

Extending equation (19) to include relative velocity as suggested by Mirels (ref. 8) and replacing 1/4 by $1/\eta$ for generality yields

$$\frac{\tau_o}{\rho(U - V_B)^2} = 0.0225\left[\frac{\nu}{(U - V_B)\delta}\right]^{1/\eta} \tag{20}$$

Rearranging and applying the definition of the local skin-friction coefficient to equation (20) gives

$$\frac{c_f}{2} = \frac{\tau_o}{\rho U^2} = 0.0225(1 - R)^{\frac{2\eta-1}{\eta}}\left(\frac{\nu}{U\delta}\right)^{1/\eta} \tag{21}$$

where $R \leqq 1$.

The key to the application of equation (21) to the prediction of local skin-friction coefficients is the determination of η. For the test data of this study, η can be determined from measured boundary-layer thickness in the following manner. Equation (2)

can be rewritten as

$$\frac{\theta}{\delta}\frac{d\delta}{dx} = \frac{\tau_o}{\rho U^2} \tag{22}$$

since θ/δ is taken to be independent of x (eq. 15(b)). Substituting equation (21) into equation (22), integrating, and rearranging yields

$$\delta = \left(\frac{0.0225}{\theta/\delta}\frac{\eta+1}{\eta}\right)^{\frac{\eta}{\eta+1}}(1-R)^{\frac{2\eta-1}{\eta+1}}\left(\frac{1}{R_x}\right)^{\frac{1}{\eta+1}}x \tag{23}$$

By using measured values of δ and θ/δ, equation (23) was solved graphically for η for the appropriate test conditions. These results are presented in figure 18. Equation (21) was then solved for c_f by using these values of η. The resulting local skin-friction coefficients are presented in figure 19.

Modified law of the wall method.- Another approach to the title problem can be made by hypothesizing that the relative velocity profiles obey the law of the wall in the form

$$\frac{\tilde{u}}{\tilde{u}_\tau} = A\log\left(\frac{y\tilde{u}_\tau}{\nu}\right) + B \tag{24}$$

where

$$\tilde{u}_\tau = \sqrt{\frac{\tau_o}{\rho}} = \tilde{U}\sqrt{\frac{\tilde{c}_f}{2}} \tag{25}$$

The local skin-friction coefficient based upon absolute velocity c_f is related to that based upon relative velocity by the equation

$$\frac{c_f}{2} = (1-R)^2\frac{\tilde{c}_f}{2} \tag{26}$$

In order to pursue this method, it is necessary to determine $\tilde{c}_f$ $\left(\text{or } c_f\right)$. The approach suggested in reference 3 was adapted to this purpose. Rewriting equation (24) by using equation (25) yields

$$\frac{\tilde{u}}{\tilde{U}} = \sqrt{\frac{\tilde{c}_f}{2}}\left[A \log\left(\frac{y\tilde{U}}{\nu}\sqrt{\frac{\tilde{c}_f}{2}}\right) + B\right]$$

or

$$\frac{\tilde{u}}{\tilde{U}} = A\sqrt{\frac{\tilde{c}_f}{2}} \log\left(\tilde{R}_y\right) + A\sqrt{\frac{\tilde{c}_f}{2}} \log\left(\sqrt{\frac{\tilde{c}_f}{2}}\right) + B\sqrt{\frac{\tilde{c}_f}{2}} \tag{27}$$

where

$$A = 5.75$$

$$B = 5.20$$

Thus, for a fixed value of $\tilde{c}_f/2$, $\tilde{u}/\tilde{U}$ can be written in the form

$$\frac{\tilde{u}}{\tilde{U}} = A' \log\left(\tilde{R}_y\right) + B'$$

where A' and B' are constants for a given value of $\tilde{c}_f/2$. Charts constructed for a range of $\tilde{c}_f$ values by using equation (27) and the measured data are presented in figures 20(a) to 20(e). The values of $\tilde{c}_f$ were obtained from the data in the same manner as previously described.

Although many of the profiles lack a clearly defined linear portion, it is nonetheless possible to determine approximate values of $\tilde{c}_f$. It is interesting to note that there is a tendency, particularly at higher values of R, for the $\tilde{u}/\tilde{U}$ profiles to drop rapidly near the wall. This effect could stem from an increase in the extent of the region of linear velocity gradient, a large laminar sublayer, or errors in the measured velocity distribution induced by the tendency of the belt to lift when in motion. These $\tilde{c}_f$ values, converted to c_f based upon absolute velocity, are shown in figure 21.

Comparison of Local Skin-Friction Coefficients

The local skin-friction coefficient is a difficult quantity to measure, and the ground-plane motion intensifies this problem. The relative integral parameter (eq. (10)), relative power law (eq. (21)), and modified power law methods all yield methods for predicting local skin-friction coefficients. No attempt has been made to establish the accuracy of the various predictions. They are, however, compared in figure 22 (as a function of

$\theta/\theta(0)$). Note that the values of c_f predicted by the modified law of the wall method are generally lower than those of the other methods.

CONCLUSIONS

The following conclusions can be reached as a result of this investigation:

1. The velocity profiles measured near a moving ground plane can be described by a relative power law formulation of the form

$$\frac{\tilde{u}}{\tilde{U}} = \left(\frac{y}{\tilde{\delta}}\right)^{1/N}$$

where $\tilde{u}/\tilde{U}$ is relative velocity ratio, $\tilde{\delta}$ is relative boundary-layer thickness, y is vertical distance from ground belt, and N is the slope of the stationary-ground-plane profile. This appears to be a particularly strong statement inasmuch as both the smooth-belt boundary layers which are near transition (the present study) and the more fully developed turbulent boundary layers on the rough belt (NASA TN D-4229) admit to this description.

2. The integral parameters (displacement thickness δ, momentum thickness θ, total skin-friction coefficient C_f, and shape factor H) can be described with reasonable accuracy by either the relative integral parameters or the relative power law variation. This conclusion must be qualified by the proviso that the variations $\theta/\theta(0)$ (relative integral parameter method) and $\tilde{\delta}/\delta(0)$ (relative power law method) observed for these tests prove to be nearly universal for smooth-belt zero-pressure-gradient boundary layers. ($\theta(0)$ is stationary-ground-plane momentum thickness and $\delta(0)$ is stationary-ground-plane boundary-layer thickness.)

3. Formulation of the velocity profiles as a modified power law variation

$$\frac{u}{U} = \left[\frac{y + a(x)}{\delta + a(x)}\right]^{1/n}$$

is not valid. (u/U is velocity ratio, $a(x) = \dfrac{\delta R^n}{1 - R^n}$ with R being ratio of ground-plane velocity to free-stream velocity, and n is reciprocal of power in power law formulation.)

4. The modified law of the wall method predicts a more rapid decrease in local skin-friction coefficient with an increase in the ratio of belt velocity to free-stream velocity than do the relative integral parameter and relative power law methods.

Langley Research Center,
National Aeronautics and Space Administration,
Hampton, Va., May 15, 1972.

REFERENCES

1. Grunwald, Kalman J.: Experimental Investigation of the Use of Slotted Test-Section Walls To Reduce Wall Interference for High-Lift-Model Testing. NASA TN D-6292, 1971.

2. Young, A. D.; and Maas, J. N.: The Behaviour of a Pitot Tube in a Transverse Total-Pressure Gradient. R. & M. No. 1770, Brit. A.R.C., 1937.

3. Clauser, Francis H.: Turbulent Boundary Layers in Adverse Pressure Gradients. J. Aeronaut. Sci., vol. 21, no. 2, Feb. 1954, pp. 91-108.

4. Turner, Thomas R.: Wind-Tunnel Investigation of a 3/8-Scale Automobile Model Over a Moving-Belt Ground Plane. NASA TN D-4229, 1967.

5. Roper, Alan T.; and Gentry, Garl L., Jr.: Turbulent-Boundary-Layer Development on a Moving Ground Belt of Rough Texture. NASA TM X-2515, 1972.

6. Foa, J. V.; and Messina, N. A.: Estimated Performance of Wheel-Supported Vehicles To Be Tested in Facility T-2. TN PT 6802 (Contract No. C-117-66 (Neg.)), Rensselaer Polytechnic Inst., Sept. 1968.

7. Schlichting, H.: Lecture Series "Boundary Layer Theory." Part II – Turbulent Flows. NACA TM 1218, 1949.

8. Mirels, Harold: Boundary Layer Behind Shock or Thin Expansion Wave Moving Into Stationary Fluid. NACA TN 3712, 1956.

TABLE I.- DATA FROM BOUNDARY-LAYER SURVEYS

(a) R = 0; U = 30.24 m/sec (99.22 ft/sec)

x = 0.347 m (1.14 ft) δ = 0.665 cm (0.262 in.)	
y/δ	u/U
0.1221	0.7352
.1565	.7538
.1985	.7693
.2366	.7871
.2748	.8044
.3130	.8186
.3473	.8286
.3893	.8441
.4733	.8731
.5420	.8914
.6193	.9171
.7023	.9417
.7710	.9578
.8473	.9717
.9237	.9829
1.0038	.9909
1.0763	.9953
1.1565	.9980
1.2366	.9988
1.3053	.9992
1.3817	.9996

x = 0.506 m (1.66 ft) δ = 0.955 cm (0.376 in.)	
y/δ	u/U
0.0851	0.6124
.1117	.6421
.1436	.6722
.1649	.6862
.1941	.7084
.2261	.7249
.2500	.7385
.2739	.7491
.3404	.7816
.4122	.8148
.4734	.8411
.5372	.8642
.6064	.8890
.6676	.9100
.7447	.9369
.8032	.9549
.8590	.9672
.9122	.9765
.9654	.9845

x = 0.713 m (2.34 ft) δ = 1.283 cm (0.505 in.)	
y/δ	u/U
0.0832	0.5989
.1050	.6279
.1248	.6496
.1525	.6735
.1644	.6909
.1922	.6937
.2020	.7050
.2416	.7287
.2812	.7511
.3208	.7719
.3604	.7896
.4059	.8118
.4515	.8338
.4970	.8521
.5485	.8726
.5980	.8909
.6535	.9102
.6970	.9231
.7485	.9400
.7980	.9545
.8475	.9668
.8951	.9729
.9446	.9837
.9941	.9889

x = 0.860 m (2.82 ft) δ = 1.430 cm (0.563 in.)	
y/δ	u/U
0.0746	0.5855
.0906	.6190
.1101	.6404
.1279	.6568
.1456	.6735
.1616	.6840
.1812	.6977
.2256	.7244
.2700	.7506
.3162	.7754
.3588	.7955
.4068	.8142
.4494	.8310
.4938	.8497
.5417	.8681
.5861	.8865
.6288	.9006
.6696	.9145
.7140	.9273
.7584	.9421
.8046	.9545
.8508	.9656
.8917	.9717
.9378	.9809
.9805	.9869

x = 1.079 m (3.54 ft) δ = 1.709 cm (0.673 in.)	
y/δ	u/U
0.0624	0.5831
.0788	.6083
.0936	.6307
.1085	.6437
.1218	.6553
.1382	.6738
.1516	.6814
.1902	.7076
.2259	.7312
.2630	.7535
.3001	.7686
.3388	.7924
.3744	.8033
.4131	.8218
.4487	.8408
.4859	.8533
.5230	.8671
.5617	.8820
.6003	.8944
.6345	.9040
.6731	.9170
.7147	.9336
.7459	.9420
.7875	.9508
.8247	.9631
.8574	.9672
.8975	.9761
.9331	.9793
.9688	.9873

TABLE I.- DATA FROM BOUNDARY-LAYER SURVEYS - Continued

(b) R = 0.19; U = 30.31 m/sec (99.45 ft/sec)

x = 0.347 m (1.14 ft) δ = 0.605 cm (0.238 in.)	
y/δ	u/U
0.1345	0.7924
.1765	.8097
.2185	.8251
.2605	.8383
.3025	.8505
.3529	.8651
.3866	.8742
.4370	.8885
.5126	.9073
.5966	.9223
.6849	.9455
.7647	.9660
.8529	.9745
.9328	.9858
1.0168	.9921
1.0966	.9961
1.1933	.9984
1.2689	.9992
1.3529	.9992

x = 0.506 m (1.66 ft) δ = 0.833 cm (0.328 in.)	
y/δ	u/U
0.1311	0.7106
.1616	.7325
.1890	.7517
.2226	.7693
.2500	.7820
.2805	.7955
.3110	.8113
.3750	.8362
.4329	.8548
.4939	.8780
.5549	.8954
.6159	.9119
.6799	.9295
.7378	.9454
.7988	.9582
.8628	.9721
.9299	.9821
.9848	.9881

x = 0.713 m (2.34 ft) δ = 1.054 cm (0.415 in.)	
y/δ	u/U
0.1318	0.7307
.1807	.7441
.1952	.7547
.2217	.7671
.2458	.7794
.2988	.7960
.3470	.8176
.3928	.8343
.4386	.8507
.4916	.8673
.5349	.8826
.5807	.8960
.6313	.9091
.6795	.9246
.7301	.9352
.7759	.9453
.8241	.9577
.8771	.9688
.9205	.9761
.9687	.9829

x = 0.860 m (2.82 ft) δ = 1.270 cm (0.500 in.)	
y/δ	u/U
0.0880	0.6685
.1040	.6866
.1240	.7075
.1460	.7263
.1640	.7403
.1860	.7540
.2040	.7639
.2480	.7863
.2820	.7972
.3340	.8187
.3640	.8306
.4080	.8489
.4540	.8659
.5020	.8817
.5560	.9011
.6040	.9124
.6560	.9270
.7020	.9396
.7520	.9521
.8040	.9624
.8560	.9705
.9060	.9790
.9580	.9885

x = 1.079 m (3.54 ft) δ = 1.448 cm (0.570 in.)	
y/δ	u/U
0.0737	0.6741
.0912	.6955
.1088	.7106
.1263	.7239
.1456	.7379
.1614	.7469
.1789	.7569
.2246	.7795
.2667	.8000
.3105	.8190
.3561	.8357
.3982	.8516
.4421	.8681
.4842	.8794
.5333	.8927
.5737	.9059
.6175	.9188
.6614	.9303
.7088	.9421
.7491	.9504
.7965	.9599
.8421	.9692
.8807	.9753
.9281	.9829
.9702	.9869

TABLE I.- DATA FROM BOUNDARY-LAYER SURVEYS - Continued

(c) R = 0.39; U = 30.37 m/sec (99.63 ft/sec)

x = 0.347 m (1.14 ft) δ = 0.764 cm (0.301 in.)	
y/δ	u/U
0.1063	0.8563
.1362	.8632
.1761	.8790
.2093	.8862
.2392	.8985
.2757	.9077
.3056	.9150
.3422	.9244
.4053	.9279
.4718	.9521
.5387	.9644
.6080	.9741
.6777	.9842
.7409	.9905
.8173	.9945
.8771	.9976
.9435	.9988
1.0033	.9992

x = 0.506 m (1.66 ft) δ = 0.759 cm (0.299 in.)	
y/δ	u/U
0.1405	0.7770
.1739	.8044
.2074	.8165
.2441	.8357
.2742	.8451
.3043	.8585
.3411	.8681
.4114	.8861
.4749	.8997
.5452	.9201
.6120	.9345
.6756	.9471
.7458	.9599
.8227	.9717
.8763	.9797
.9431	.9849

x = 0.713 m (2.34 ft) δ = 0.922 cm (0.363 in.)	
y/δ	u/U
0.1433	0.7915
.1763	.8064
.1956	.8137
.2287	.8272
.2562	.8357
.2837	.8475
.3361	.8618
.3912	.8773
.4463	.8893
.5041	.9004
.5702	.9186
.6088	.9301
.6567	.9428
.7218	.9523
.7924	.9635
.8347	.9716
.8926	.9793
.9449	.9841
.9772	.9897

x = 0.860 m (2.82 ft) δ = 1.069 cm (0.421 in.)	
y/δ	u/U
0.1259	0.7733
.1436	.7885
.1734	.7999
.1995	.8121
.2280	.8232
.2447	.8308
.2945	.8449
.3444	.8619
.3848	.8742
.4323	.8894
.4822	.8990
.5439	.9142
.6010	.9275
.6556	.9409
.7173	.9517
.7767	.9620
.8385	.9721
.8979	.9802
.9596	.9856

x = 1.079 m (3.54 ft) δ = 1.219 cm (0.480 in.)	
y/δ	u/U
0.1125	0.7806
.1312	.7922
.1458	.7996
.1708	.8124
.1917	.8197
.2229	.8321
.2521	.8415
.2937	.8546
.3438	.8688
.3771	.8787
.4208	.8903
.4625	.9026
.5000	.9096
.5500	.9247
.5854	.9298
.6292	.9382
.6687	.9432
.7104	.9511
.7542	.9594
.7979	.9684
.8354	.9724
.8792	.9793
.9229	.9837
.9625	.9873

TABLE I.- DATA FROM BOUNDARY-LAYER SURVEYS - Continued

(d) R = 0.58; U = 30.40 m/sec (99.75 ft/sec)

x = 0.347 m (1.14 ft) δ = 0.579 cm (0.228 in.)	
y/δ	u/U
0.1404	0.9028
.1842	.9106
.2368	.9179
.2763	.9235
.3158	.9295
.3596	.9358
.4035	.9400
.4474	.9458
.5351	.9545
.6228	.9611
.7193	.9709
.7982	.9761
.8904	.9849
.9825	.9893
1.0746	.9941
1.1491	.9961
1.2368	.9980
1.3246	.9988

x = 0.506 m (1.66 ft) δ = 0.704 cm (0.277 in.)	
y/δ	u/U
0.1913	0.8649
.2238	.8789
.2671	.8927
.2996	.8997
.3321	.9075
.3682	.9141
.4440	.9252
.5199	.9387
.5884	.9500
.6607	.9574
.7292	.9663
.8014	.9745
.8809	.9801
.9495	.9865

x = 0.713 m (2.34 ft) δ = 0.792 cm (0.312 in.)	
y/δ	u/U
0.1567	0.8623
.1967	.8700
.2308	.8804
.2660	.8893
.2949	.8964
.3269	.9026
.3974	.9160
.4551	.9259
.5160	.9348
.5833	.9436
.6506	.9536
.7115	.9614
.7756	.9692
.8429	.9773
.9135	.9821
.9776	.9881

x = 0.860 m (2.82 ft) δ = 0.945 cm (0.372 in.)	
y/δ	u/U
0.1425	0.8362
.1720	.8590
.2043	.8708
.2231	.8771
.2473	.8838
.2742	.8896
.3306	.9032
.3790	.9128
.4355	.9239
.4866	.9324
.5484	.9421
.6048	.9508
.6559	.9586
.7043	.9648
.7581	.9701
.8065	.9753
.8683	.9829
.9194	.9859
.9731	.9897

x = 1.079 m (3.54 ft) δ = 1.143 cm (0.450 in.)	
y/δ	u/U
0.1200	0.8411
.1378	.8555
.1622	.8665
.1844	.8733
.2089	.8801
.2289	.8868
.2756	.8961
.3133	.9031
.3600	.9152
.4022	.9230
.4511	.9310
.4933	.9382
.5378	.9453
.5822	.9516
.6400	.9594
.6689	.9627
.7156	.9680
.7578	.9729
.8044	.9777
.8511	.9829
.8933	.9857
.9355	.9877
.9822	.9913

TABLE I.- DATA FROM BOUNDARY-LAYER SURVEYS - Continued

(e) R = 0.77; U = 30.34 m/sec (99.54 ft/sec)

x = 0.347 m (1.14 ft) δ = 0.594 cm (0.234 in.)	
y/δ	u/U
0.1308	0.[illegible]
.1795	.9342
.2222	.9379
.2692	.9417
.3077	.9455
.3547	.9479
.3932	.9521
.4487	.9540
.4786	.9570
.5214	.9611
.6068	.9648
.6923	.9709
.7778	.9765
.8718	.9826
.9487	.9870
1.0427	.9925
1.1197	.9945
1.2137	.9961
1.2949	.9980
1.3803	.9996

x = 0.506 m (1.66 ft) δ = 0.691 cm (0.272 in.)	
y/δ	u/U
0.1912	0.9154
.2353	.9261
.2647	.9350
.3015	.9400
.3382	.9442
.3787	.9500
.4154	.9533
.4485	.9562
.5221	.9599
.6029	.9664
.6691	.9709
.7426	.9749
.8162	.9793
.8897	.9849
.9632	.9881

x = 0.713 m (2.34 ft) δ = 0.775 cm (0.305 in.)	
y/δ	u/U
0.2098	0.9250
.2492	.9344
.2689	.9369
.3016	.9411
.3311	.9465
.3705	.9515
.4066	.9536
.4689	.9565
.5377	.9635
.5967	.9675
.6689	.9716
.7311	.9757
.7967	.9793
.8623	.9833
.9311	.9861
1.0000	.9889

x = 0.860 m (2.82 ft) δ = 0.866 cm (0.341 in.)	
y/δ	u/U
0.1818	0.9123
.2111	.9227
.2405	.9311
.2757	.9379
.3021	.9417
.3636	.9500
.4164	.9545
.4809	.9586
.5396	.9627
.5953	.9668
.6510	.9709
.7126	.9749
.7713	.9781
.8270	.9813
.8915	.9841
.9472	.9881

x = 1.079 m (3.54 ft) δ = 1.067 cm (0.420 in.)	
y/δ	u/U
0.1476	0.9109
.1738	.9204
.1976	.9264
.2167	.9302
.2429	.9344
.2905	.9399
.3381	.9466
.3857	.9507
.4310	.9557
.4810	.9594
.5262	.9631
.5738	.9664
.6262	.9700
.6714	.9729
.7190	.9757
.7690	.9793
.8143	.9813
.8619	.9861
.9119	.9869
.9571	.9885

TABLE I.- DATA FROM BOUNDARY-LAYER SURVEYS - Concluded

(f) $R \approx 1.00$ (fig. 4); $U = 30.48$ m/sec (100 ft/sec)

x = 0.347 m (1.14 ft) δ = 0.546 cm (0.215 in.)	
y/δ	u/U
0.1488	0.9537
.1953	.9533
.2419	.9549
.2977	.9558
.3442	.9586
.3860	.9599
.4279	.9623
.4744	.9652
.5674	.9688
.6698	.9741
.7488	.9789
.8465	.9837
.9395	.9865
1.0326	.9905
1.1395	.9941
1.2279	.9961
1.3209	.9984
1.4046	.9992

x = 0.506 m (1.66 ft) δ = 0.615 cm (0.242 in.)	
y/δ	u/U
0.1322	0.9725
.1818	.9672
.2190	.9656
.2603	.9643
.3058	.9643
.3388	.9660
.3843	.9664
.4215	.9668
.5041	.9676
.5868	.9717
.6735	.9753
.7521	.9797
.8347	.9841
.9215	.9877
1.0000	.9901
1.0826	.9917
1.1653	.9949
1.2479	.9972
1.3306	.9992
1.4132	.9996

x = 0.713 m (2.34 ft) δ = 0.510 cm (0.201 in.)	
y/δ	u/U
0.2587	0.9602
.3085	.9622
.3632	.9626
.4080	.9639
.4577	.9651
.5174	.9671
.6070	.9679
.7065	.9716
.8060	.9740
.9055	.9773
1.0100	.9793
1.1045	.9809
1.2040	.9841
1.3035	.9865
1.4030	.9885
1.5025	.9917
1.6020	.9941
1.7015	.9957
1.8010	.9961
1.9005	.9980
2.0000	.9996

x = 0.860 m (2.82 ft) δ = 0.737 cm (0.290 in.)	
y/δ	u/U
0.1103	0.9833
.1448	.9857
.1793	.9865
.2172	.9789
.2483	.9761
.2828	.9757
.3276	.9745
.3552	.9729
.4207	.9753
.4965	.9765
.5586	.9781
.6276	.9805
.7000	.9821
.7828	.9833
.8655	.9861
.9655	.9893
1.0414	.9917
1.1345	.9933
1.2138	.9949
1.3000	.9965
1.3897	.9976
1.4724	.9988
1.5621	.9992
1.6448	.9996

x = 1.079 m (3.54 ft) δ = 0.838 cm (0.330 in.)	
y/δ	u/U
0.0970	0.9925
.1364	.9865
.1636	.9829
.1848	.9801
.2182	.9757
.2485	.9749
.2758	.9745
.3091	.9745
.3697	.9749
.4303	.9753
.4879	.9753
.5545	.9781
.6121	.9789
.6697	.9809
.7303	.9821
.7970	.9845
.8545	.9865
.9152	.9873
.9788	.9897
1.0333	.9909
1.0939	.9921
1.1576	.9929
1.2212	.9949
1.2788	.9961
1.3394	.9976
1.4030	.9980
1.4576	.9984

TABLE II.- SUMMARY OF GROSS PARAMETERS FROM PROFILE MEASUREMENTS

x		R	U		R_x	δ		δ^*		θ		H	N	$\tilde{\delta}$		$\tilde{\delta}^*$		$\tilde{\theta}$		$\tilde{H}$
m	ft		m/sec	ft/sec		cm	in.	cm	in.	cm	in.			cm	in.	cm	in.	cm	in.	
0.506	1.66	0	30.20	99.07	0.942×10^6	0.955	0.376	0.1882	0.0741	0.1123	0.0442	1.676	4.98	0.955	0.376	0.1882	0.0741	0.1123	0.0442	1.676
		.193	30.18	99.01	.944	.833	.328	.1389	.0547	.0912	.0359	1.522	4.53	.833	.328	.1722	.0678	.0991	.0390	1.740
		.386	30.27	99.30	.937	.759	.299	.1013	.0399	.0716	.0282	1.415	4.53	.818	.322	.1651	.0650	.0861	.0339	1.915
		.578	30.28	99.35	.937	.704	.277	.0704	.0277	.0549	.0216	1.286	4.62	.803	.316	.1671	.0658	.0790	.0311	2.114
		.769	30.37	99.65	.933	.691	.272	.0424	.0167	.0376	.0148	1.132	4.29	.848	.334	.1844	.0726	.0912	.0359	2.022
.713	2.34	0	30.08	98.70	1.337	1.283	.505	.2367	.0932	.1504	.0592	1.678	4.84	1.283	.505	.2522	.0993	.1504	.0592	1.678
		.194	30.14	98.90	1.331	1.054	.415	.1854	.0730	.1179	.0464	1.574	4.74	1.105	.435	.2301	.0906	.1260	.0496	1.825
		.387	30.23	99.17	1.322	.922	.363	.1247	.0491	.0884	.0348	1.412	4.70	.988	.389	.2035	.0801	.1067	.0420	1.909
		.579	30.29	99.38	1.315	.792	.312	.0782	.0308	.0620	.0244	1.263	4.74	.914	.360	.1857	.0731	.0940	.0370	1.977
		.776	30.43	99.82	1.334	.775	.305	.0470	.0185	.0414	.0163	1.131	4.55	.975	.384	.2096	.0825	.1008	.0397	2.079
.860	2.82	0	30.14	98.89	1.610	1.430	.563	.2715	.1069	.1722	.0678	1.576	4.93	1.430	.563	.2715	.1069	.1722	.0678	1.576
		.193	30.25	99.23	1.598	1.270	.500	.2055	.0809	.1372	.0540	1.499	4.67	1.300	.512	.2545	.1002	.1496	.0589	1.702
		.386	30.25	99.23	1.598	1.069	.421	.1427	.0562	.1026	.0404	1.390	4.56	1.128	.444	.2324	.0915	.1262	.0497	1.840
		.578	30.27	99.32	1.594	.945	.372	.0902	.0355	.0721	.0284	1.252	4.29	1.046	.412	.2141	.0843	.1120	.0441	1.914
		.777	30.05	98.59	1.613	.866	.341	.0518	.0204	.0462	.0182	1.124	4.03	1.123	.442	.2327	.0916	.1176	.0463	1.980
1.079	3.54	0	30.18	99.03	2.012	1.709	.673	.3129	.1232	.2037	.0802	1.537	5.12	1.709	.673	.3129	.1232	.2037	.0802	1.537
		.193	30.27	99.31	1.995	1.448	.570	.2189	.0862	.1552	.0611	1.412	5.06	1.496	.589	.2715	.1069	.1732	.0682	1.566
		.385	30.32	99.46	1.982	1.219	.480	.1461	.0575	.1123	.0442	1.301	4.89	1.278	.503	.2377	.0936	.1481	.0583	1.605
		.577	30.38	99.66	1.977	1.143	.450	.0986	.0388	.0813	.0320	1.213	4.63	1.278	.503	.2329	.0917	.1361	.0536	1.711
		.768	30.46	99.94	1.978	1.067	.420	.0607	.0239	.0541	.0213	1.120	4.56	1.349	.531	.2611	.1028	.1405	.0553	1.859

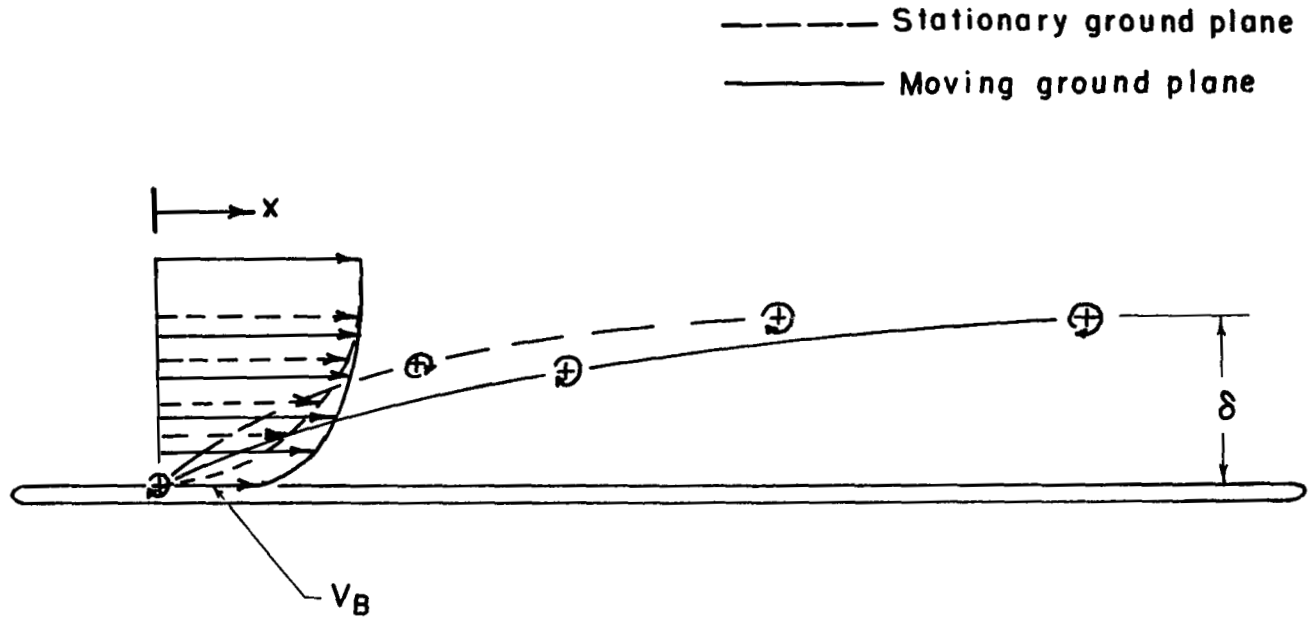

Figure 1.- Boundary-layer development over a moving ground plane.

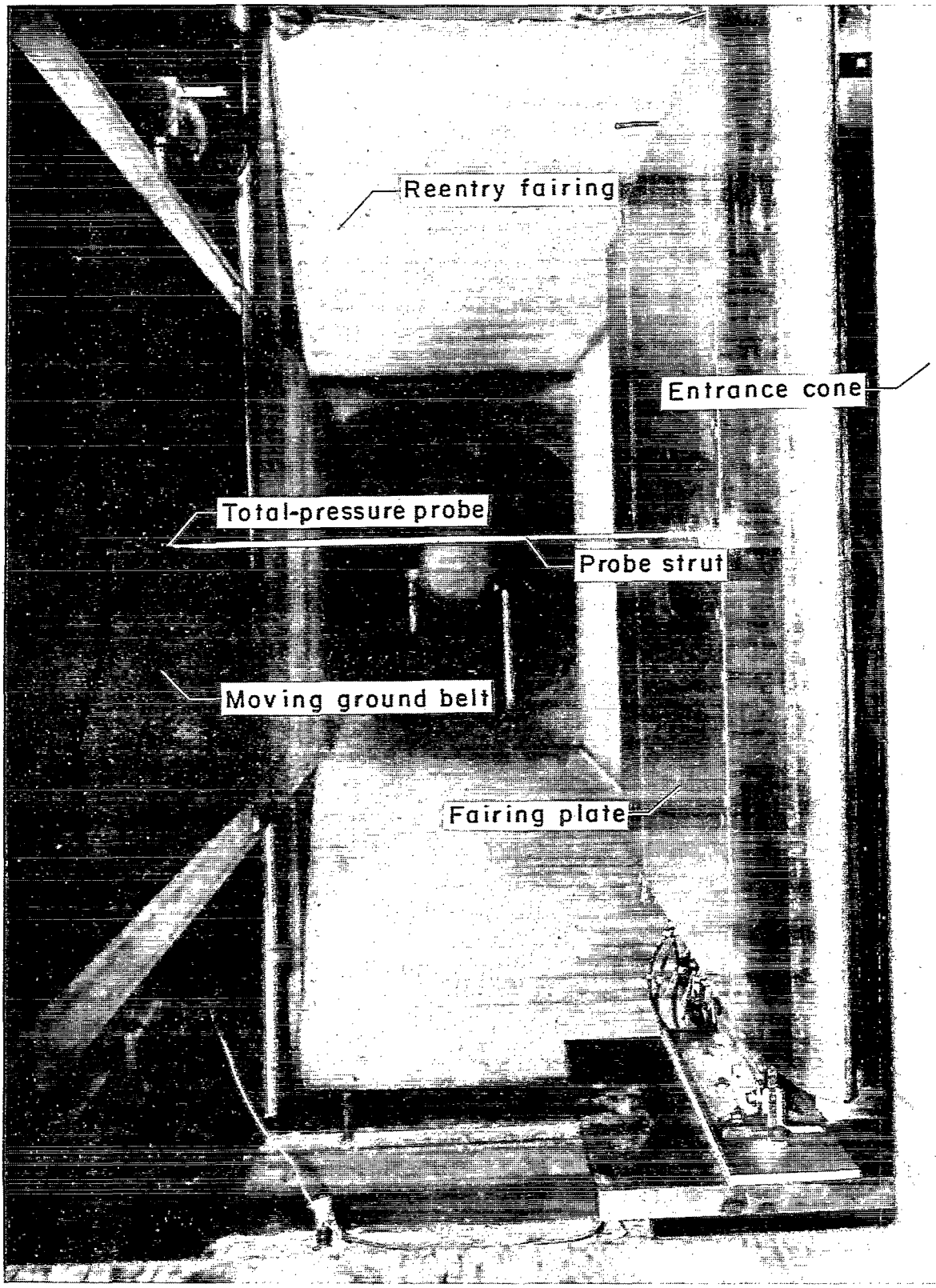

L-69-6014.1

(a) View from tunnel looking downstream.

Figure 2.- Total-pressure probe and ground-belt arrangement.

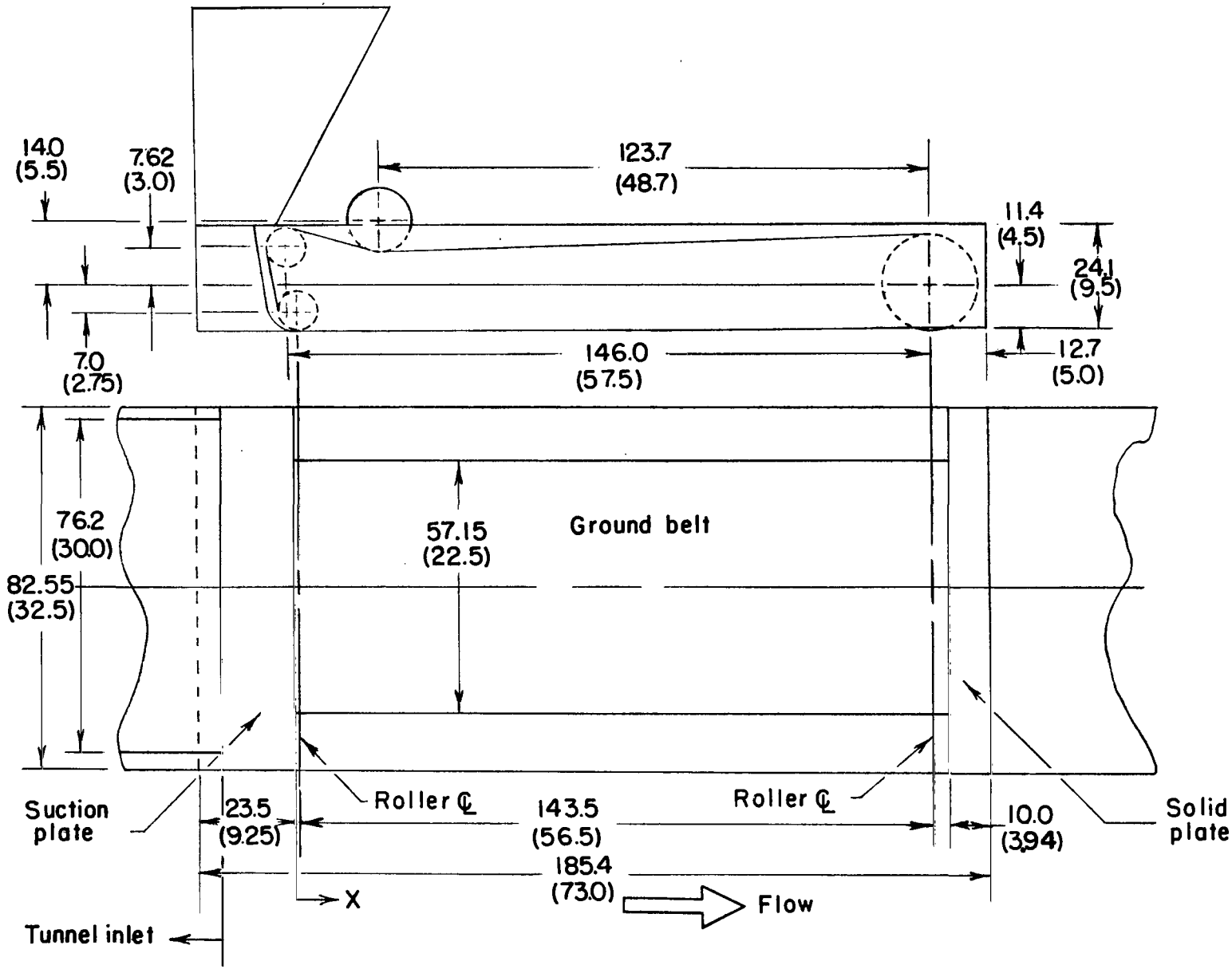

(b) General arrangement of moving ground belt. Dimensions are in centimeters (inches).

Figure 2.- Concluded.

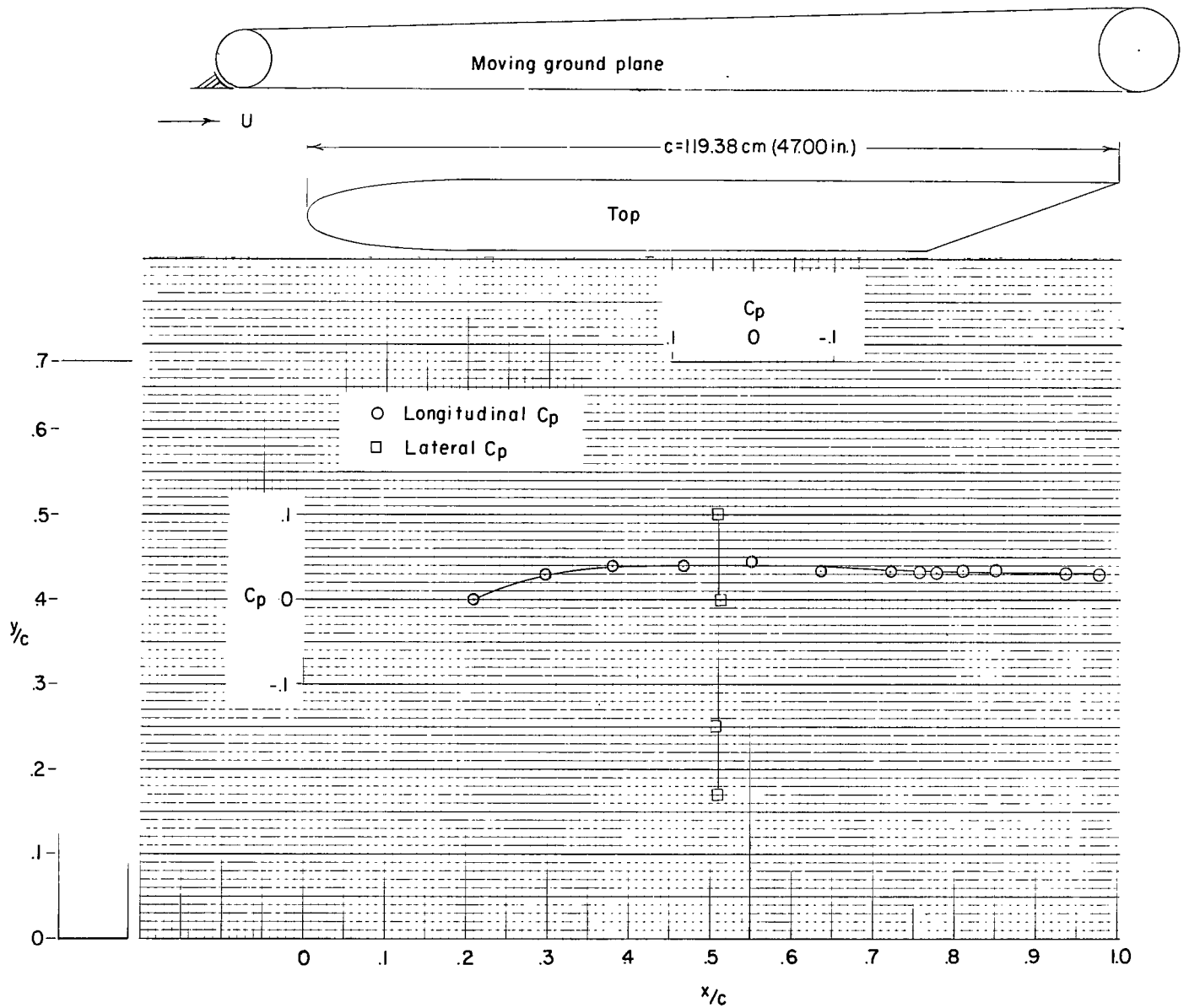

Figure 3.- Typical pressure distribution on fairing plate.

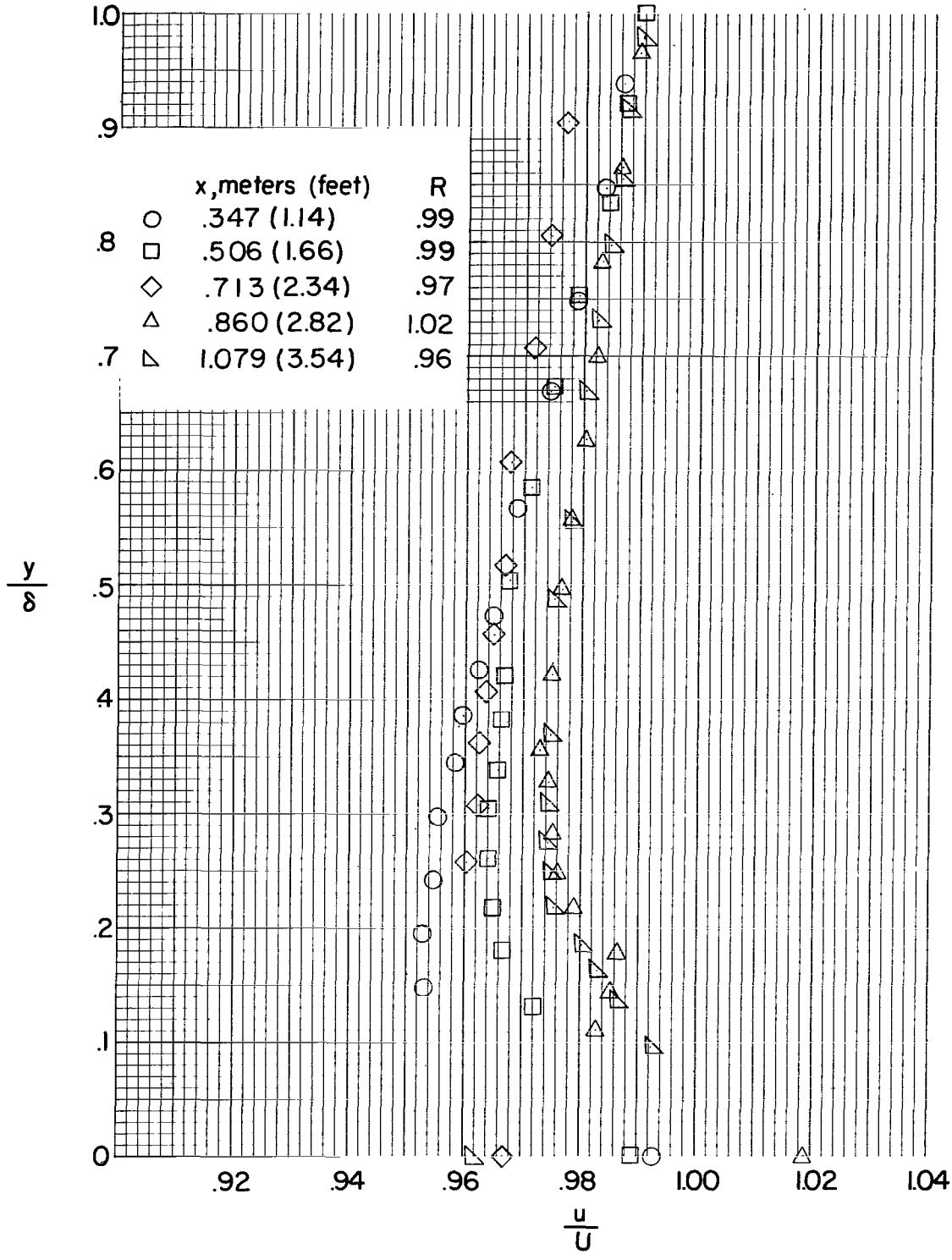

Figure 4.- Effect of incomplete boundary-layer removal.

(1) Blasius ; $c_f = 1.328\ R_x^{-1/2}$

(2) Prandtl- Schlichting ; $c_f = 0.455(\log_{10} R_x)^{-2.58} - A/R_x$

(3) Schultz – Grunow ; $c_f = 0.427\ (\log_{10} R_x - 0.407)^{-2.64}$

A = Constant

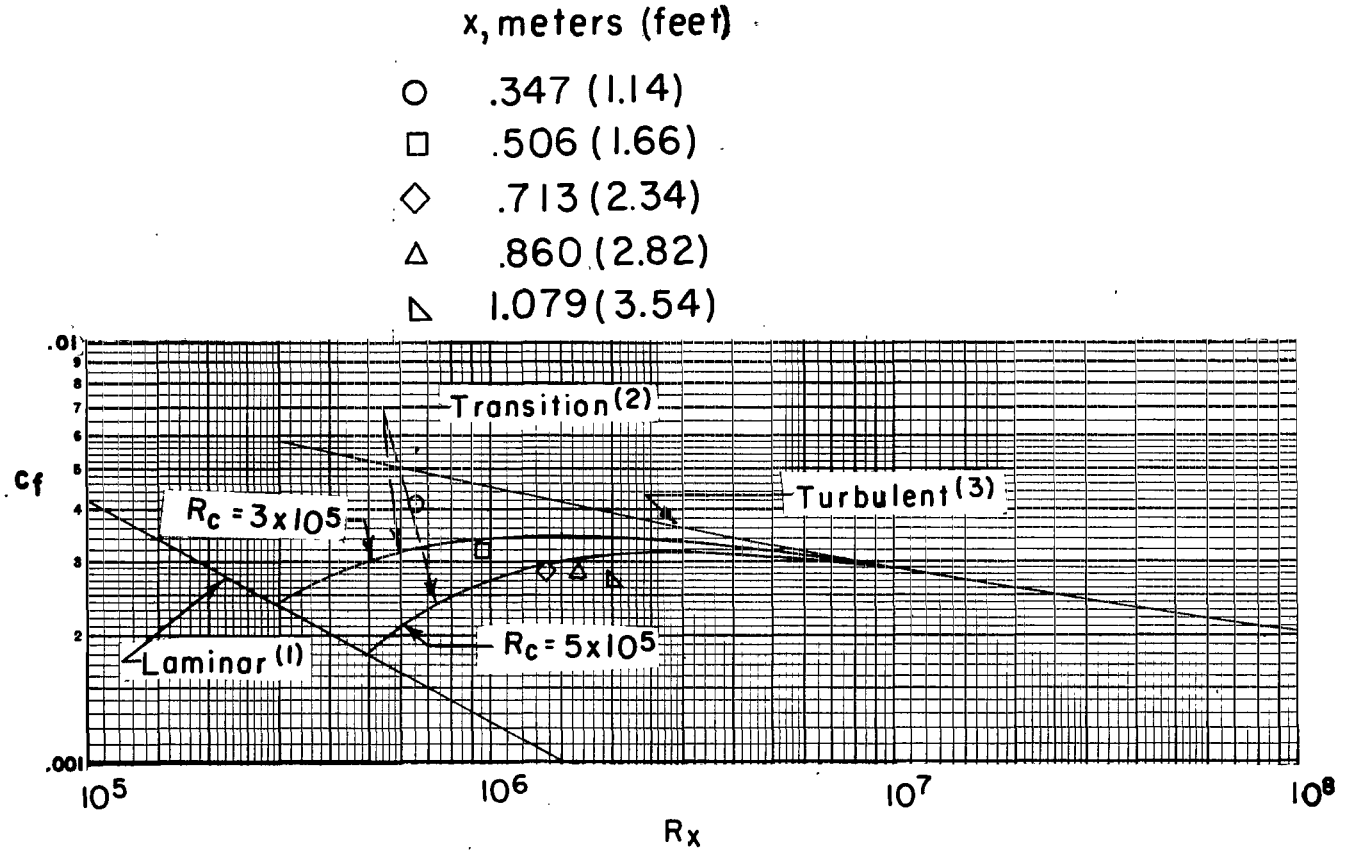

(a) Boundary-layer regime.

Figure 5.- Reynolds number effects. R = 0.

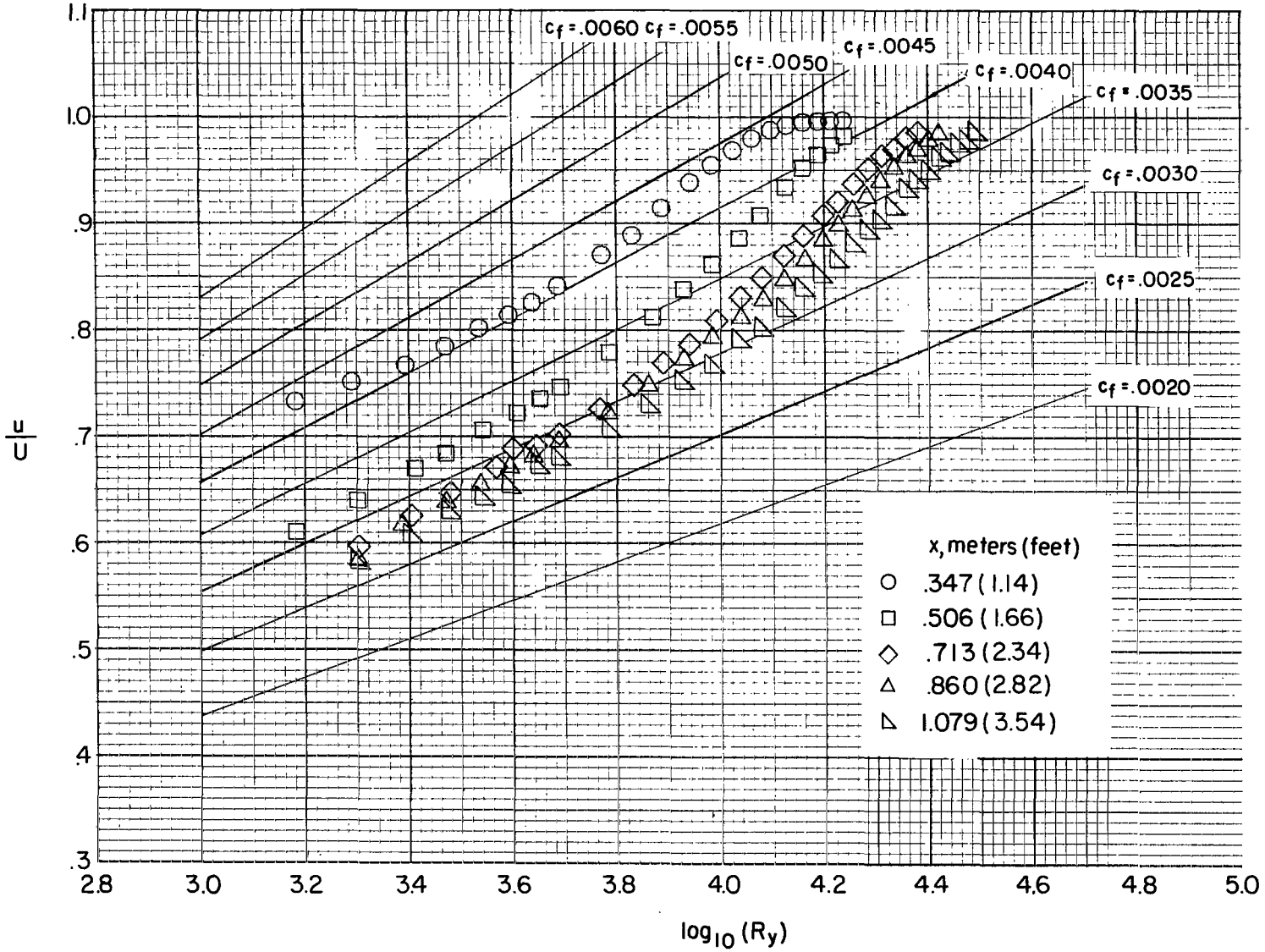

(b) Determination of local skin-friction drag coefficient.

Figure 5.- Concluded.

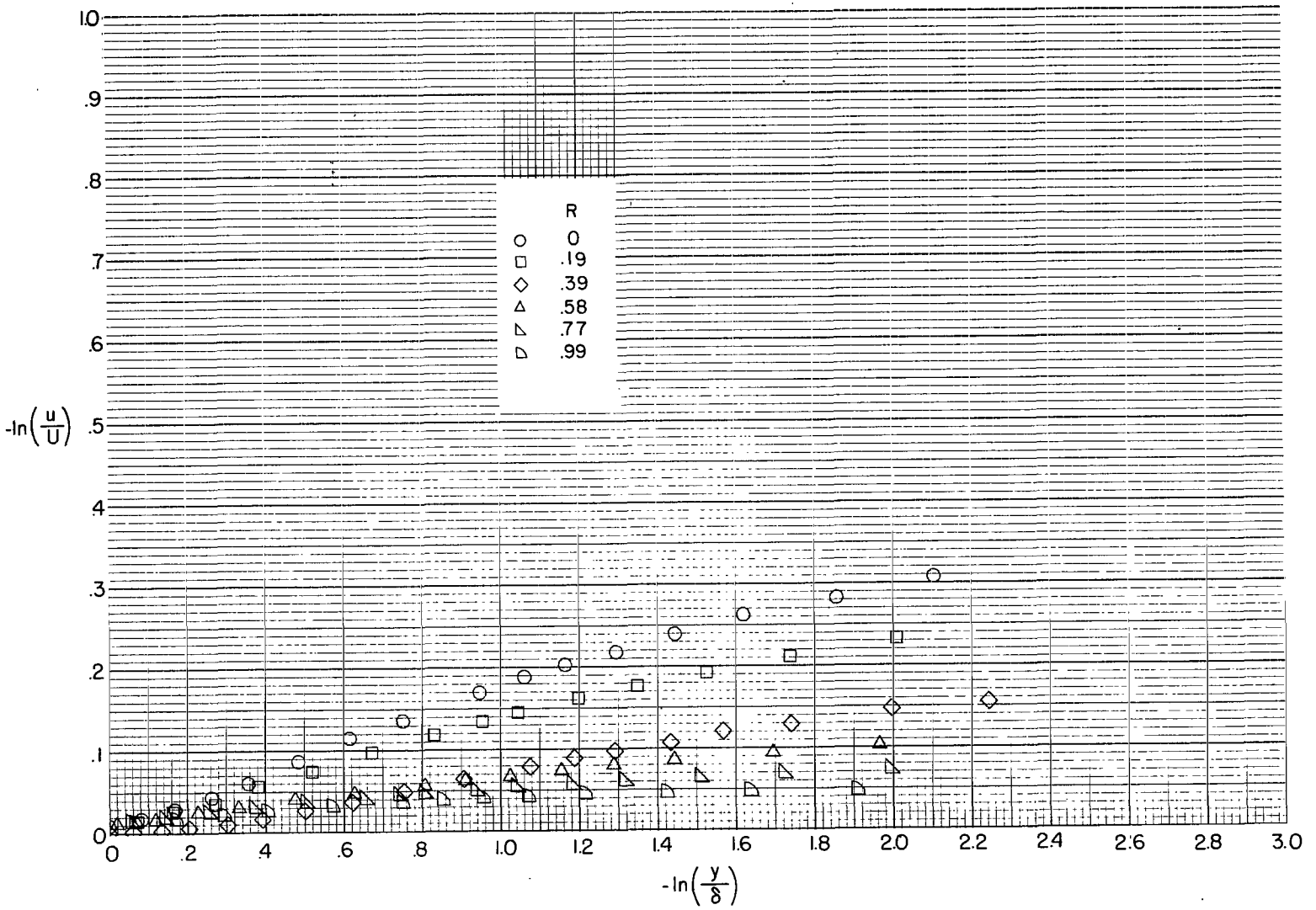

(a) x = 0.347 meter (1.14 feet).

Figure 6.- Measured velocity profiles.

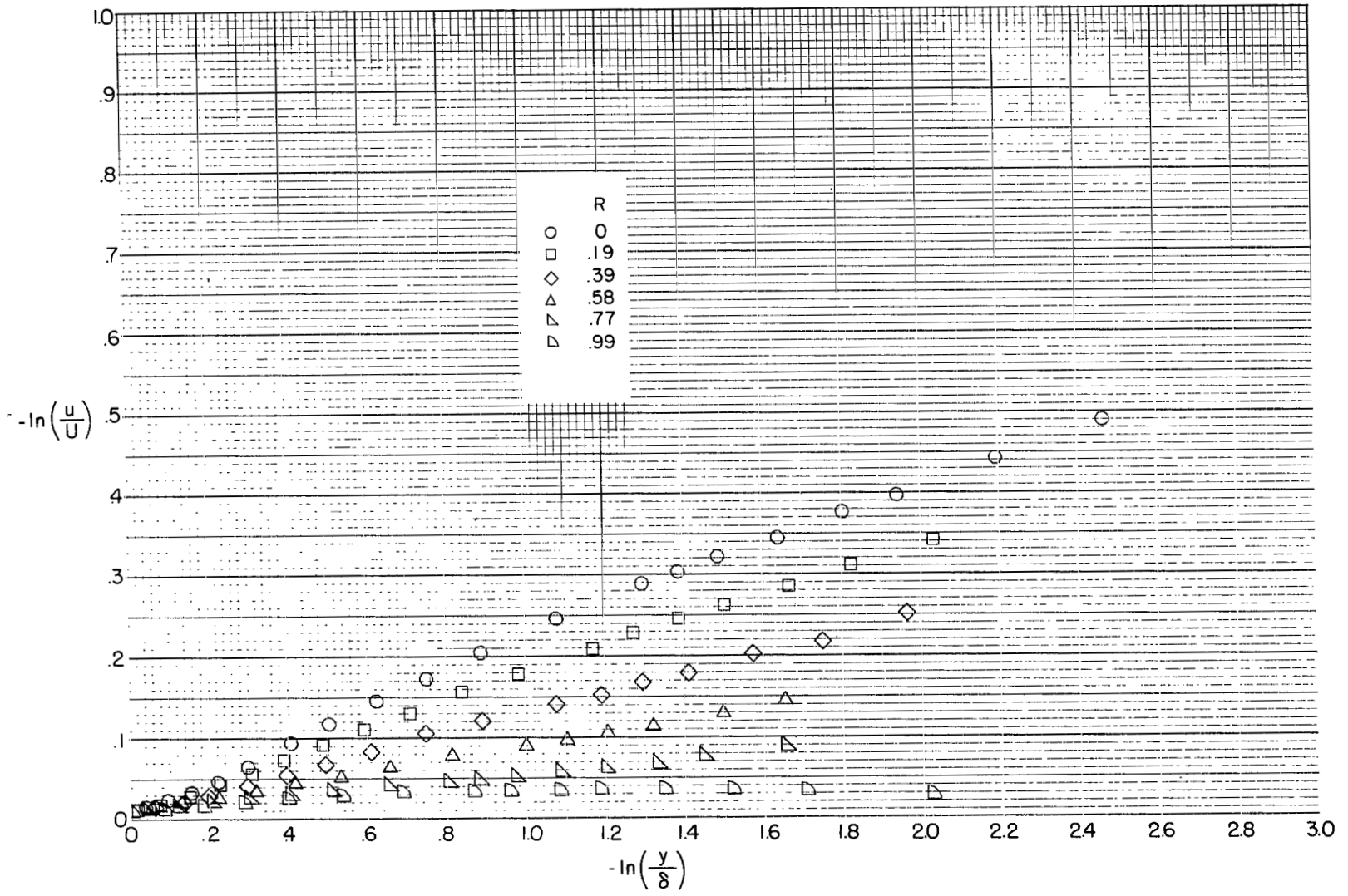

(b) x = 0.506 meter (1.66 feet).

Figure 6.- Continued.

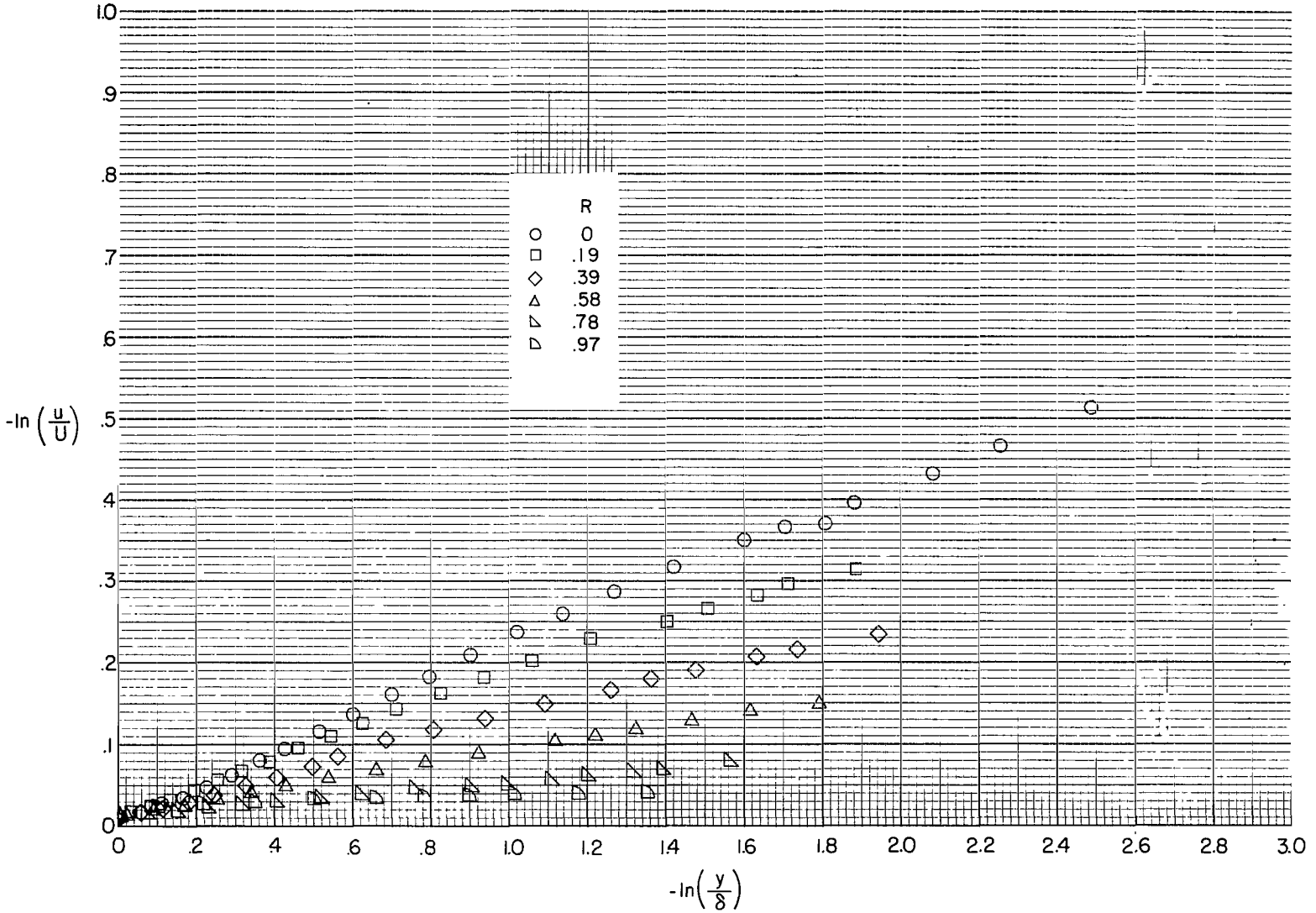

(c) x = 0.713 meter (2.34 feet).

Figure 6.- Continued.

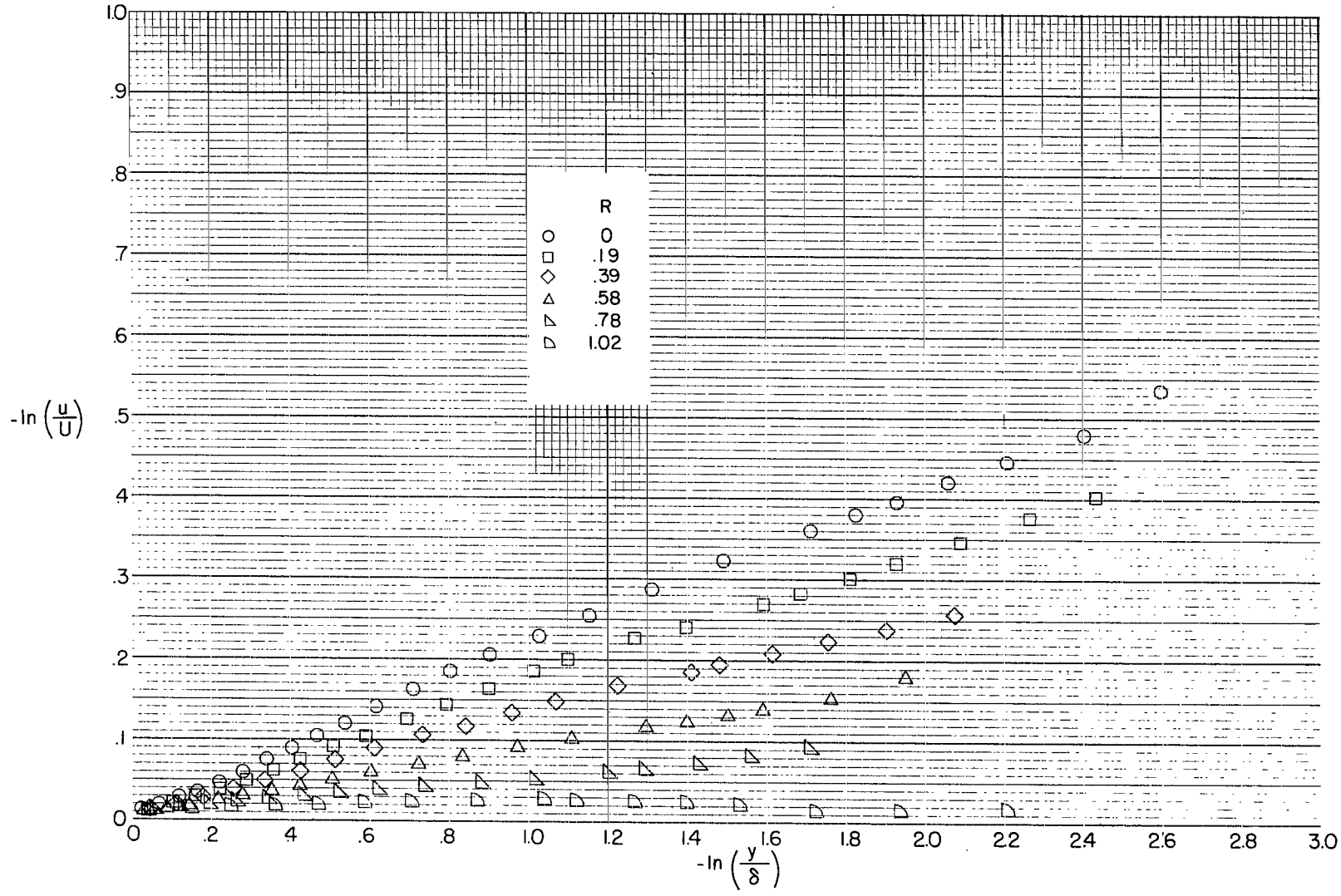

(d) x = 0.860 meter (2.82 feet).

Figure 6.- Continued.

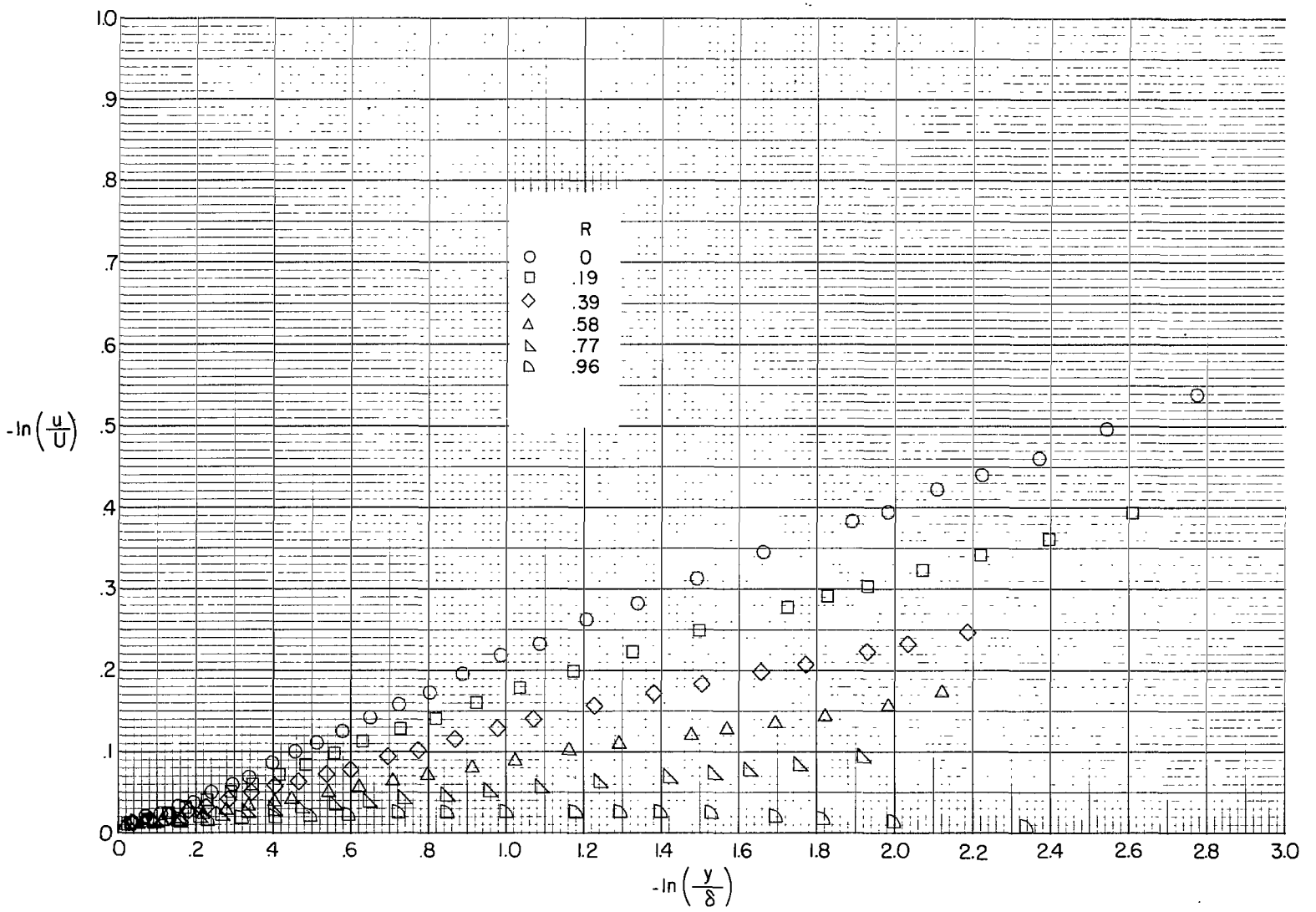

(e) x = 1.079 meters (3.54 feet).

Figure 6.- Concluded.

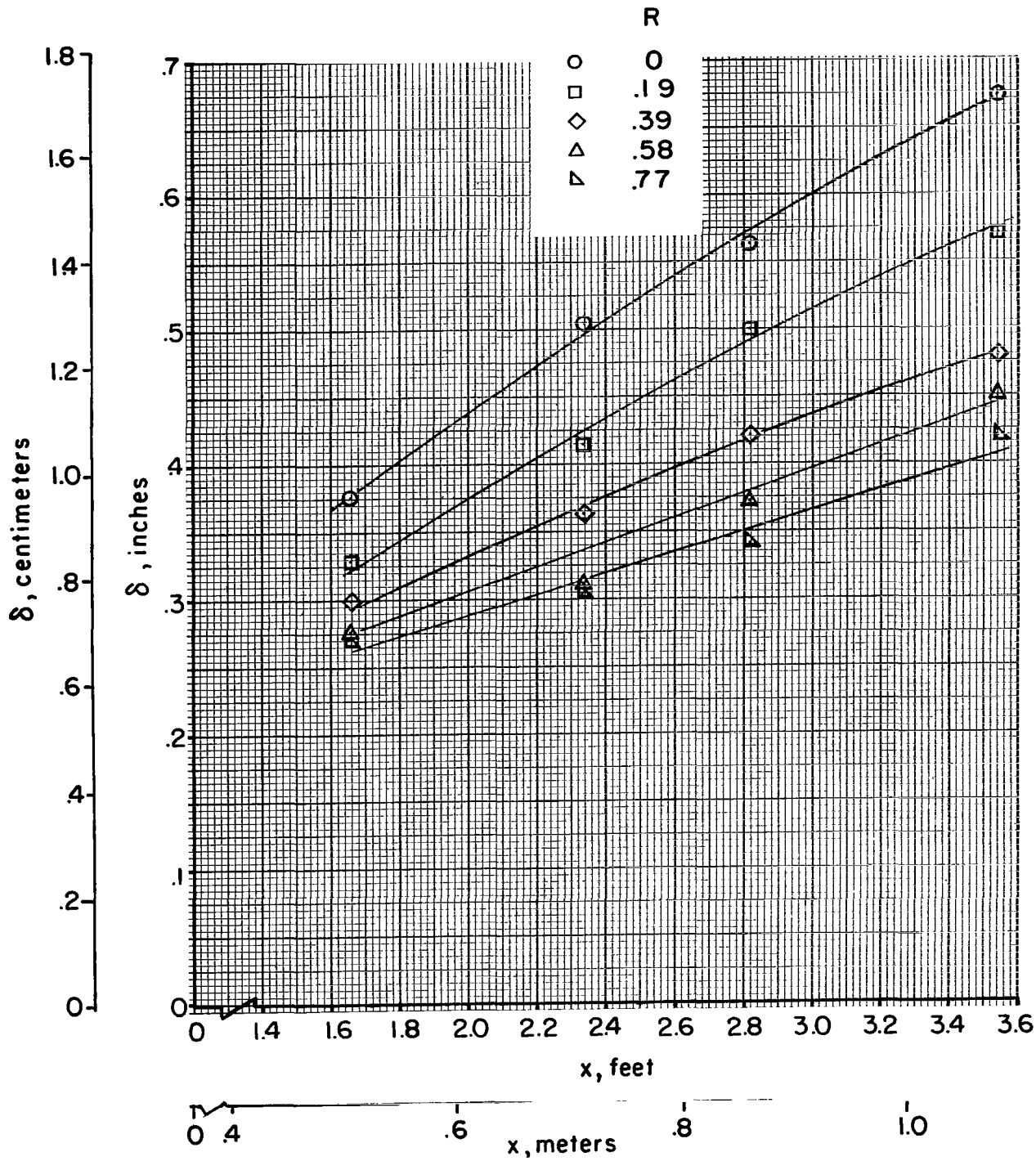

(a) Boundary-layer thickness.

Figure 7.- Experimentally determined integral parameter variation.

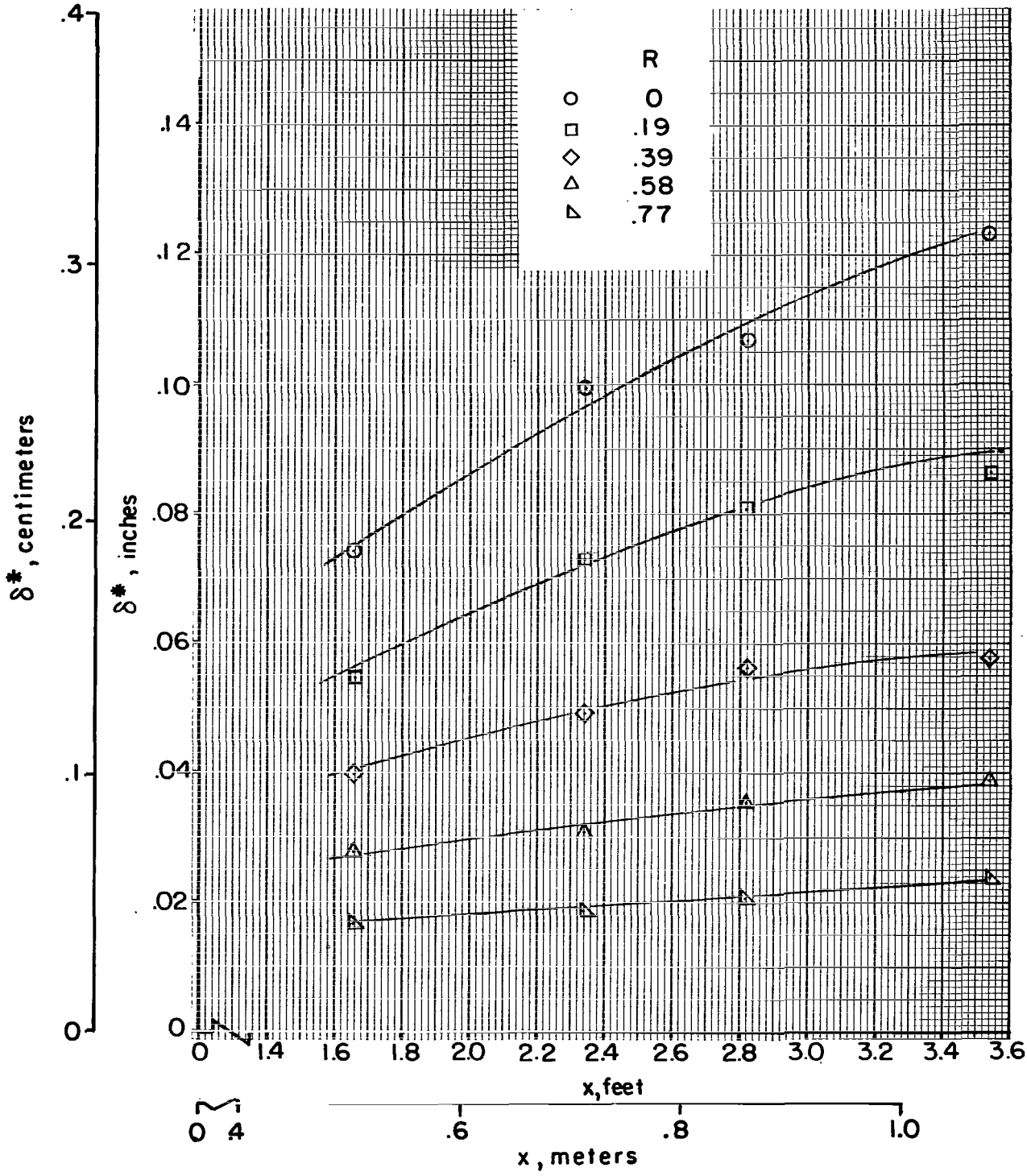

(b) Displacement thickness.

Figure 7.- Continued.

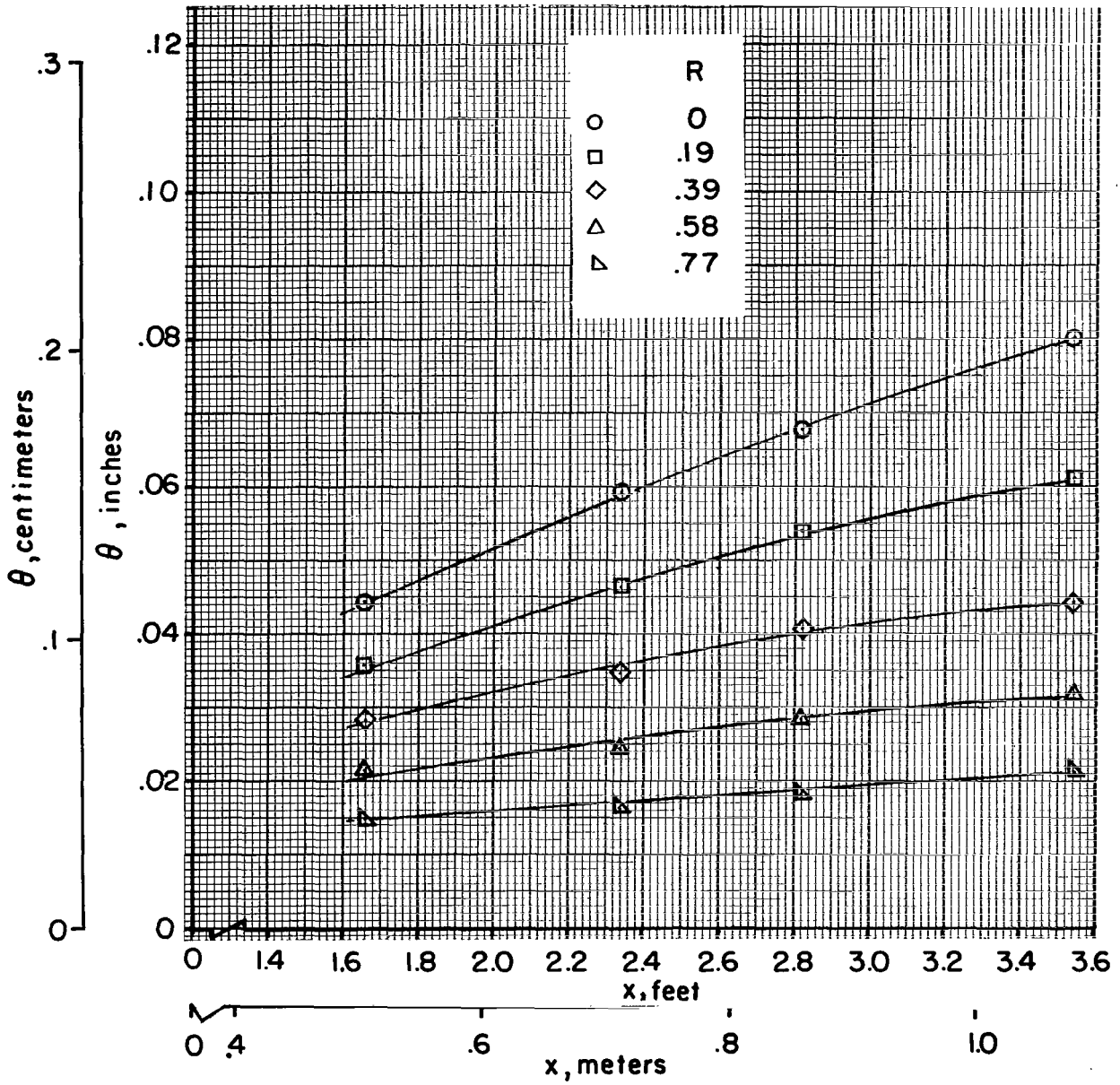

(c) Momentum thickness.

Figure 7.- Continued.

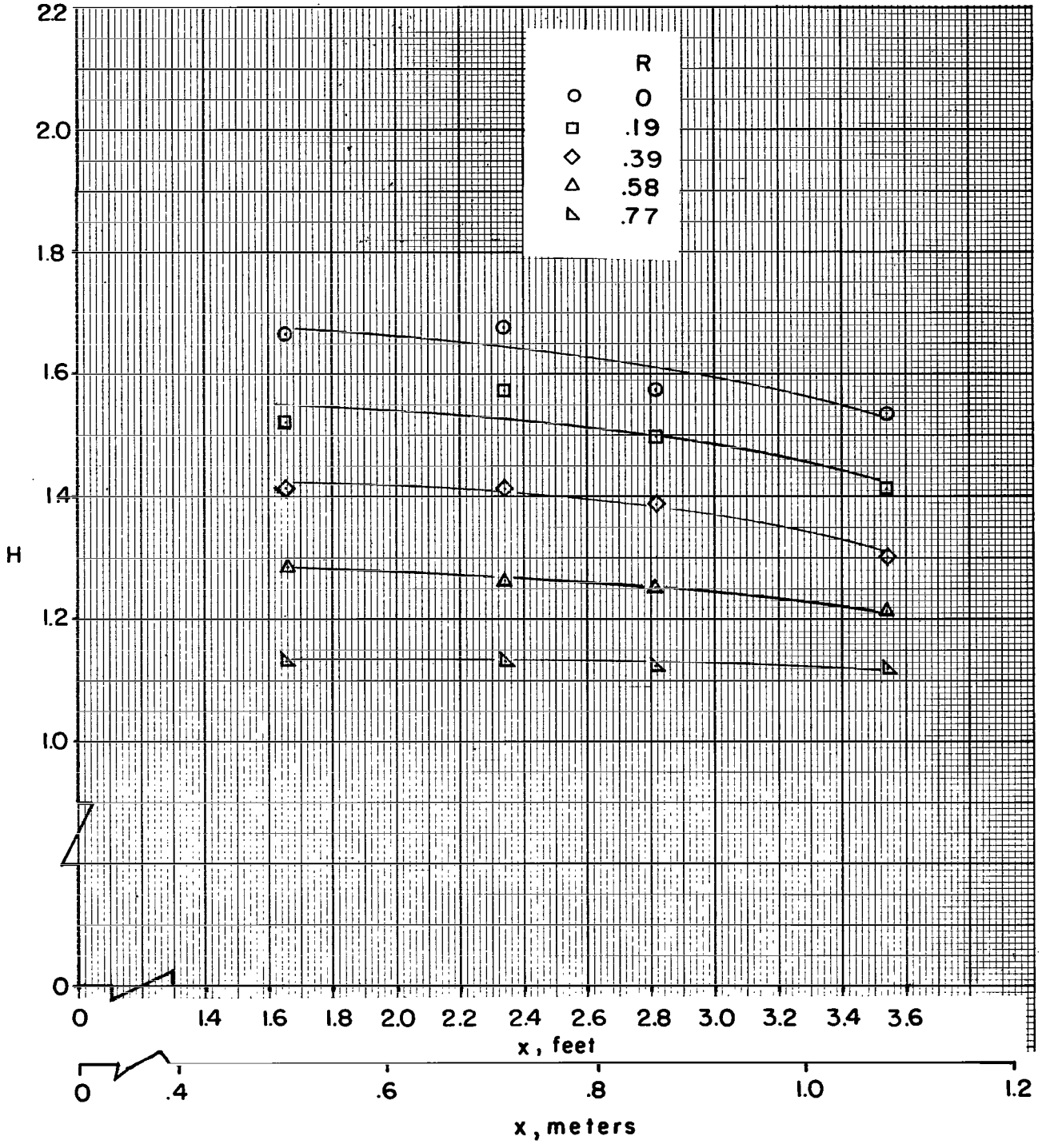

(d) Shape factor.

Figure 7.- Concluded.

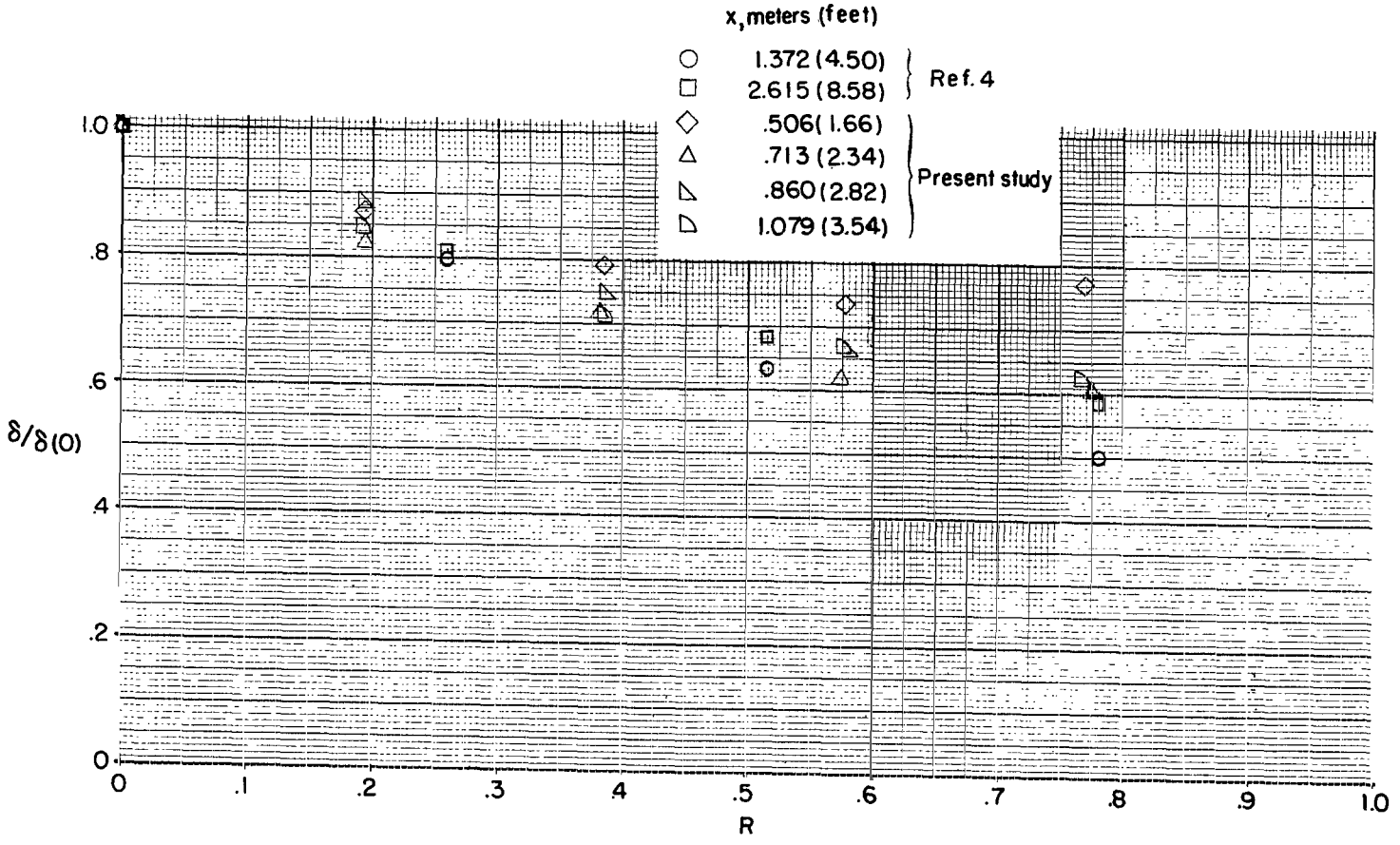

Figure 8.- Experimentally determined variation of boundary-layer thickness with belt speed ratio.

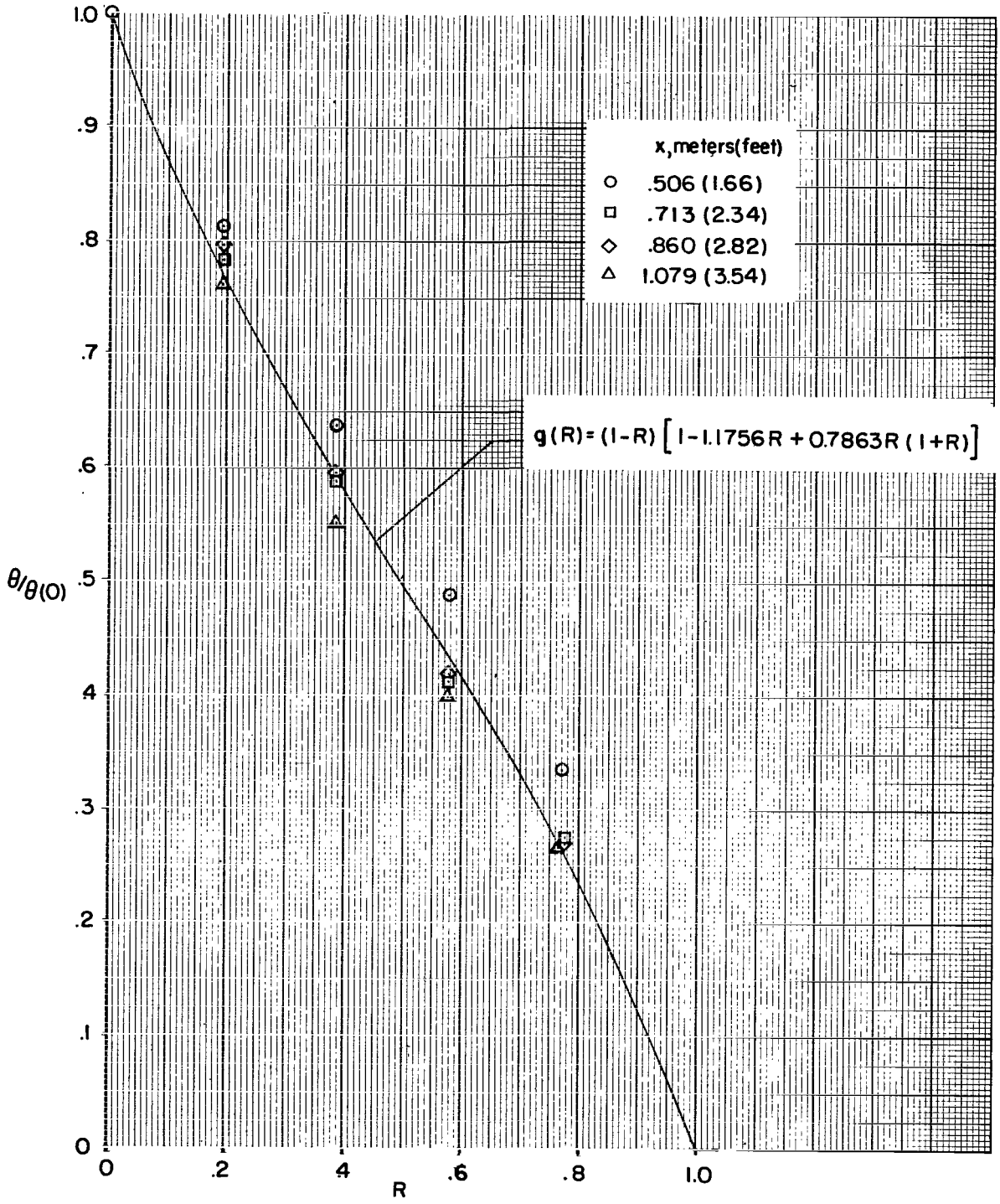

Figure 9.- Comparison of g(R) with experimental $\theta/\theta(0)$ data.

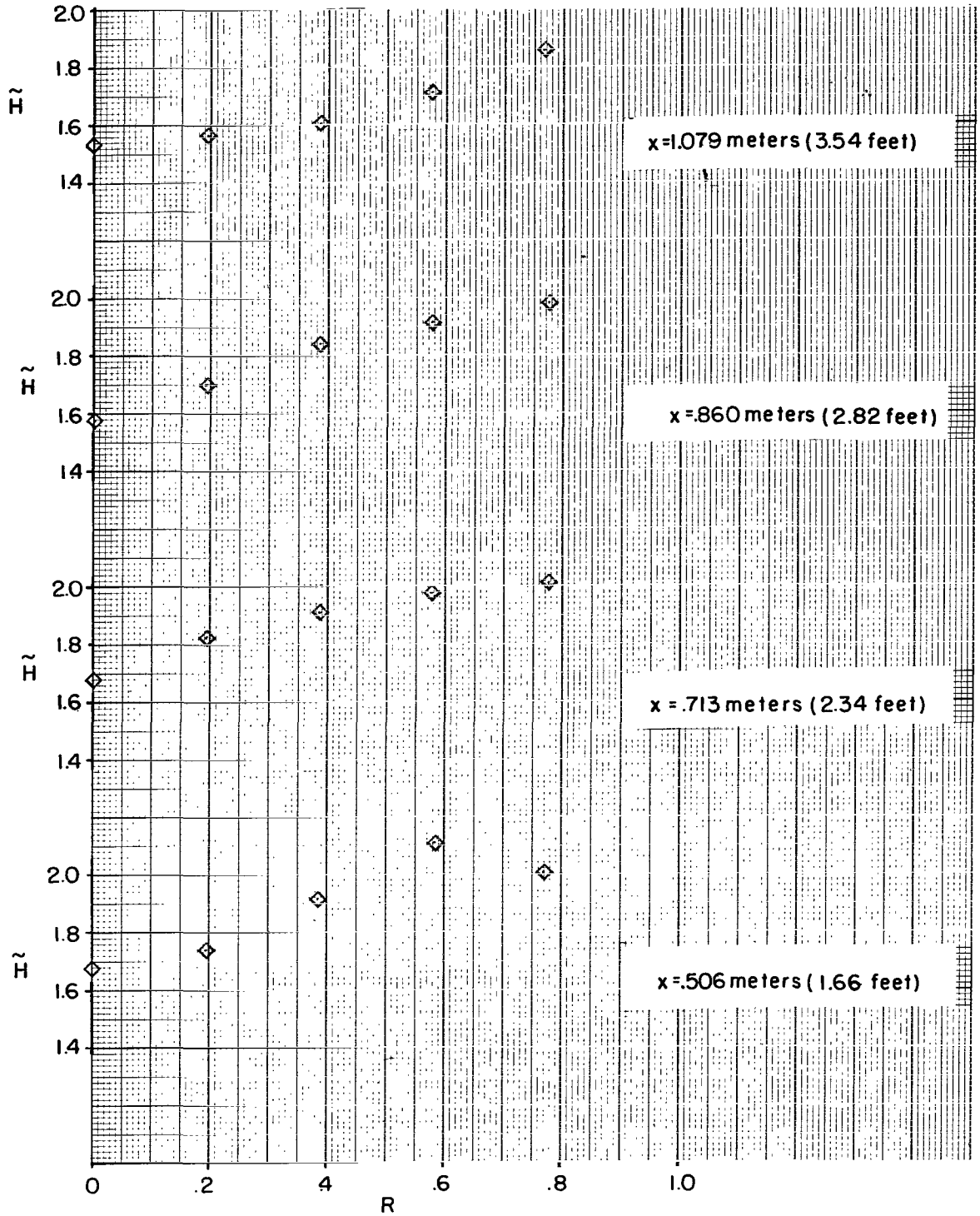

Figure 10.- Experimentally determined variation of relative shape factor with belt speed ratio.

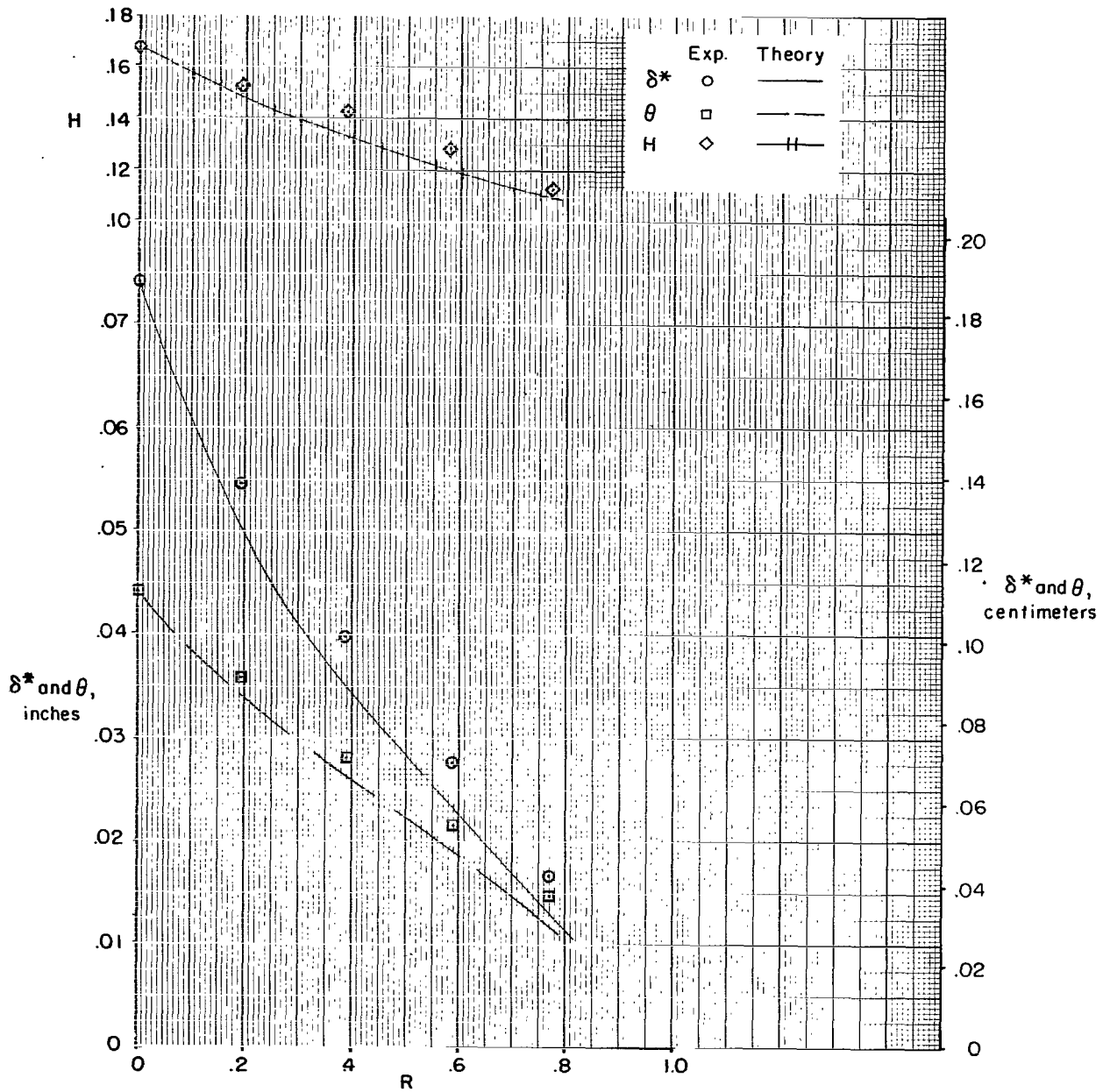

(a) x = 0.506 meter (1.66 feet).

Figure 11.- Comparison of experimental and calculated values of the integral parameters.

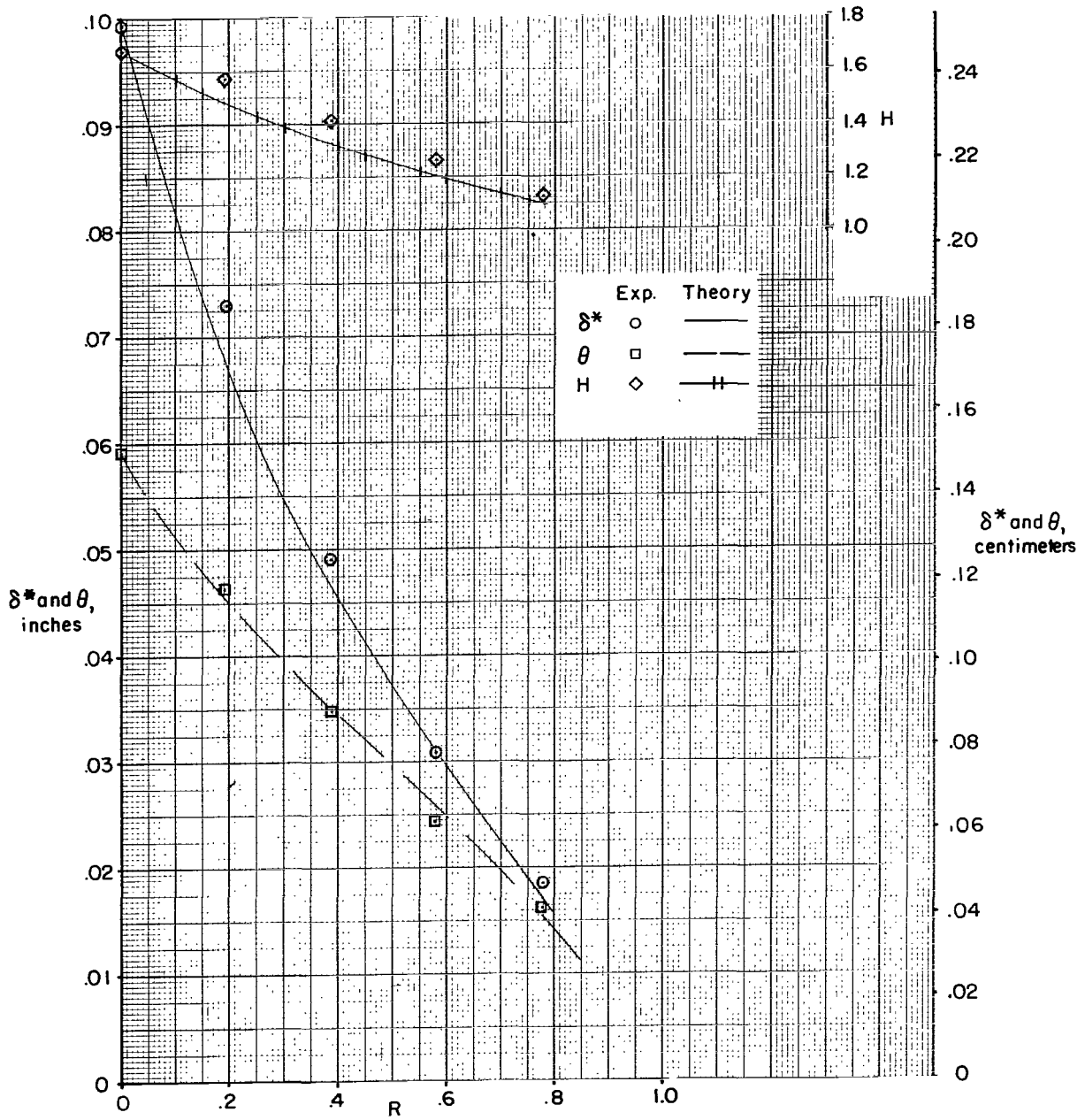

(b) x = 0.713 meter (2.34 feet).

Figure 11.- Continued.

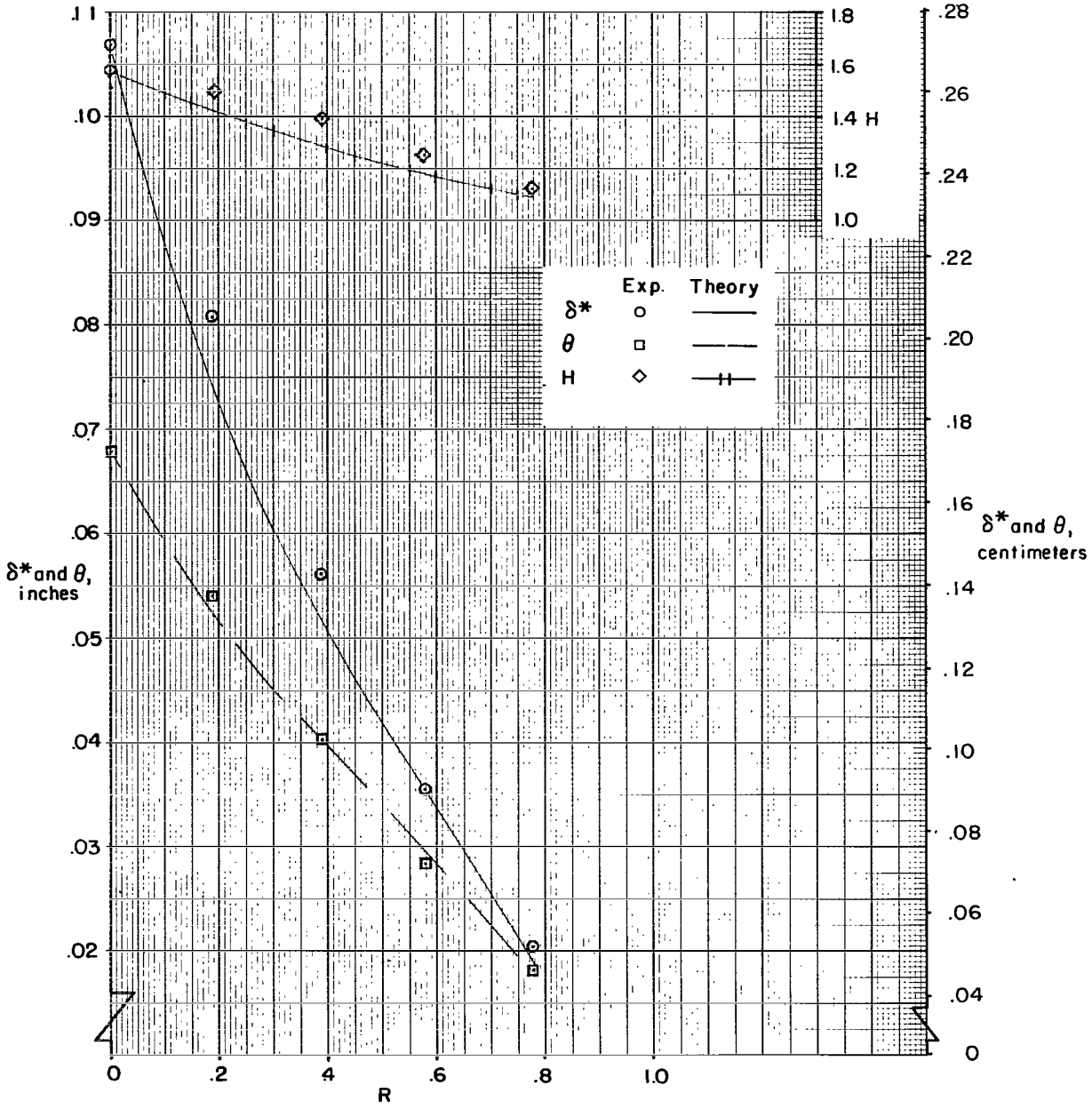

(c) x = 0.860 meter (2.82 feet).

Figure 11.- Continued.

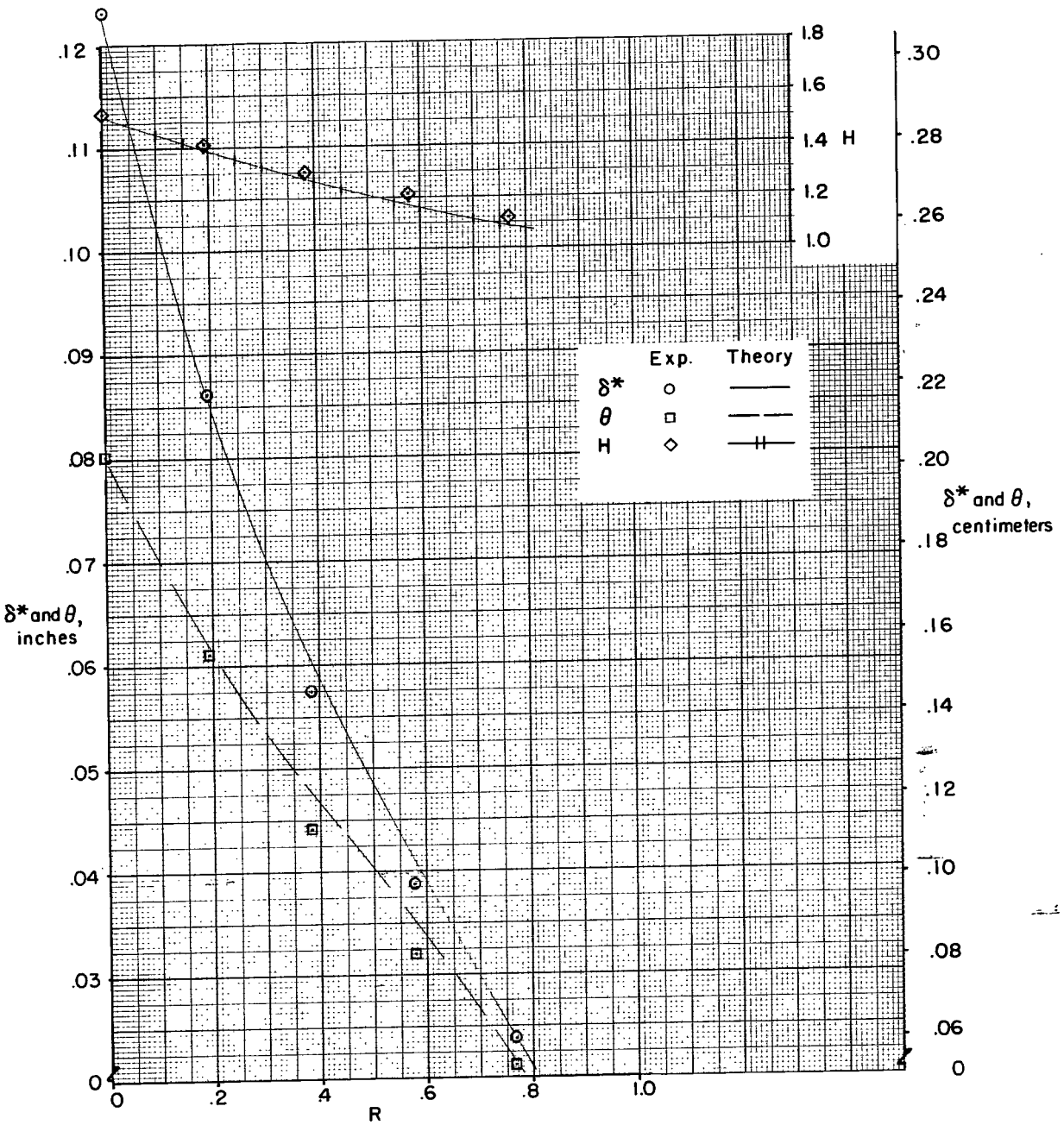

(d) x = 1.079 meters (3.54 feet).

Figure 11.- Concluded.

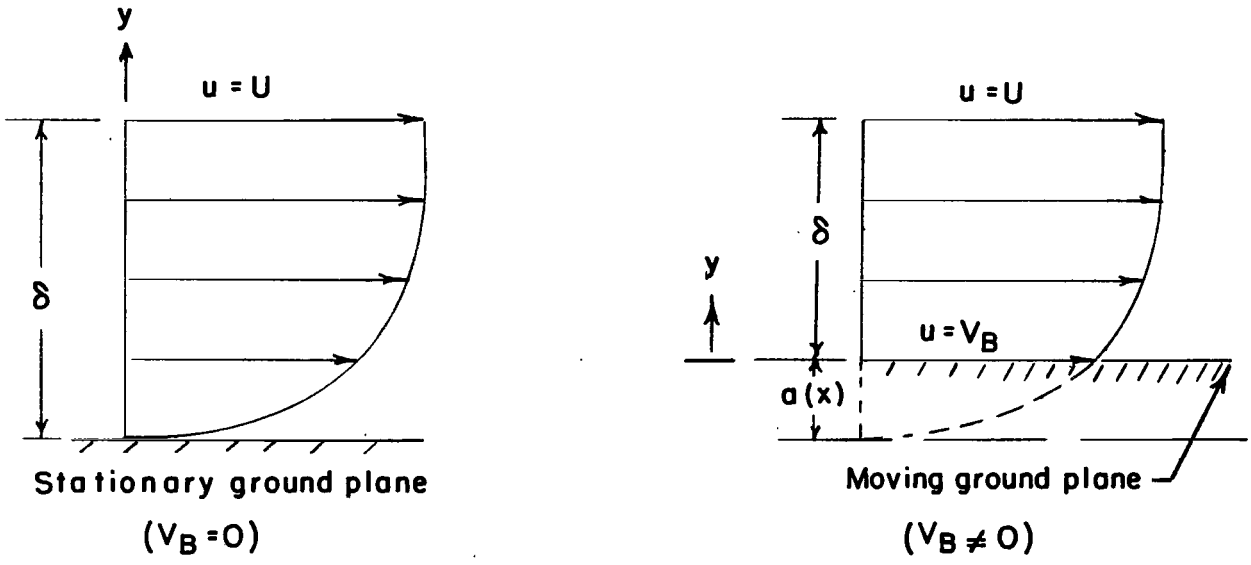

Figure 12.- Sketch of modified power law velocity profile.

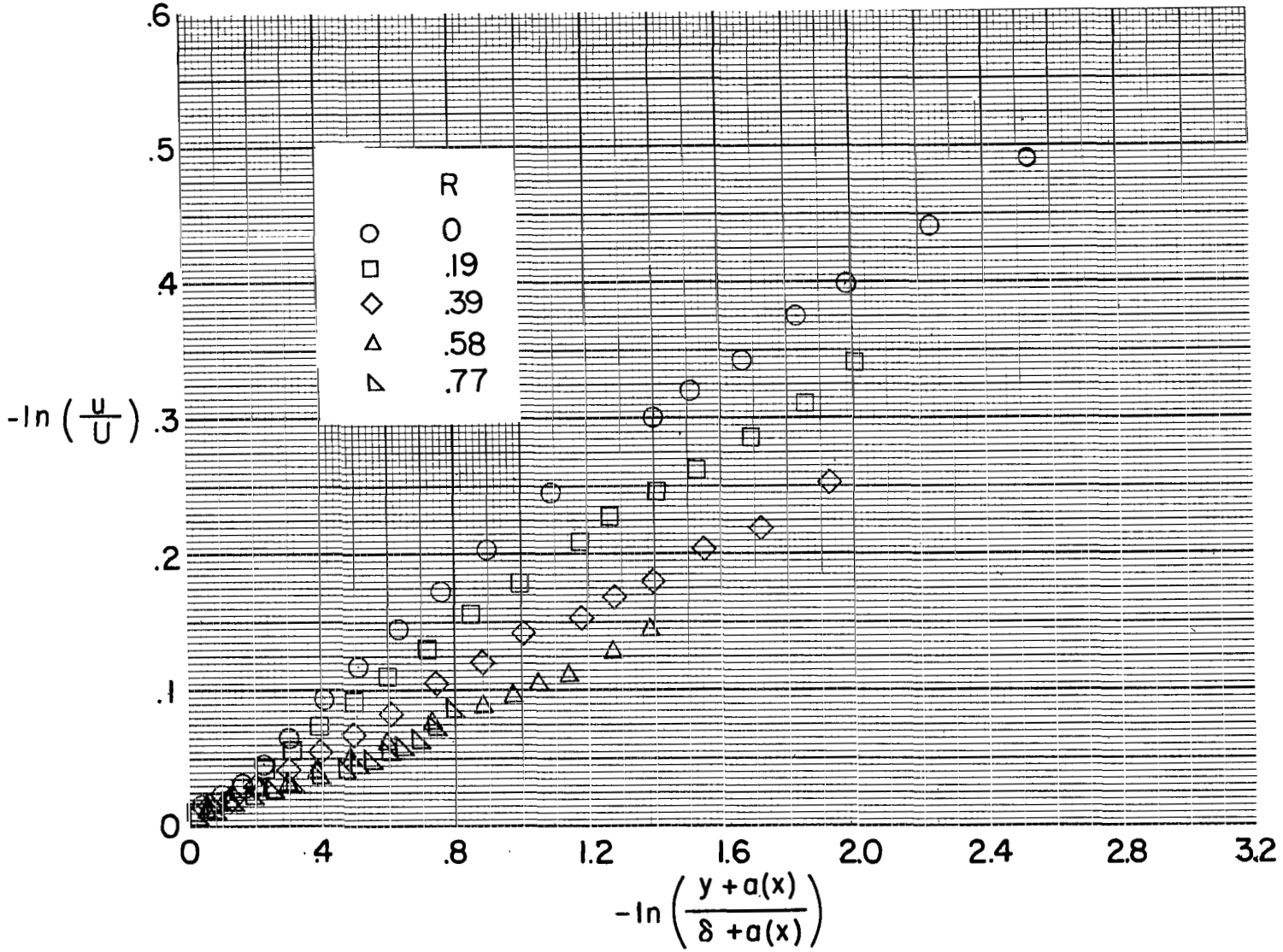

(a) x = 0.506 meter (1.66 feet).

Figure 13.- Modified power law velocity profiles.

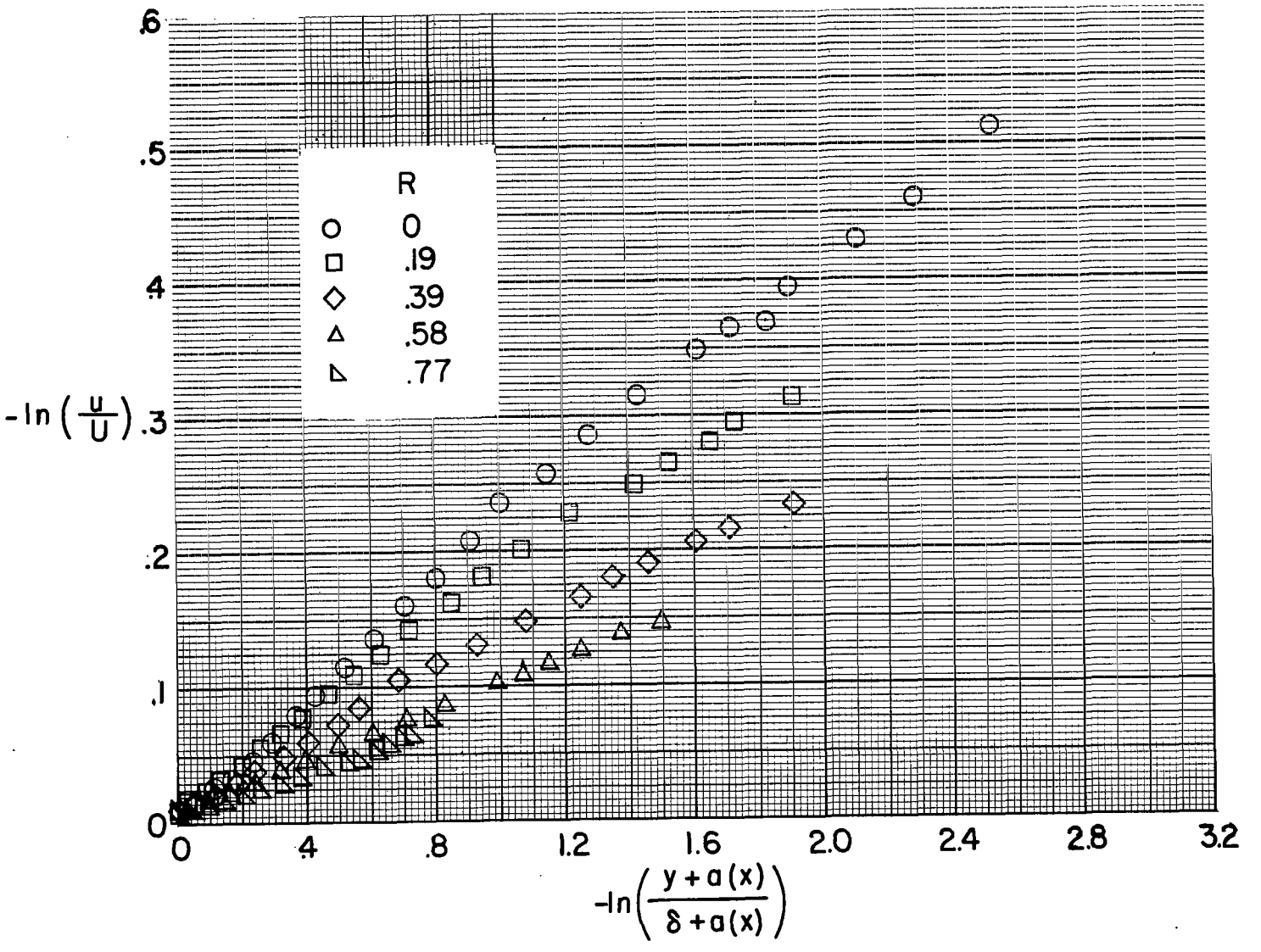

(b) x = 0.713 meter (2.34 feet).

Figure 13.- Continued.

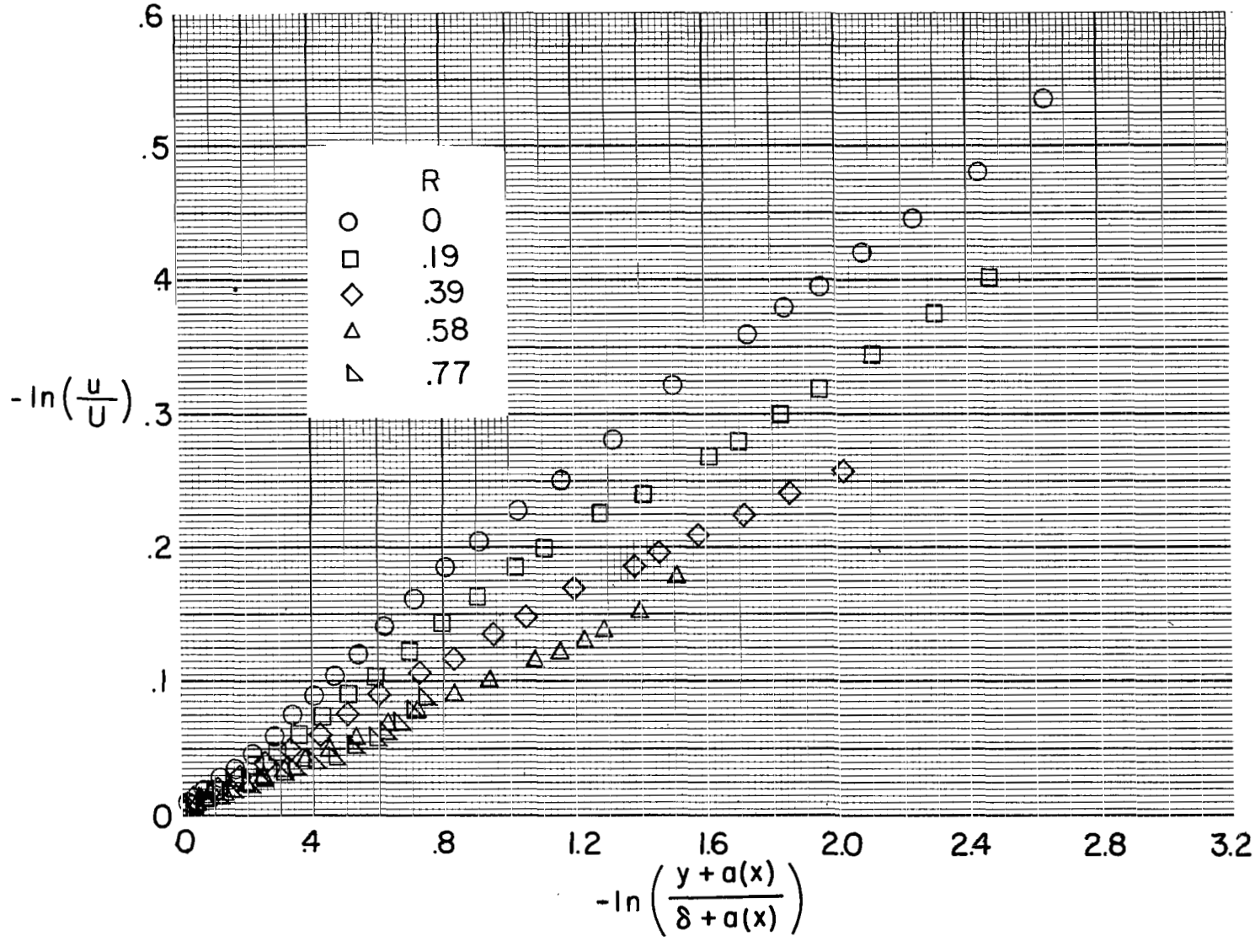

(c) x = 0.860 meter (2.82 feet).

Figure 13.- Continued.

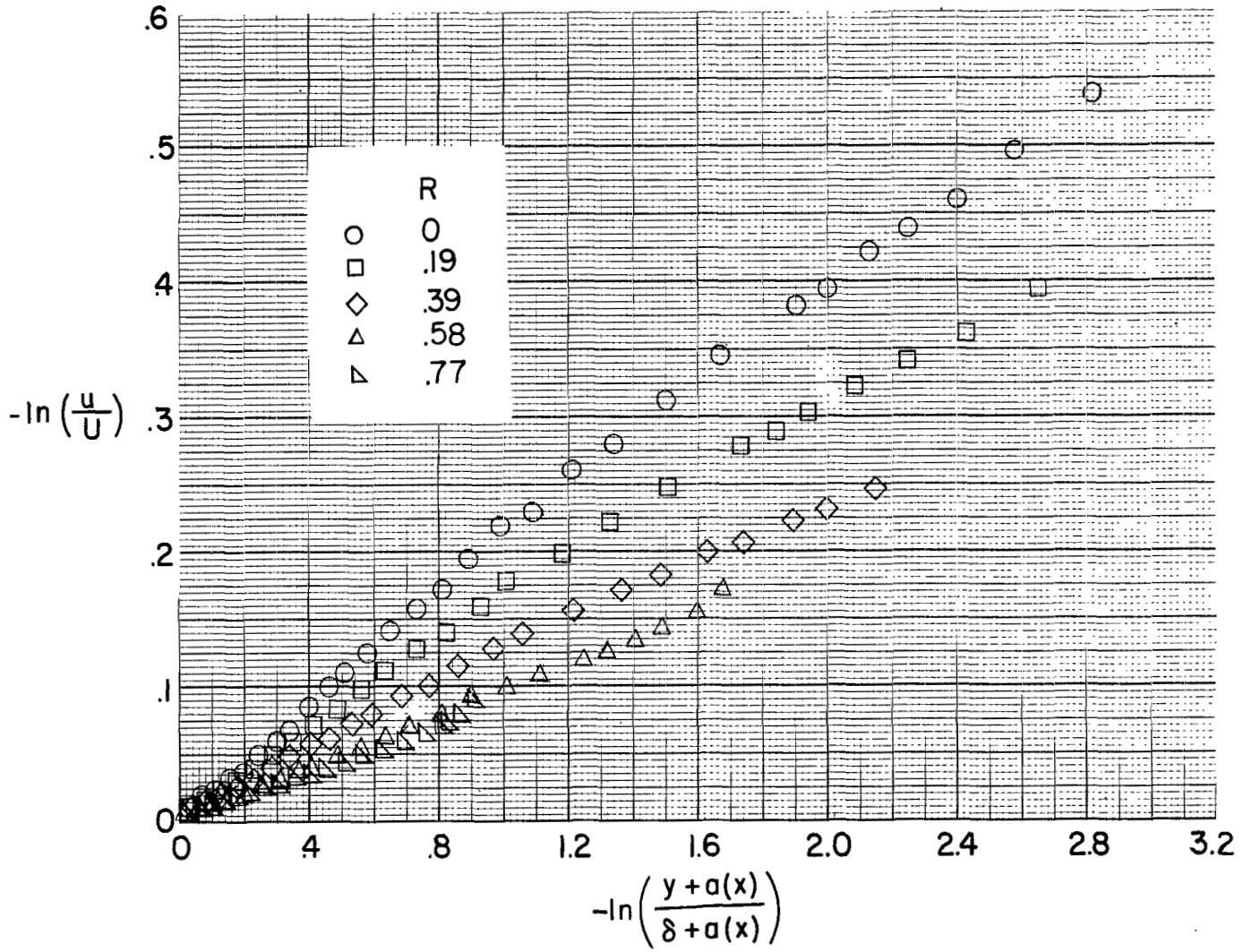

(d) x = 1.079 meters (3.54 feet).

Figure 13.- Concluded.

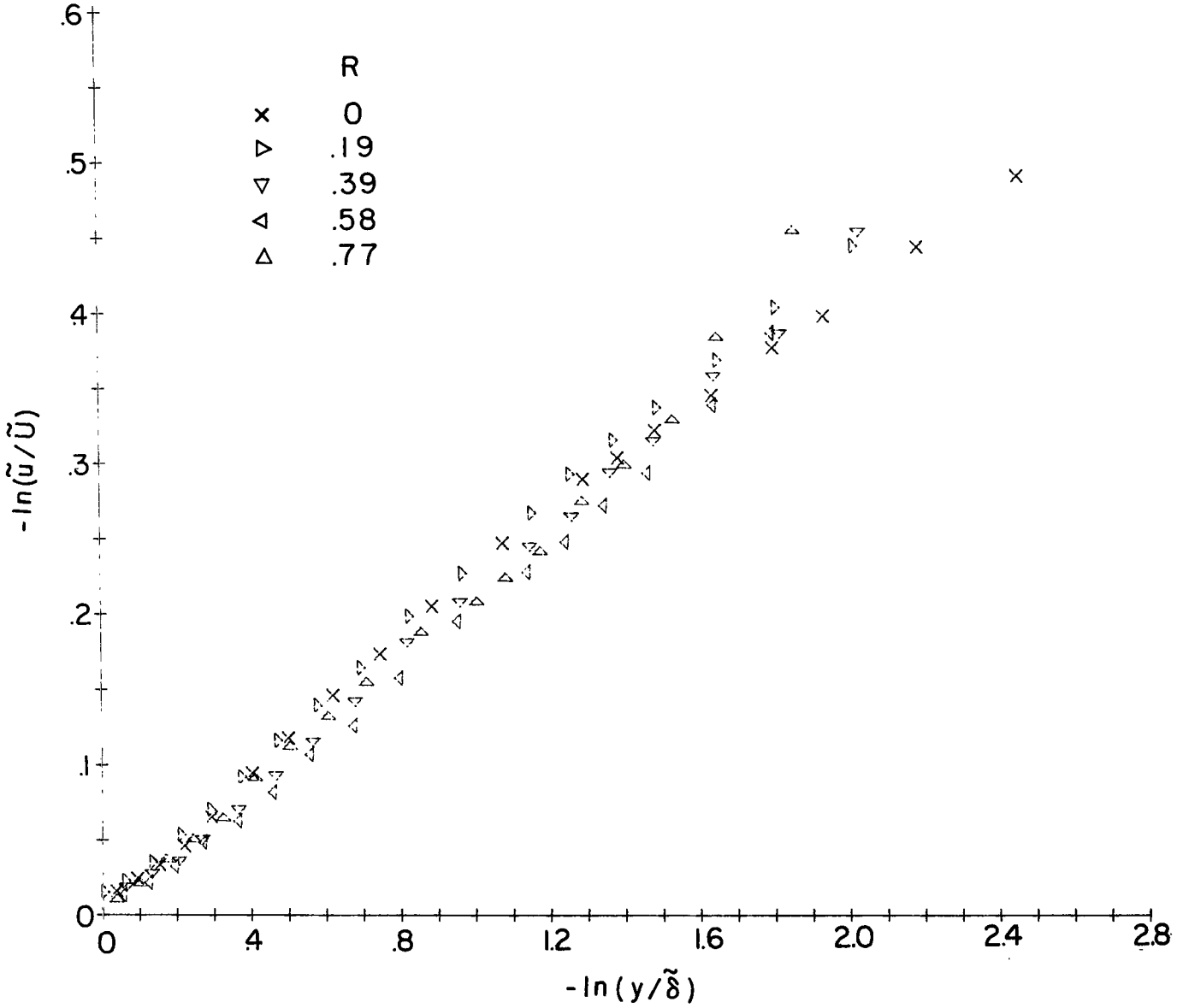

(a) x = 0.506 meter (1.66 feet).

Figure 14.- Relative power law velocity profiles.

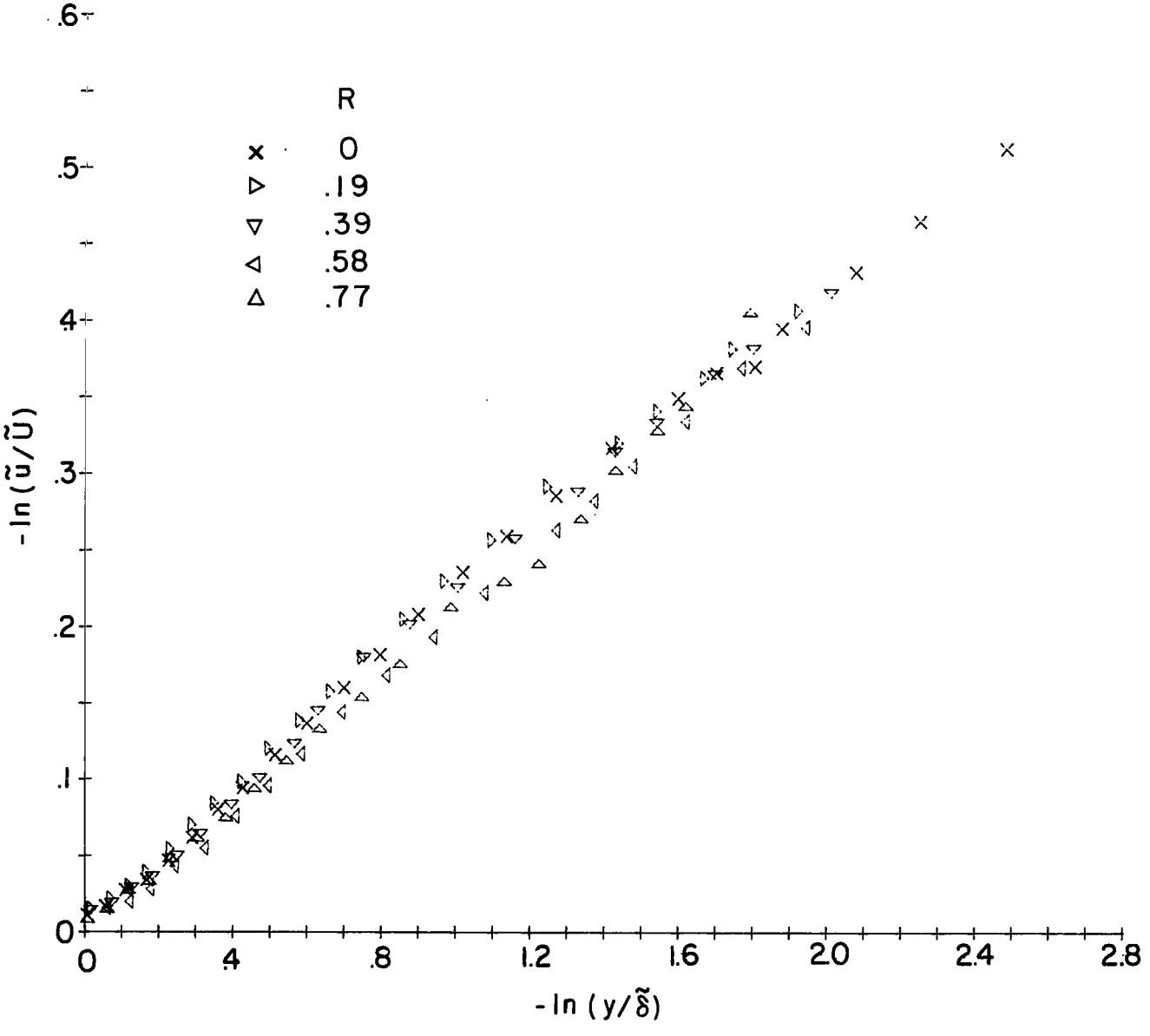

(b) x = 0.713 meter (2.34 feet).

Figure 14.- Continued.

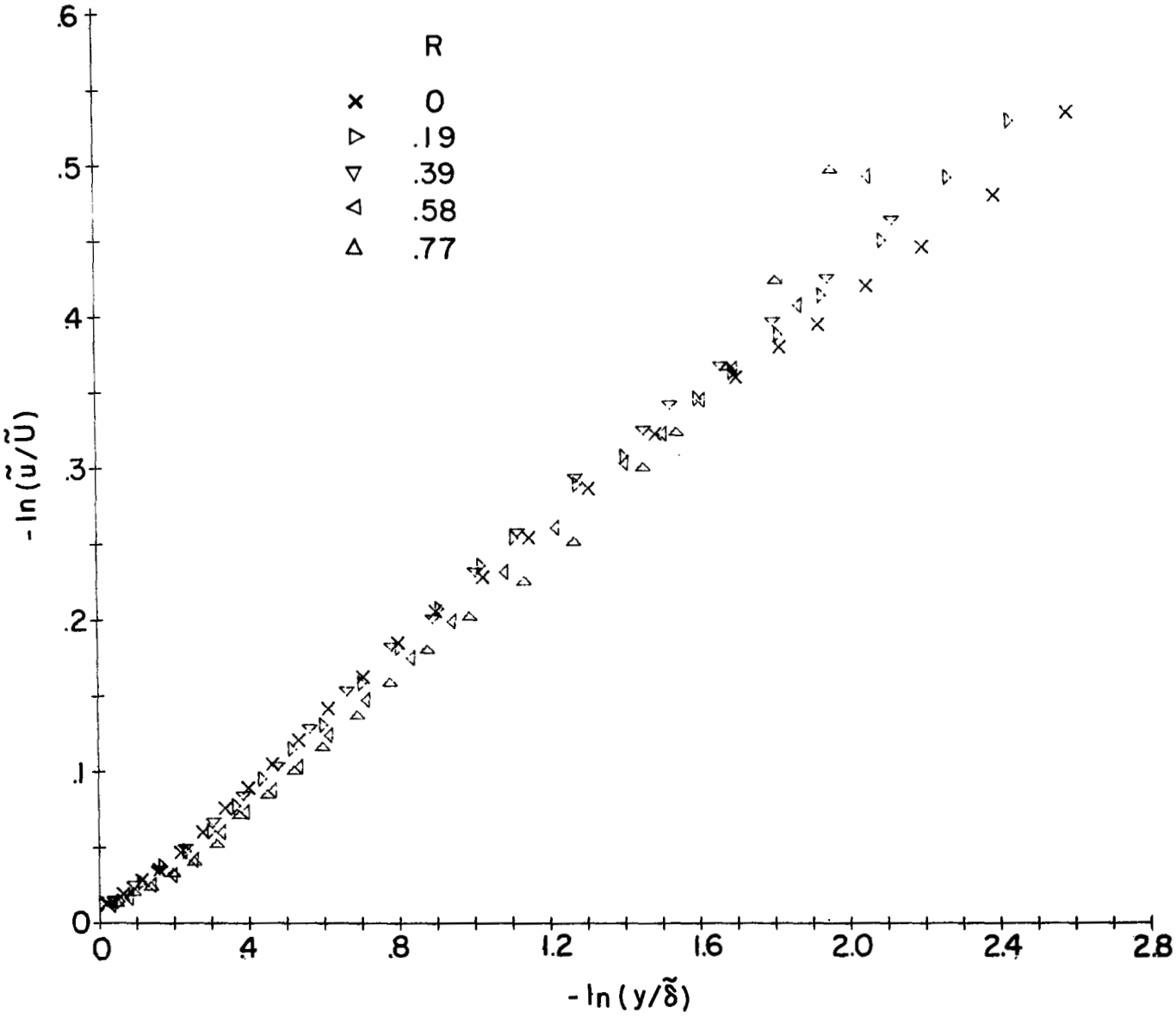

(c) x = 0.860 meter (2.82 feet).

Figure 14.- Continued.

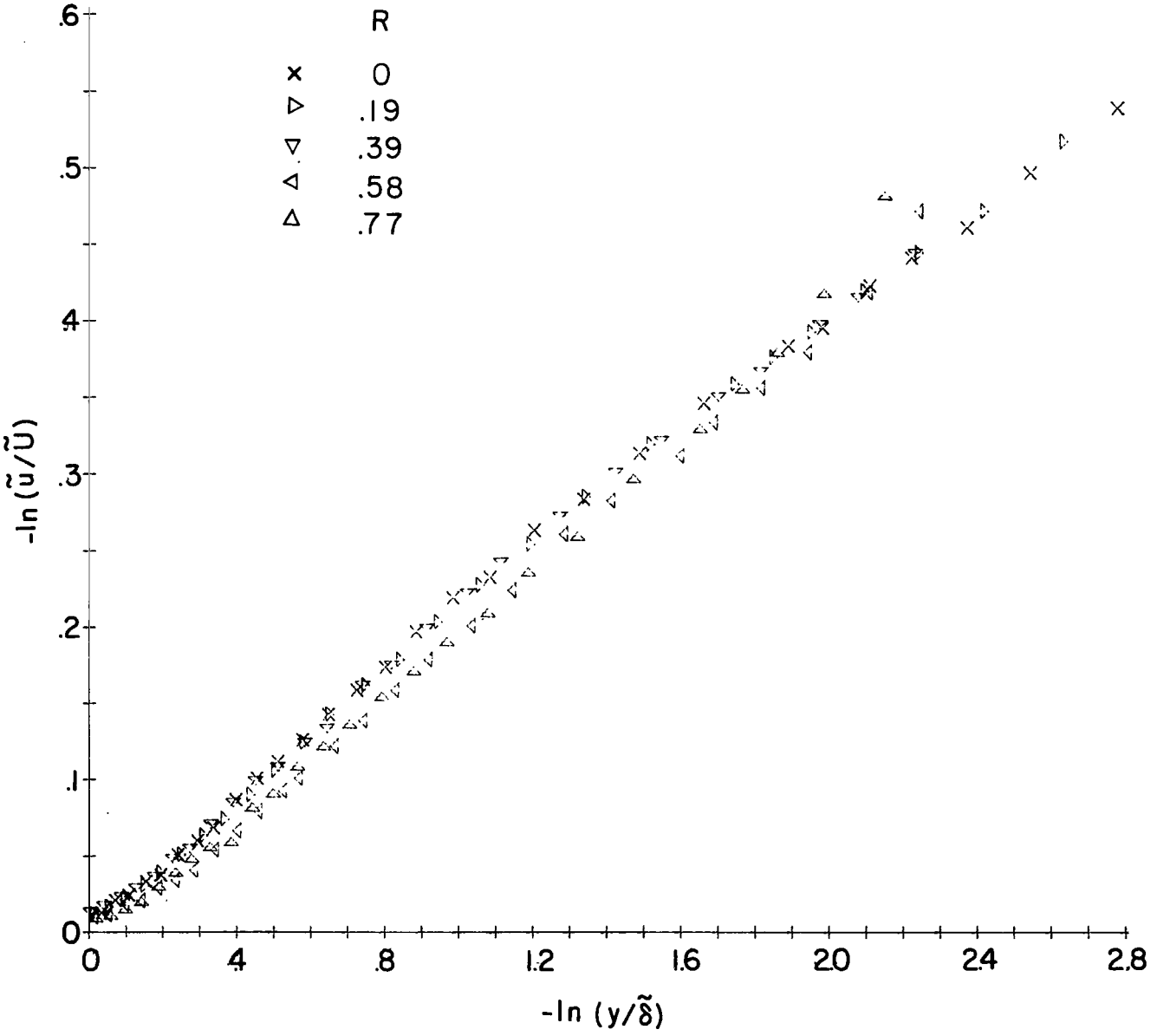

(d) x = 1.079 meters (3.54 feet).

Figure 14.- Continued.

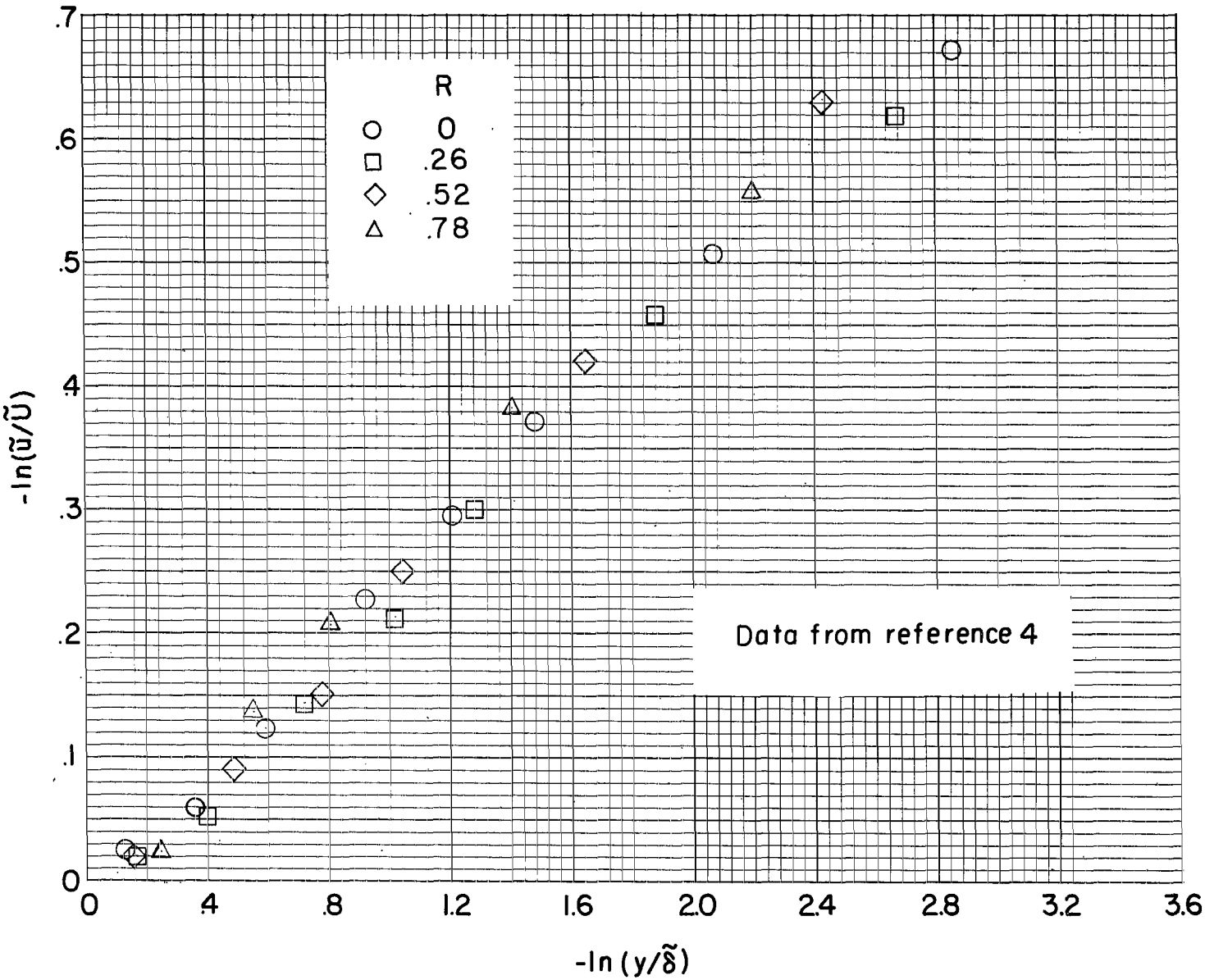

(e) x = 1.372 meters (4.50 feet).

Figure 14.- Continued.

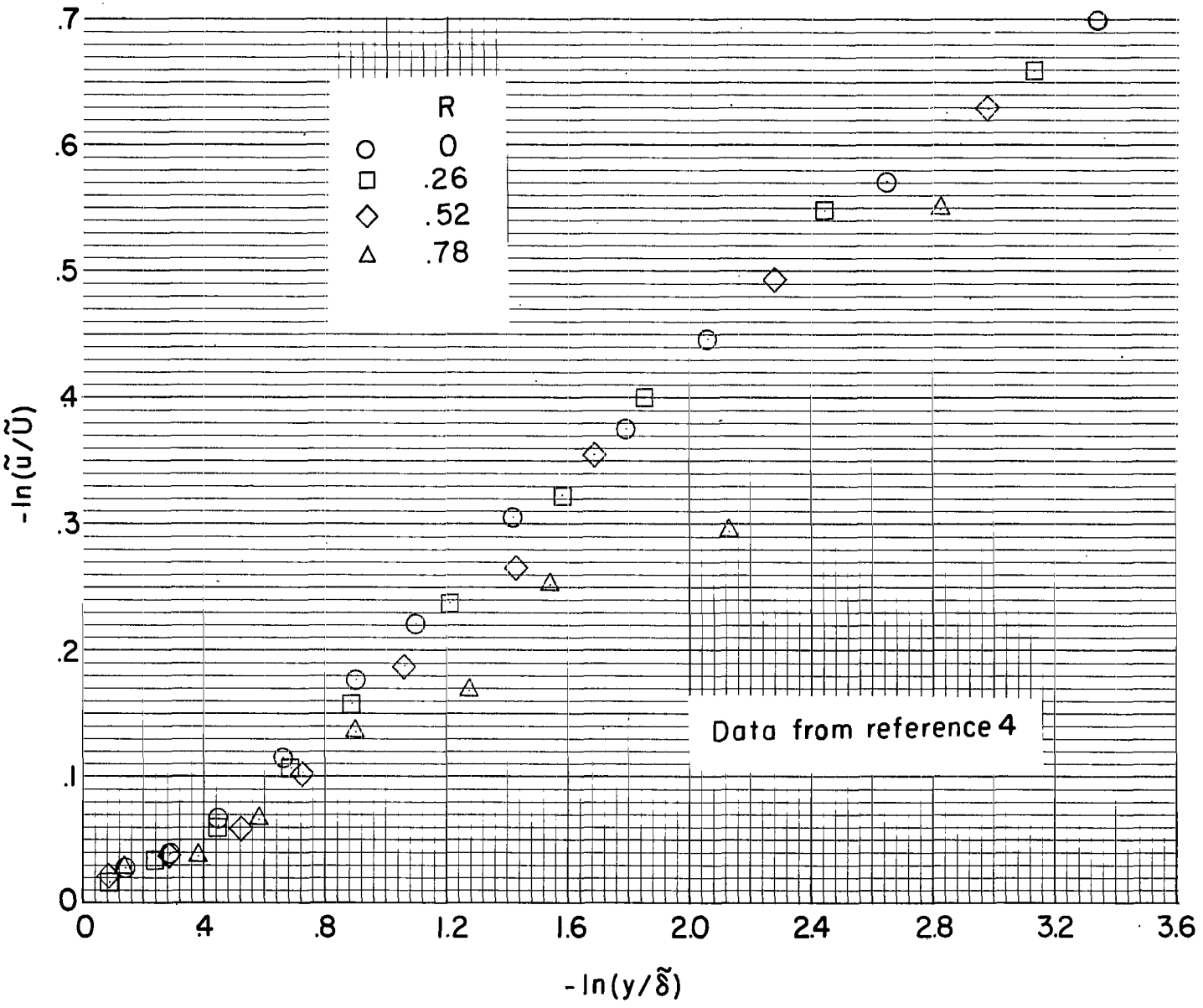

(f) x = 2.615 meters (8.58 feet).

Figure 14.- Concluded.

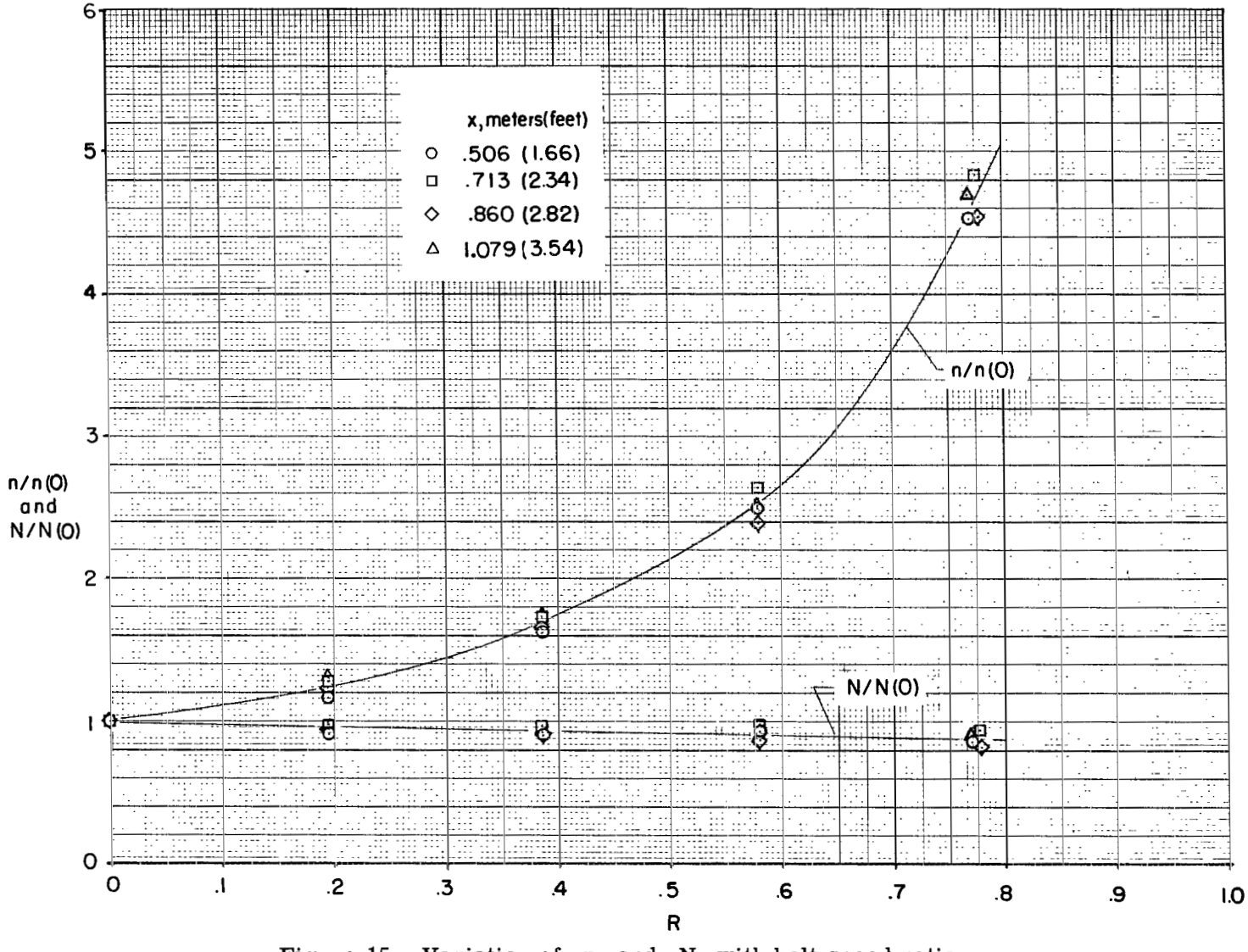

Figure 15.- Variation of n and N with belt speed ratio.

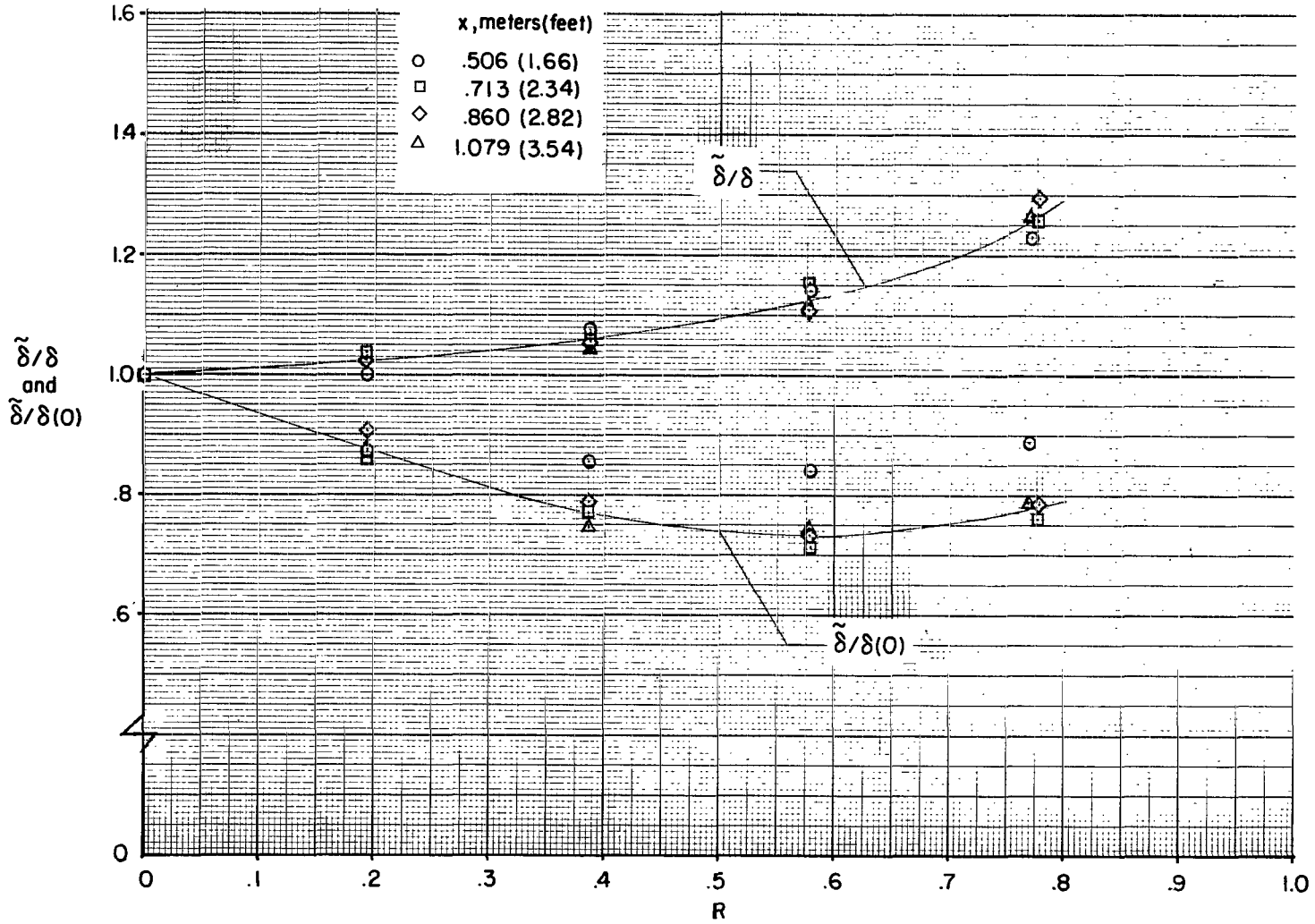

Figure 16.- Variation of boundary-layer thickness and relative boundary-layer thickness with belt speed ratio.

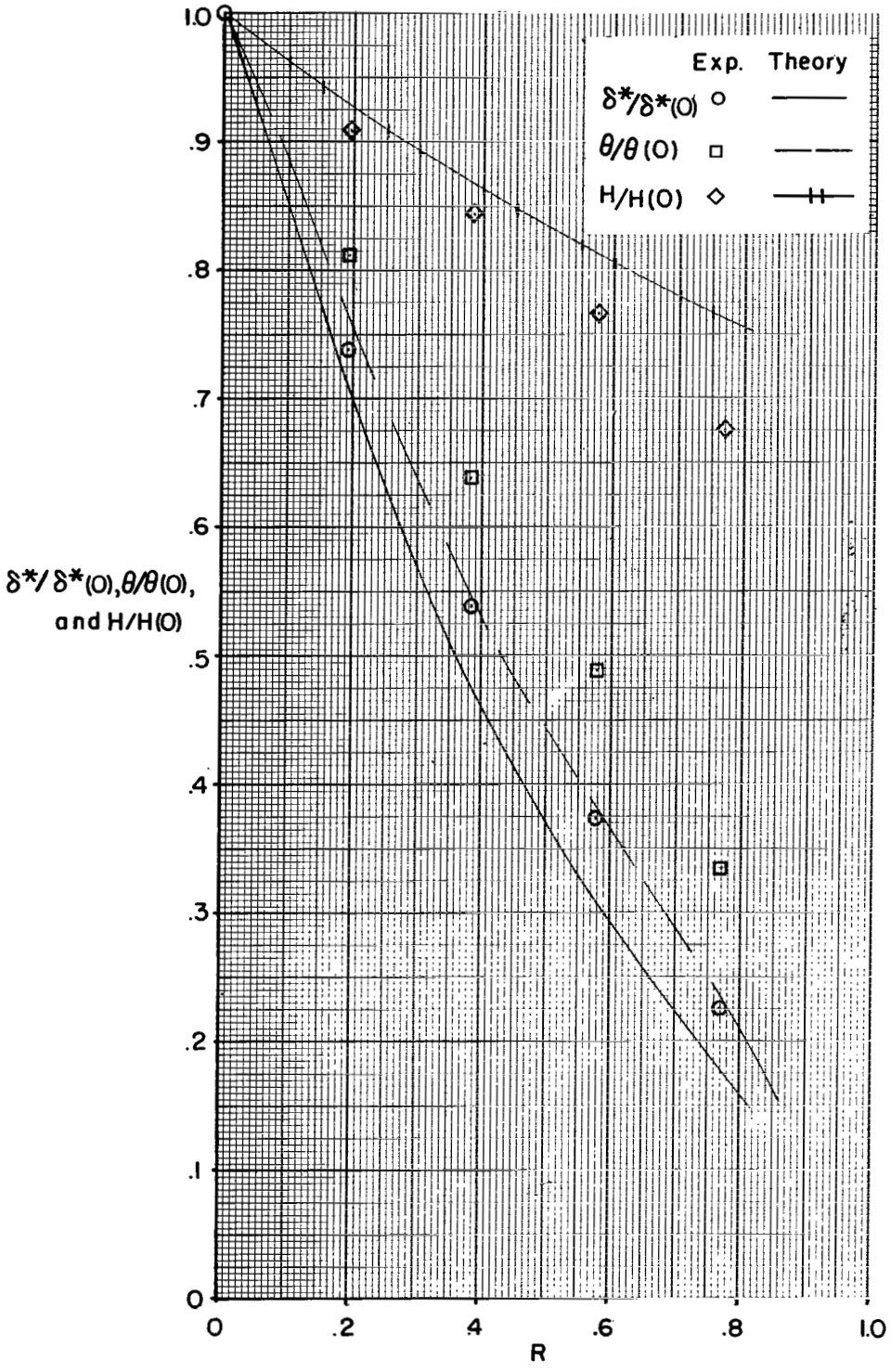

(a) x = 0.506 meter (1.66 feet).

Figure 17.- Comparison of experimental and calculated values of integral parameters.

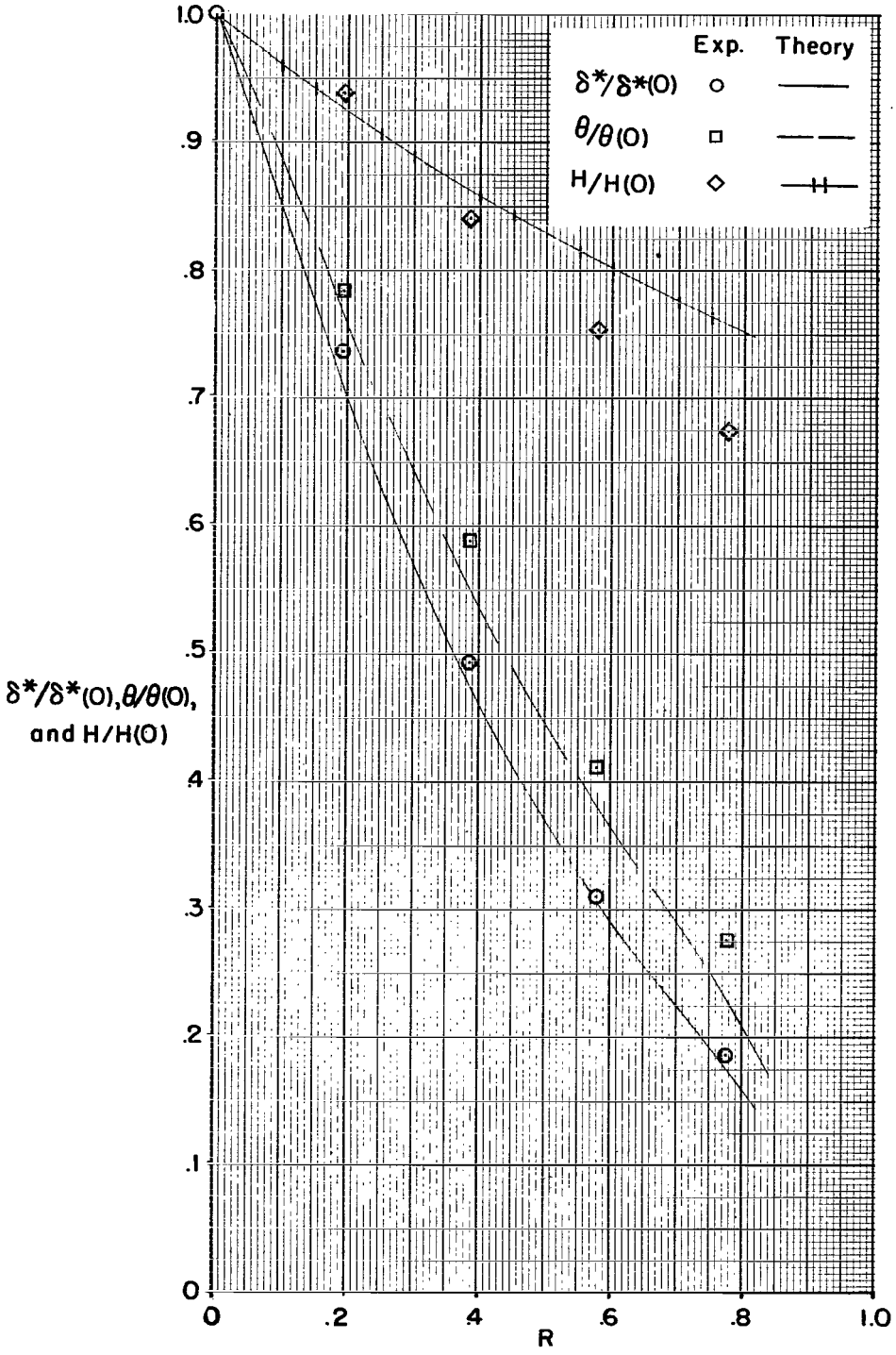

(b) x = 0.713 meter (2.34 feet).

Figure 17.- Continued.

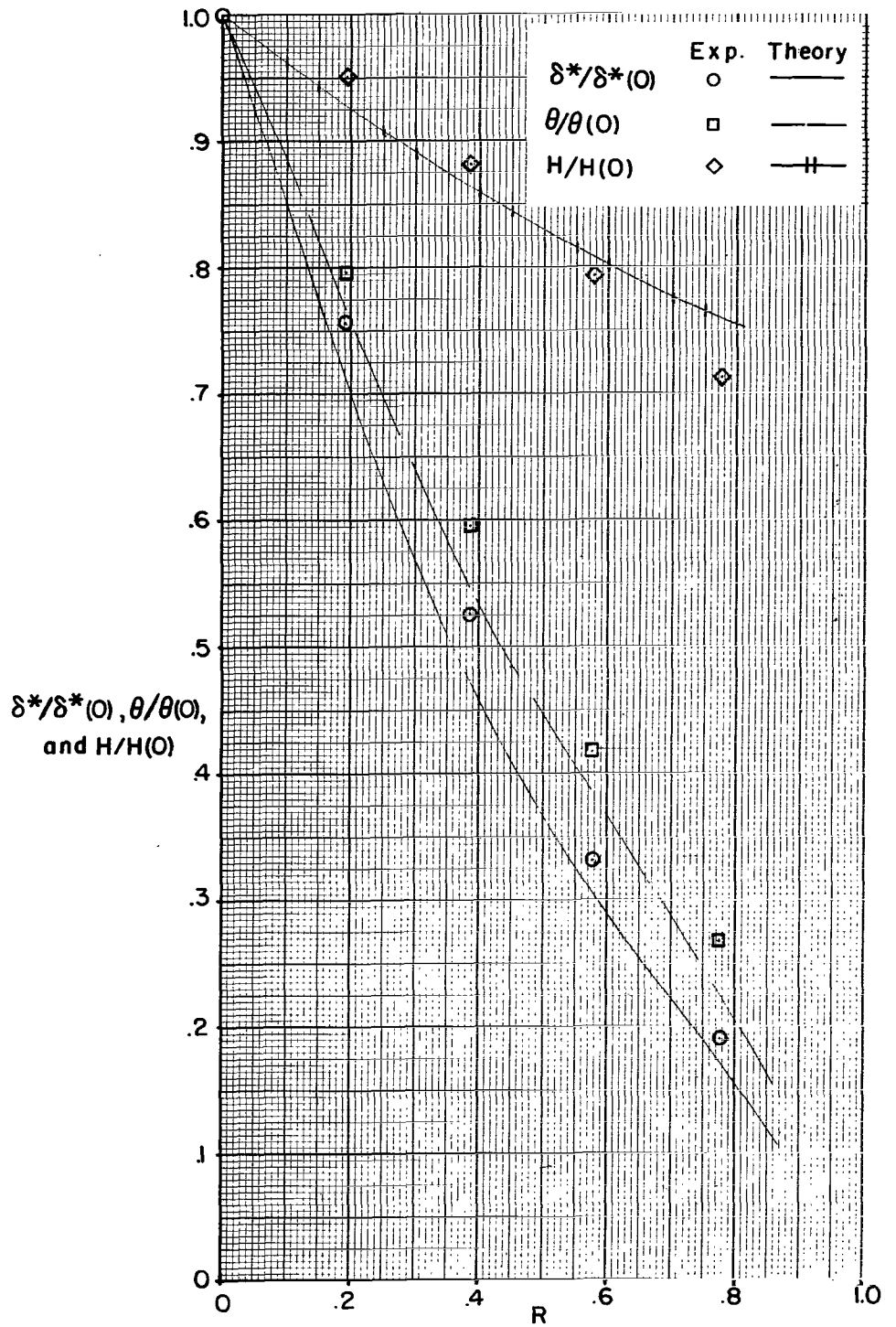

(c) x = 0.860 meter (2.82 feet).

Figure 17.- Continued.

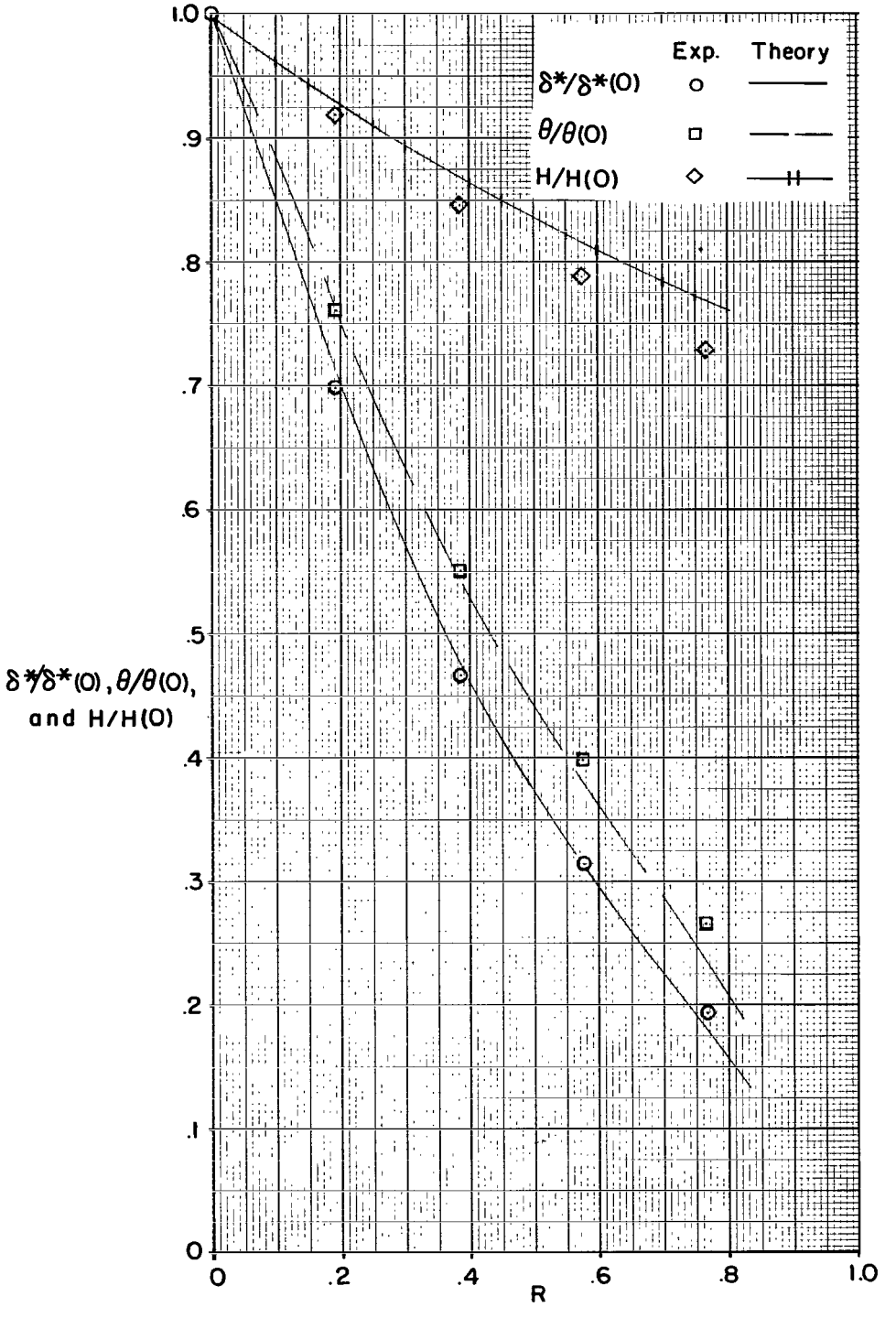

(d) x = 1.079 meters (3.54 feet).

Figure 17.- Concluded.

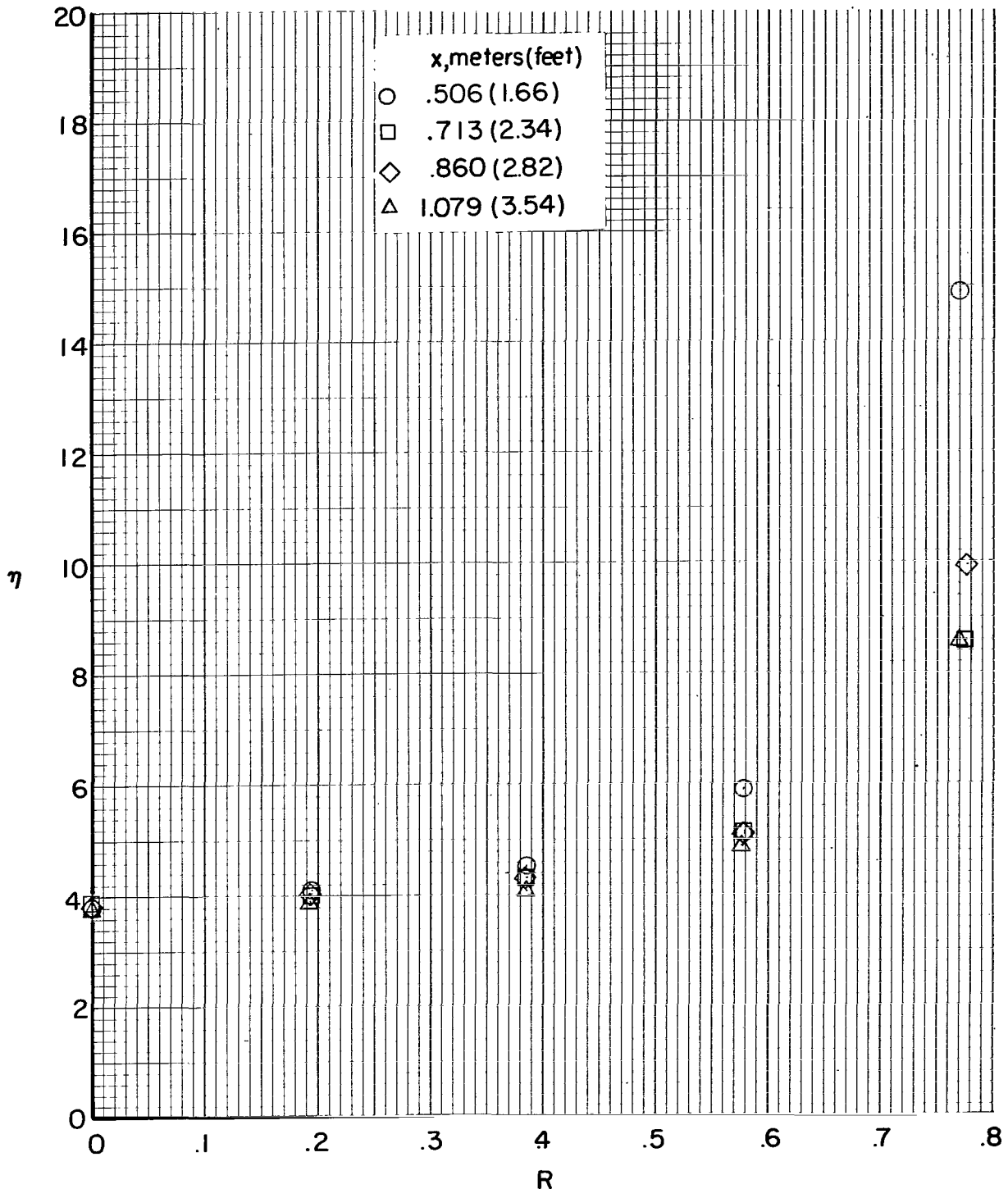

Figure 18.- Variation of the reciprocal of exponent in the Blasius shear-stress expression as a function of R.

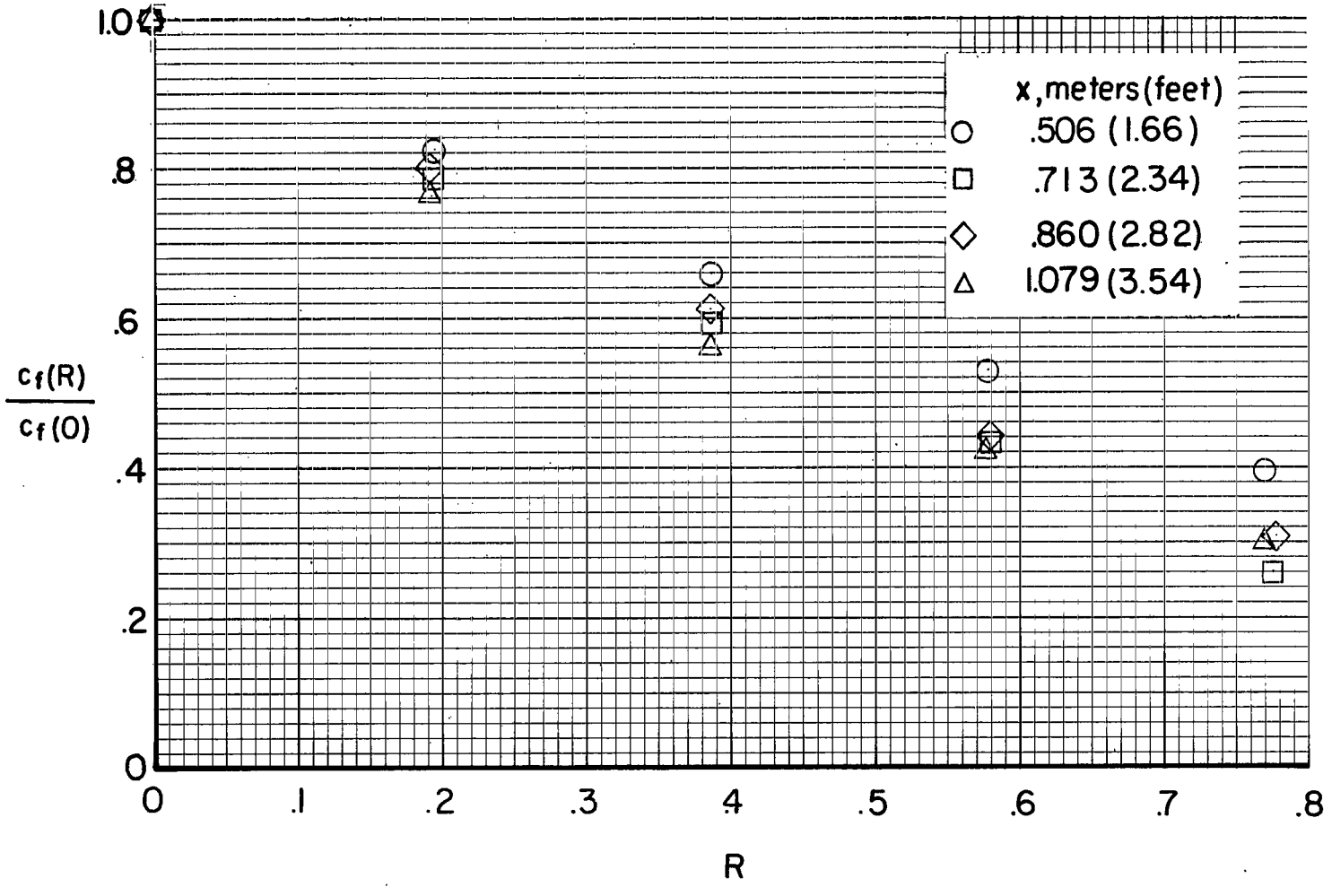

Figure 19.- Local skin-friction coefficients determined by the relative power law method.

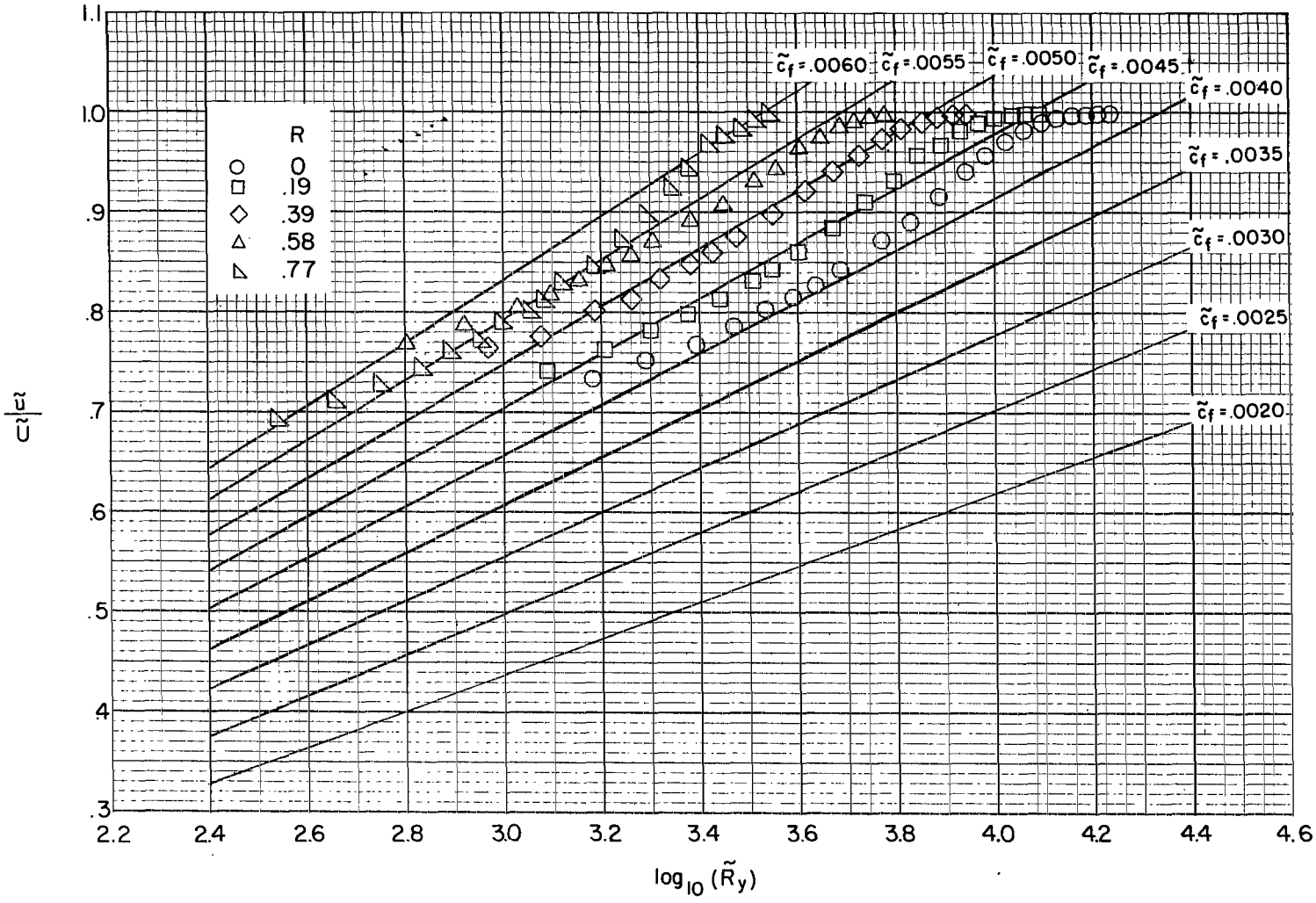

(a) x = 0.347 meter (1.14 feet).

Figure 20.- Skin-friction coefficients determined by modified law of the wall method.

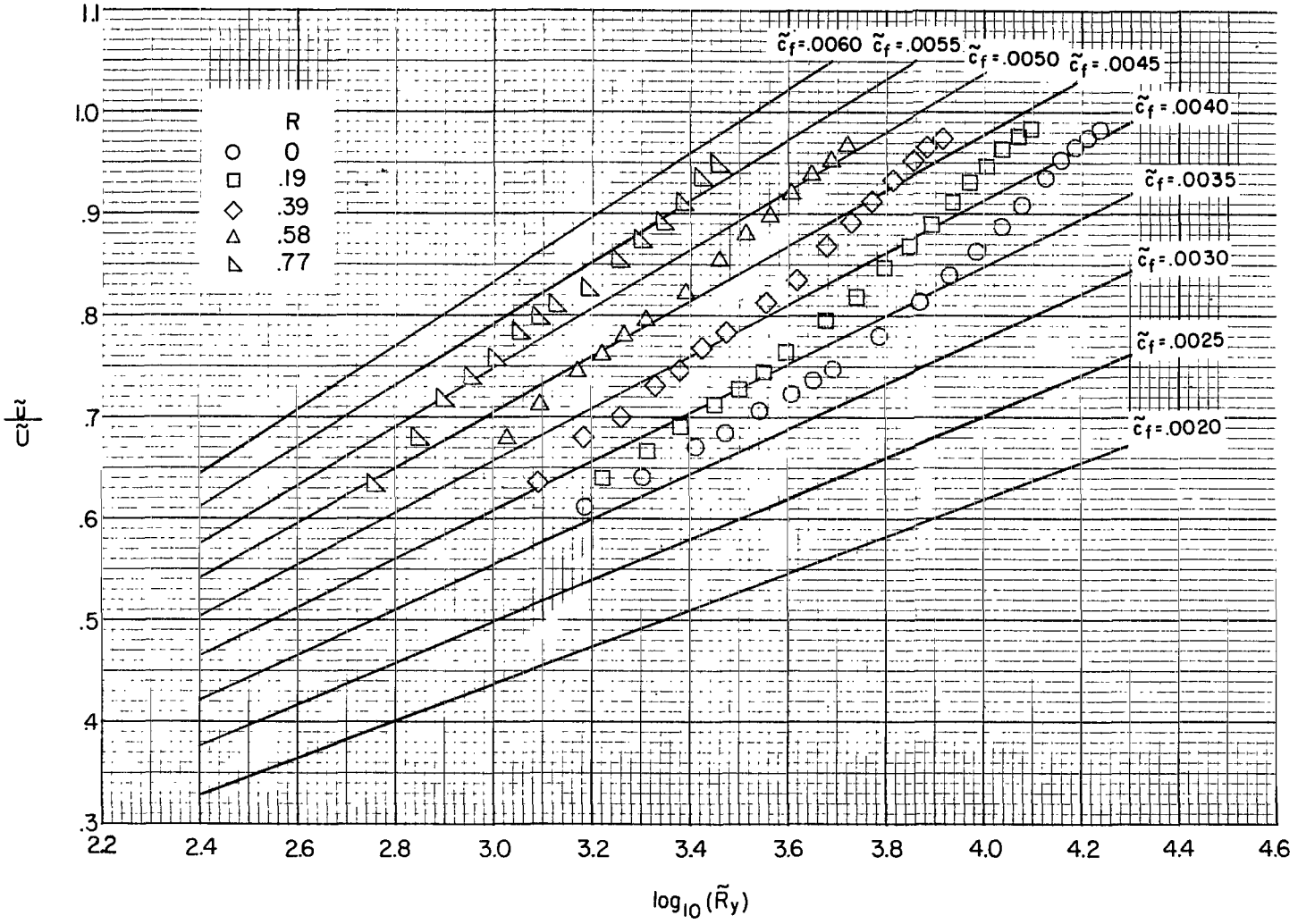

(b) x = 0.506 meter (1.66 feet).

Figure 20.- Continued.

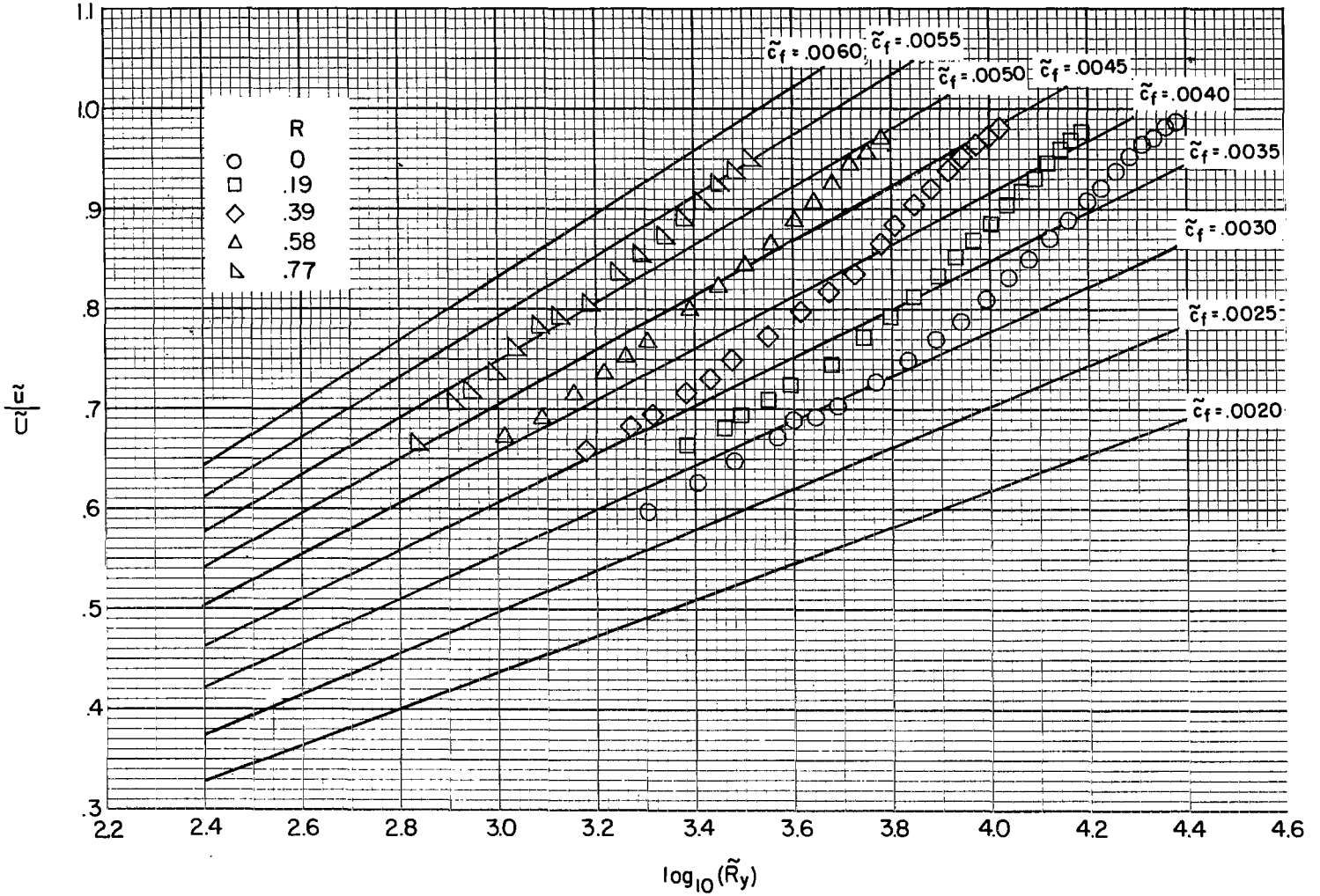

(c) x = 0.713 meter (2.34 feet).

Figure 20.- Continued.

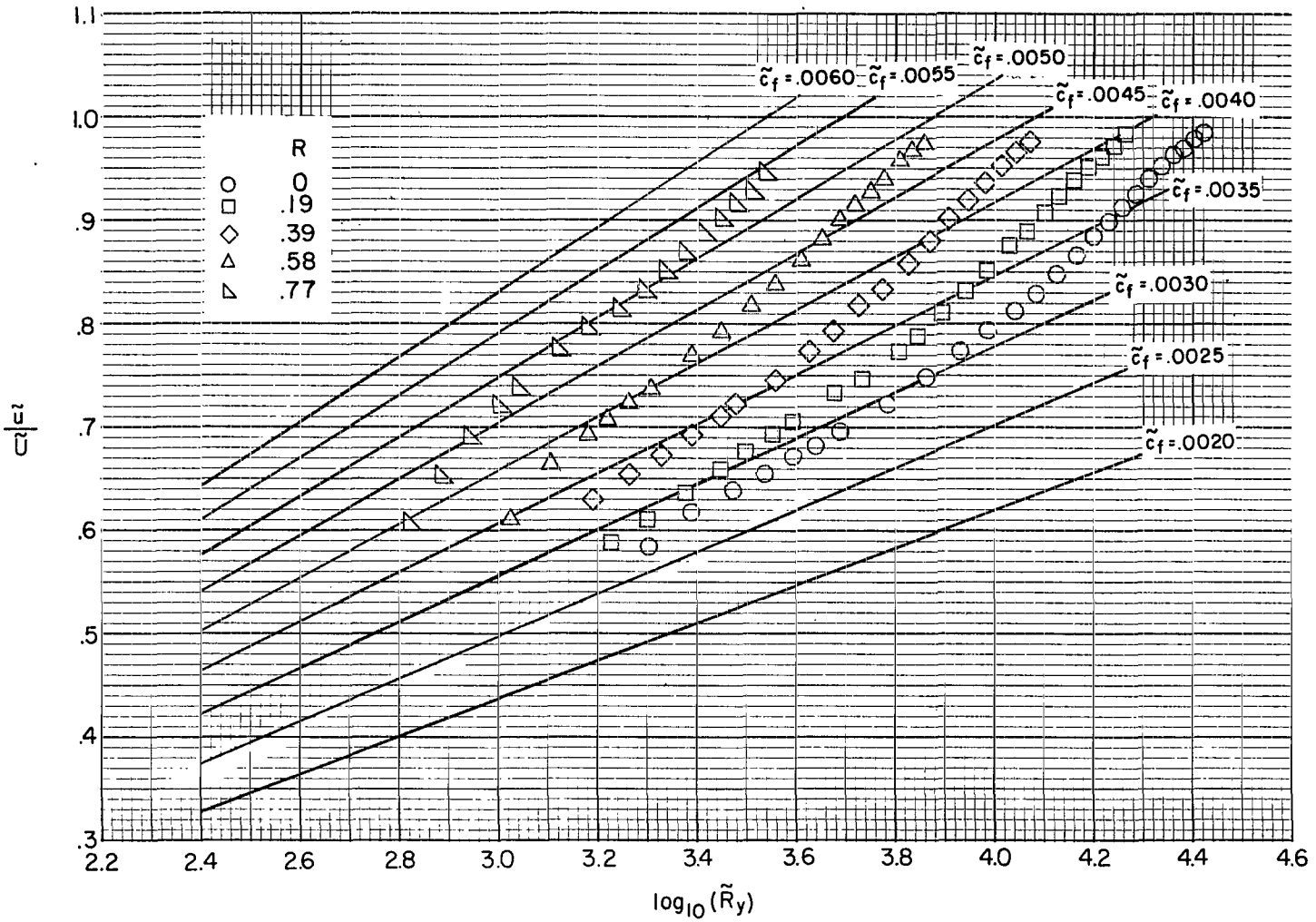

(d) x = 0.860 meter (2.82 feet).

Figure 20.- Continued.

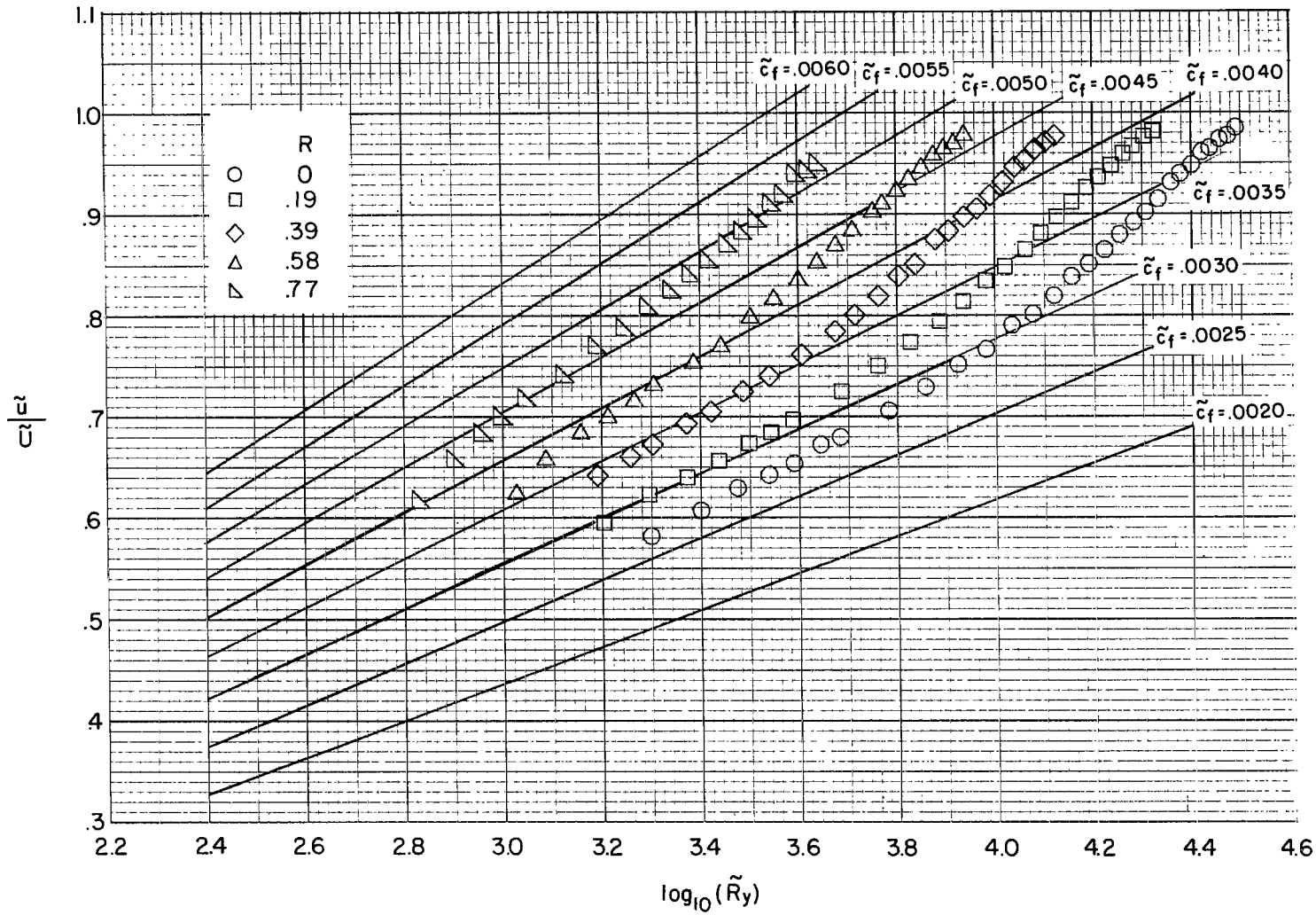

(e) x = 1.079 meters (3.54 feet).

Figure 20.- Concluded.

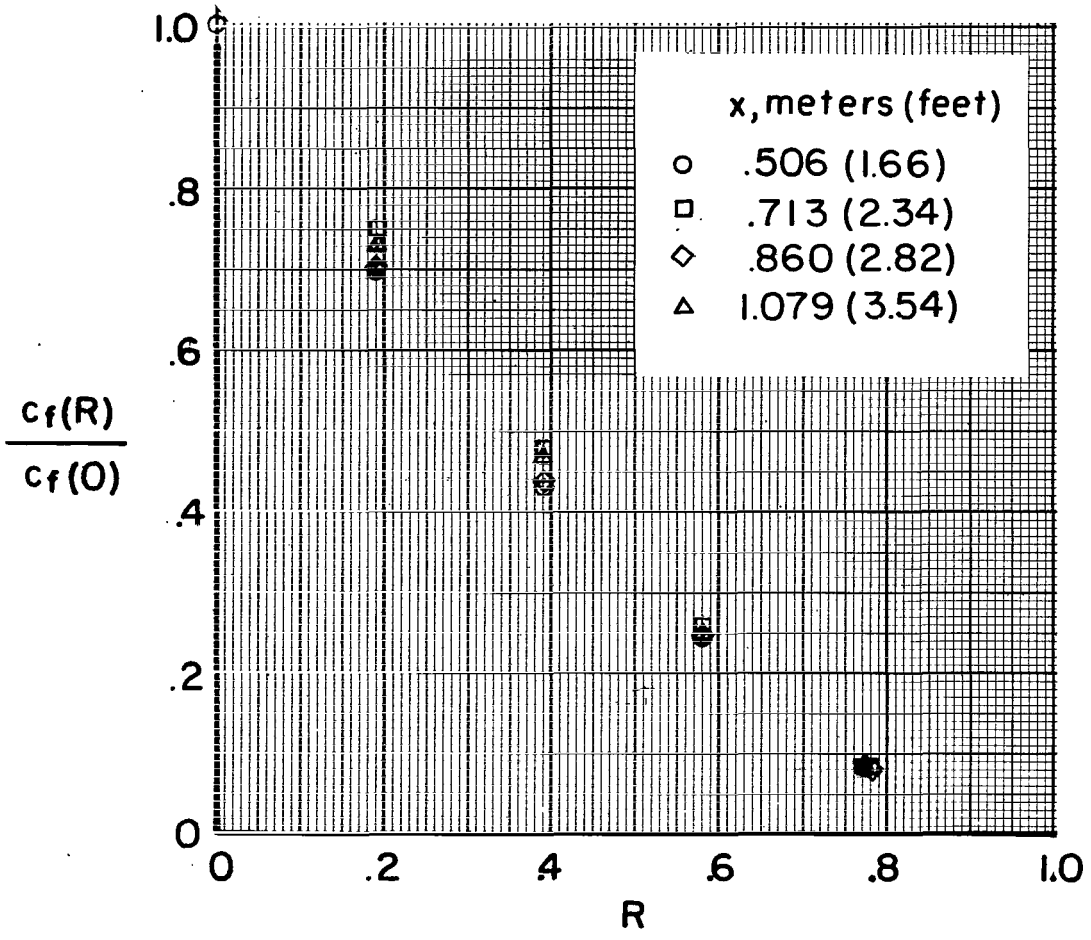

Figure 21.- Local skin-friction coefficients determined by the modified law of the wall method.

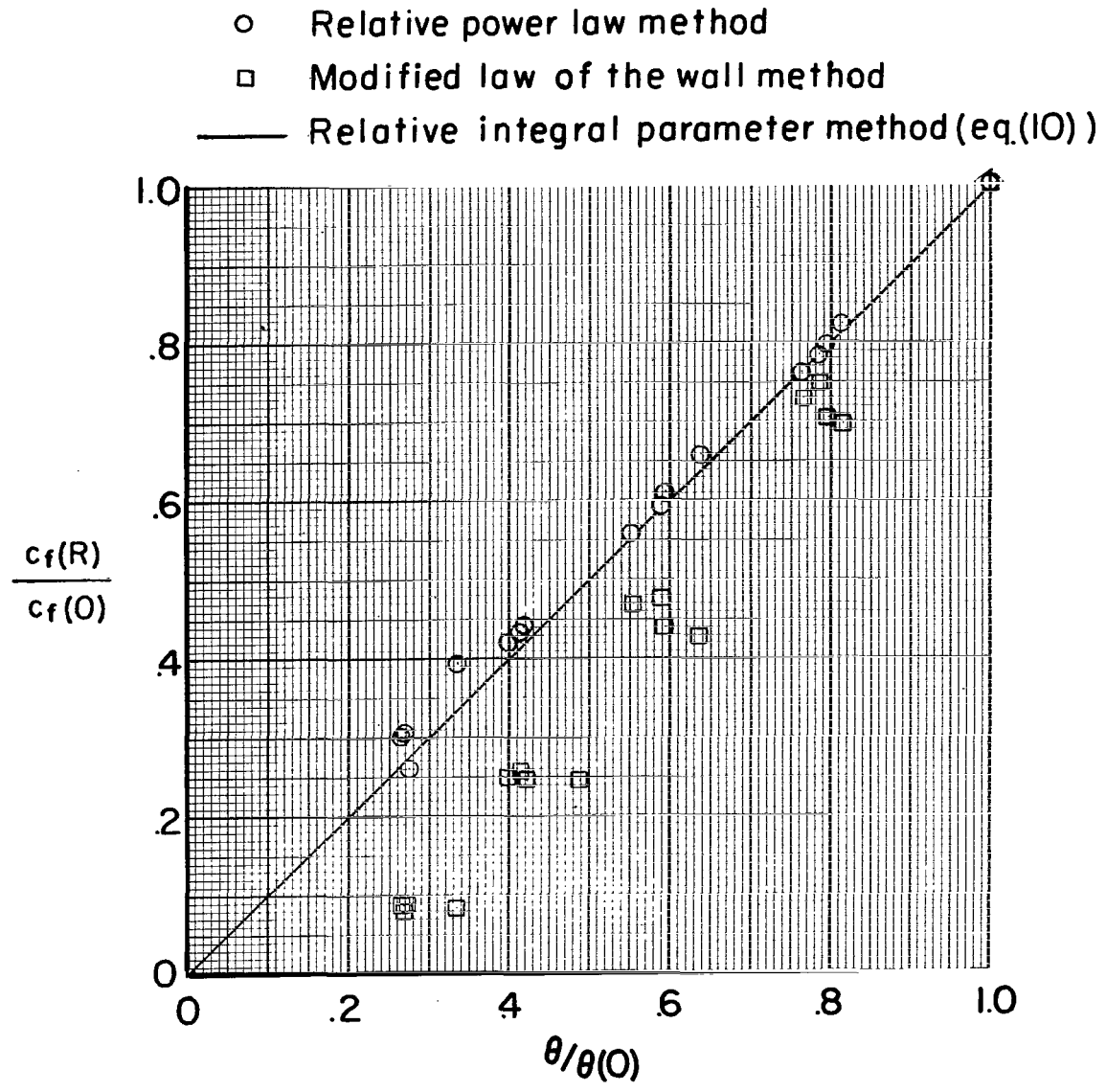

Figure 22.- Comparison of local skin-friction coefficients determined by relative integral parameter method, relative power law method, and modified law of the wall method.

NASA-Langley, 1972 —— 12 L-7872

"The aeronautical and space activities of the United States shall be conducted so as to contribute . . . to the expansion of human knowledge of phenomena in the atmosphere and space. The Administration shall provide for the widest practicable and appropriate dissemination of information concerning its activities and the results thereof."

—NATIONAL AERONAUTICS AND SPACE ACT OF 1958

NASA SCIENTIFIC AND TECHNICAL PUBLICATIONS

TECHNICAL REPORTS: Scientific and technical information considered important, complete, and a lasting contribution to existing knowledge.

TECHNICAL NOTES: Information less broad in scope but nevertheless of importance as a contribution to existing knowledge.

TECHNICAL MEMORANDUMS: Information receiving limited distribution because of preliminary data, security classification, or other reasons.

CONTRACTOR REPORTS: Scientific and technical information generated under a NASA contract or grant and considered an important contribution to existing knowledge.

TECHNICAL TRANSLATIONS: Information published in a foreign language considered to merit NASA distribution in English.

SPECIAL PUBLICATIONS: Information derived from or of value to NASA activities. Publications include conference proceedings, monographs, data compilations, handbooks, sourcebooks, and special bibliographies.

TECHNOLOGY UTILIZATION PUBLICATIONS: Information on technology used by NASA that may be of particular interest in commercial and other non-aerospace applications. Publications include Tech Briefs, Technology Utilization Reports and Technology Surveys.

Details on the availability of these publications may be obtained from:

SCIENTIFIC AND TECHNICAL INFORMATION OFFICE

NATIONAL AERONAUTICS AND SPACE ADMINISTRATION

Washington, D.C. 20546